Evaluation of membrane crystallization for the recovery of freshwater and mineral salts from high-saline wastewater

WITS
UNIVERSITY

By

Indira Camryn Theresa Chimanlal

A dissertation submitted to the Faculty of Science, School of Chemistry, University of the Witwatersrand, Johannesburg, in fulfillment of the requirements for the degree of Master of Science (Chemistry)

Supervisor: Dr. H. Richards

Co-supervisor: Dr. L. Nthunya

Date: 5 June 2023

DECLARATION

I declare that this dissertation is my own, unaided work. It is undergoing submission toward the degree of Master of Science at the University of the Witwatersrand, Johannesburg. Furthermore, this work has not been submitted before for any other degree at any other university.

Signature of candidate

Indira Chimanlal

DEDICATION

This work is dedicated to my loving parents who have always supported and helped me through everything that I do. Thank you for all your sacrifices, it did not go unnoticed. I hope that this makes you proud and I love you immensely. This work is also dedicated to my very special foi, Kirti, you have supported me through everything, guided me, and you have always been there for me. Your wisdom, smile, and laughter remain in my heart forever. You were proud of me. I love you.

ACKNOWLEDGEMENTS

I was able to produce this work with the assistance of many people who have offered support, help, and advice when I needed it. I would like to acknowledge Dr. Heidi Richards for the financial acquisition that funded this project and for the support offered during this project. I would like to thank Prof. Cejna Anne Quist-Jensen (Aalborg University) who provided me with support, guidance, and assistance during my time spent in Denmark. I would also like to acknowledge Dr. Lebea Nthunya for all the assistance and guidance provided in this project.

I wish to express my gratitude to the Danish International Development Agency (DANIDA) and the University of the Witwatersrand for their financial support during my studies.

I would like to acknowledge the great support offered by Dr. Shaeen Chetty. Even though you were not my supervisor, you were there whenever I needed help no matter what time of day it was. You offered to support me each time I had a problem and you assisted me with finding solutions. I cannot express enough how grateful I am.

I would like to acknowledge the contribution of my friends to the Environmental and Analytical Chemistry research group. Thank you for looking out for me, supporting me, and lending a much-needed helping hand. I would like to extend my gratitude to the Chemistry and Bioscience research group at Aalborg University who welcomed me with open arms and created a friendly and inviting atmosphere. Thank you for assisting me to progress my research and for providing guidance whenever I experienced challenges. I thoroughly enjoyed my time spent there. It was truly a memorable experience, something I would not trade for anything.

I would like to acknowledge my parents throughout this phase in my life. You have supported me, guided me, and encouraged me. I would like to acknowledge my very special aunt who always kept my best interests at heart and provided me with the best wisdom and strength when I needed it the most. You helped shape me into the person I am today. Whenever I experienced challenging moments throughout this degree and contemplated quitting, when each failure contributed to my frustration, and when difficulties got in the way of my well-being, my family was always around to comfort and encourage me to continue.

To my friends and family, I could not have made it this far without you. You have supported me in great ways. You have been there to celebrate my successes and encouraged the rise from my falls. Thank you for allowing me to reach greater heights. Words cannot describe what you mean to me and your impact on my life. Thank you for always assisting me whenever I needed

help, when I did not know whom to turn to, you were there. I am blessed to have such people in my life. To my nieces, Eliana, and Gianna, I hope to be a good role model to you. Thank you for all the joy you bring to my life. To the many pets in my life, you have always put a smile on my face when I needed it most and you have brought me happiness. You may not understand what goes on, but you have left paw prints in my heart.

PUBLICATIONS

This dissertation is largely based on articles that were produced from this study. Both published articles and those in preparation make up this dissertation and the details thereof are provided below for reference:

Membrane distillation crystallization for water and mineral recovery : The occurrence of fouling and its control during wastewater treatment

Indira Chimanlal, Lebea N. Nthunya, Cejna Anne Quist-Jensen, and Heidi Richards

Published in Frontiers in Chemical Engineering, (2022) Vol. 4, ISSN = 2673-2718

DOI=10.3389/fceng.2022.1066027

Nanoparticle-Enhanced PVDF Flat-Sheet Membranes for Seawater Desalination in Direct Contact Membrane Distillation

Indira Chimanlal, Lebea N. Nthunya, Oranso T. Mahlangu, Bastian Kirkebæk, Aamer Ali, Cejna A. Quist-Jensen, and Heidi Richards

Published in Membranes, MDPI, (2023) Vol. 13(3), 317

https://doi.org/10.3390/membranes13030317

The Evaluation of Modified Synthetic Flat-Sheet PVDF Membranes for Membrane Distillation Crystallization (MDC) Using Simulated Wastewater

Indira Chimanlal, Lebea N. Nthunya, Cejna Quist-Jensen, Heidi Richards

(Manuscript in preparation)

CANDIDATE CONTRIBUTION TO ARTICLES

Membrane distillation crystallization for water and mineral recovery: The occurrence of fouling and its control during wastewater treatment

Indira Chimanlal, Lebea N. Nthunya, Cejna Quist-Jensen, and Heidi Richards

Candidate contribution: Principle author responsible for investigation; methodology; validation; writing and editing.

Nanoparticle-Enhanced PVDF Flat-Sheet Membranes for Seawater Desalination in Direct Contact Membrane Distillation

Indira Chimanlal, Lebea N. Nthunya, Oranso T. Mahlangu, Bastian Kirkebæk, Aamer Ali, Cejna Quist-Jensen, and Heidi Richards

Candidate contribution: Principle author who was responsible for investigation; formal analysis; methodology; writing and editing.

The Evaluation of Modified Synthetic Flat-Sheet PVDF Membranes for Membrane Distillation Crystallization (MDC) Using Simulated Wastewater

Indira Chimanlal, Lebea N. Nthunya, Cejna Quist-Jensen, and Heidi Richards

Candidate contribution: Principle author involved in the investigation and methodology; data analysis; writing and editing

OTHER RESEARCH OUTPUTS

Book chapter

Hybrid membrane processes equipped with crystallization unit for simultaneous recovery of freshwater and minerals from saline wastewater in *Innovative Trends in Removal of Refractory Pollutants from Pharmaceutical Wastewater*

Tshepiso Mpala, Indira Chimanlal, Heidi Richards, Anita Etale, Lebea N. Nthunya

(In press)

TABLE OF CONTENTS

LIST OF FIGURES

LIST OF TABLES

NOMENCLATURE

AFM	Atomic force microscopy
CNTs	Carbon nanotubes
DCMD	Direct contact membrane distillation
DMac	Dimethylacetamide
DMF	Dimethylformamide
EDS	Energy dispersive x-ray spectroscopy
fCNTs	Functionalised carbon nanotubes
FTIR	Fourier transform infrared Spectroscopy
IC	Ion chromatography
ICP-OES	Inductively coupled plasma optical emission spectroscopy
LEP	Liquid entry pressure
MCr	Membrane crystallisation
MD	Membrane distillation
MDC	Membrane distillation crystallisation
NPs	nanoparticles
POTS	1H,1H,2H,2H-Perfluorooctyl triethoxysilane
PTFE	Polytetrafluoroethylene
PVDF	Polyvinylidene-fluoride
PVP	Polyvinylpyrrolidone
PXRD	Powder x-ray diffraction
SEM/EDX	Scanning electron microscopy/ energy dispersive x-ray spectroscopy
TEM	Transmission electron microscopy
TEOS	Tetraethyl orthosilicate
WCA	Water contact angle
XRD	X-ray diffraction

CHAPTER ONE – INTRODUCTION

1.1 Background

Water scarcity has been a distressing crisis in many countries around the world for years and will continue to pose a threat in the future. Approximately 2.2 billion people around the world are unable to access clean and safe drinking water (UNICEF, 2019). Particularly for developing countries, other factors such as degenerating wastewater treatment infrastructure, reducing freshwater sources, and financial constraints contribute to the enormity of water scarcity (Farmani *et al.*, 2021). Moreover, high salt content in water is yet another contributing factor to water shortages because it requires intensive pre-treatment to ensure its suitability for consumption (Vineis *et al.*, 2011). This is a consequence of wastewater discharged from industrial sources and when left untreated can prove to be detrimental for many species. Some of the disadvantages of high saline water include deteriorating water quality and aquatic health, eutrophication, plant dehydration, and ecological imbalances (Sparenberg *et al*, 2020; Dow *et al.*, 2022). Approximately 309 million people in developing African countries experience intermittent water supply where drinking water is supplied for less than a full day (Farmani *et al.*, 2021; Loubser *et al*., 2021). In addition to a water scarcity crisis, mineral shortages present itself as an emerging economic problem. Mineral shortages typically arise due to the growing industrial and economic sector thus further stimulating greater demand for these resources. The increased pressure generated by the renewable energy sector also encourages a greater demand for minerals as they are used in products such as electric generators for wind turbines, electric vehicles, and solar panels (Calvo and Valero, 2022). Therefore, research was directed toward wastewater treatment with an aim to recover valuable components such as mineral salts, nutrients, organic products, and freshwater. The utilization of wastewater for mineral resource reclamation has the potential to drive a circular economy and provide an alternative avenue apart from the conventional methods (Kharraz *et al.*, 2022). Moreover, this is advantageous for the environment as harmful and hazardous wastewater can be adequately treated prior to discharge.

Due to the small percentage of drinkable water on earth, clean drinking water is commonly produced from treated wastewater. Examples of membrane separation processes that are used to treat wastewater include nanofiltration (NF), ultrafiltration (UF), microfiltration (MF), and reverse osmosis (RO). Other methods include electrodialysis (ED) and membrane bioreactors (MBR), and evaporation ponds that are used to retrieve valuable salt components in the water.

However, these procedures have their associated disadvantages. Processes such as RO are limited by operating pressures (Hickenbottom and Cath, 2014), MBR processes experience poor effluent quality due to the presence of organic contaminants (Kharraz *et al.*, 2022), and evaporation ponds suffer from high water losses to the environment.

The gravity of the setbacks discussed herein motivate the need to find sustainable technology that may assist to alleviate the problems experienced. One such solution is membrane crystallisation (MCr), otherwise known as membrane distillation crystallisation (MDC), which was first introduced by Curcio *et al*. (2001). This technique is an augmented form of membrane distillation (MD) with an added crystallisation component which MD does not include. It is relatively new but is an avenue of membrane application technology that is gaining popularity. This technology has demonstrated its potential in sustainably providing solutions to the water and mineral shortage crises. Principally, this technology utilises a hydrophobic membrane as an interface, which separates a warmer feed side from a cooler permeate region. The feed solution is heated below boiling point, thereby facilitating a water phase change. The water vapour that is generated passes through the hydrophobic membrane, which is condensed by a colder permeate stream, thereby collecting freshwater from a previously polluted feed stream. The temperature difference initiated across the membrane interface introduces a vapour pressure gradient which is the driving force of this technique. The gradual elimination of water from the feed solution drives the solution to supersaturation which allows the salt constituents to be crystallised.

A unique advantage of this technology is that it can utilise renewable energy sources, therefore making it a sustainable technology. It can treat brine and has the ability to achieve near zero liquid discharge (ZLD) (Balis *et al.*, 2022). It can also achieve higher total water recoveries compared to MD alone (Balis *et al.*, 2022). Furthermore, it is not hindered by osmotic pressure and can operate independently of the feed concentration, therefore even industrial wastewater can be utilised (Shi *et al.*, 2022). It is not energetically intensive as it can operate at lower temperatures and pressures (Quist-Jensen *et al.*, 2017), and it can simultaneously provide freshwater and mineral salts (Hickenbottom and Cath, 2014). However, the success of this technology is limited due to disadvantages such as membrane fouling and wetting. The former is the result of feed contaminant deposition onto the membrane surface or within its pores thereby leading to pore blocking. (Pramanik *et al.*, 2016). Common types of fouling include inorganic (scaling), organic and biofouling (Drioli *et al.*,2015). Fouling can lead to structural damage and overall performance deterioration. This problem is alleviated using pre-treatment

strategies to eliminate or reduce the foulants in the feed solution, or membrane cleaning to restore its original performance. MDC has the added benefit of reducing the occurrence of scaling as compared to MD, however it does not completely prevent it from happening (Shi *et al.*, 2022). Membrane wetting occurs when water in its liquid state passes through the membrane and provides an avenue for the permeation of any minerals or contaminants in the feed solution. This can be circumvented using hydrophobic membranes. Consequences of this includes a reduction of mass transfer and declining process efficiency. Other disadvantages include polarization effects namely: temperature and concentration polarisation. Temperature polarization results in reduced heat transfer which diminishes the driving force, additionally, concentration polarization stimulates scaling as it facilitates an increase in the solute concentration at the feed-membrane interface. Moreover, this reduces mass transfer across the membrane (Hickenbottom and Cath, 2014). In this work membrane crystallization was evaluated using a selection of synthesised polyvinylidene fluoride (PVDF) membranes containing additives to improve their properties. Moreover, these membranes were comparatively assessed alongside commercial polytetrafluoroethylene (PTFE) membranes. These membranes were evaluated through a series of Direct Contact Membrane Distillation (DCMD) experiments using simulated seawater (3.5 wt% NaCl), after which they were evaluated in MDC application using simulated acid mine drainage (AMD), which has not yet been widely reported in literature thus far. AMD was targeted in this study as it is highly prevalent in South Africa due to the high level of mining activity especially in inland provinces. Its high occurrence provides an opportunity of waste reclamation due to the harmful environmental and health risks AMD poses.

CHAPTER TWO – LITERATURE REVIEW

2 Membrane distillation crystallization for water and mineral recovery: The occurrence of fouling and its control during wastewater treatment

The information presented in this chapter was published as a review article in the journal Frontiers in Chemical Engineering. This work was authored by Indira Chimanlal, Lebea N. Nthunya, Cejna Anne Quist-Jensen, and Heidi Richards and titled "Membrane distillation crystallization for water and mineral recovery: The occurrence of fouling and its control during wastewater treatment".

2.1 Introduction

Presently, about 4 billion people globally are affected by water scarcity (Mekonnen and Hoekstra, 2016). Water scarcity is influenced by an increase in urbanization and industrialization, population growth, and climate change (Ahmed, Hashaikeh and Hilal, 2020). Additionally, mineral resource depletion is emerging as an industrial problem. Thus, the decline in raw materials results in energy and financial challenges in several industries (Quist-Jensen *et al.*, 2016). The shortage of raw materials consequently minimizes industrial production required to meet the market demand. Therefore, recycling mineral resources from waste streams while recovering freshwater is imperative. This avenue circumvents the search for freshwater sources due to their steady depletion. A progressively attractive technique addressing the issues of mineral and freshwater shortages is membrane distillation crystallization (MDC). Interestingly, MDC affords simultaneous recovery of both mineral crystals and freshwater from high-saline wastewater (Quist-Jensen *et al.*, 2016). Technically, MDC is a hybrid process consisting of membrane distillation (MD) and a crystallization reactor wherein the feed solution is concentrated in the MD system to reach supersaturation, followed by crystallization to recover the minerals (Quist-Jensen *et al.*, 2017). Particularly, MDC can overcome challenges associated with common wastewater treatment options such as reverse osmosis (RO) and nanofiltration (NF) (Pramanik, Shu and Jegatheesan, 2017). Additionally, MDC operates at low temperatures and pressures, uses simple configuration, and consumes less energy compared to other thermal processes (Bouchrit *et al.*, 2017; Pramanik, Shu and

Jegatheesan, 2017). This review aims to unpack the principles and process characteristics of MDC for mineral and water recovery. Secondly, membrane fouling, and scale control measures are highlighted. Furthermore, process parameter optimization towards permeate flux, and crystal growth and selectivity are discussed. Additionally, membrane fabrication and modification strategies are reviewed to provide further insight into the development of more efficient and competitive membranes. Lastly, the latest developments towards MDC application are reported.

2.2 Principles of membrane distillation crystallization (MDC)

Membrane distillation (MD) has been extensively evaluated for the desalination of seawater and the treatment of high saline industrially discharged wastewater. During desalination processes, concentrated brines are generated and discharged to the environment. However, these brines could be treated further to recover mineral resources. Drioli, Ali and Macedonio (2015) regard mineral resources to be more economically valuable compared to fresh water produced from MD processes. In their study, the researchers presented a proof-of-concept to extract mineral resources from MD desalination plants (Drioli, Ali and Macedonio, 2015). In this regard, MDC emerged as a new technology with similar mechanisms to MD. The MDC saturates the feed solution to recover mineral crystals. The feed solution is concentrated through the MD process while recovering fresh water (Pramanik *et al.*, 2016). In this process, the feed solution becomes concentrated towards super-saturation, thus enabling nucleation and mineral crystallization while simultaneously recovering freshwater on the permeate side of the membrane (**Figure 2.1**) (Quist-Jensen *et al.*, 2016). To facilitate selective passage of water in vapour state while exclusively retaining liquid, this technique requires the use of a hydrophobic membrane (Das, Dutta and Singh, 2021). This process operates in various MD modes namely, direct contact membrane distillation (DCMD), air gap membrane distillation (AGMD), sweep gas membrane distillation (SGMD), and vacuum membrane distillation (VMD) (Pramanik *et al.*, 2016; Quist-Jensen *et al.*, 2016). The detailed description of each mode is reported elsewhere (Nthunya *et al.*, 2019). Interestingly, the water recovery in MDC ranges from 50 – 90%, thus emerging as an alternative water desalination technology (Quist-Jensen *et al.*, 2019). According to Quist-Jensen et al. (2019), MDC can increase water production, mineral recovery and advance zero-liquid discharge (Quist-Jensen *et al.*, 2019). The advantages and disadvantages of this technique are summarized in **Table 2.1**.

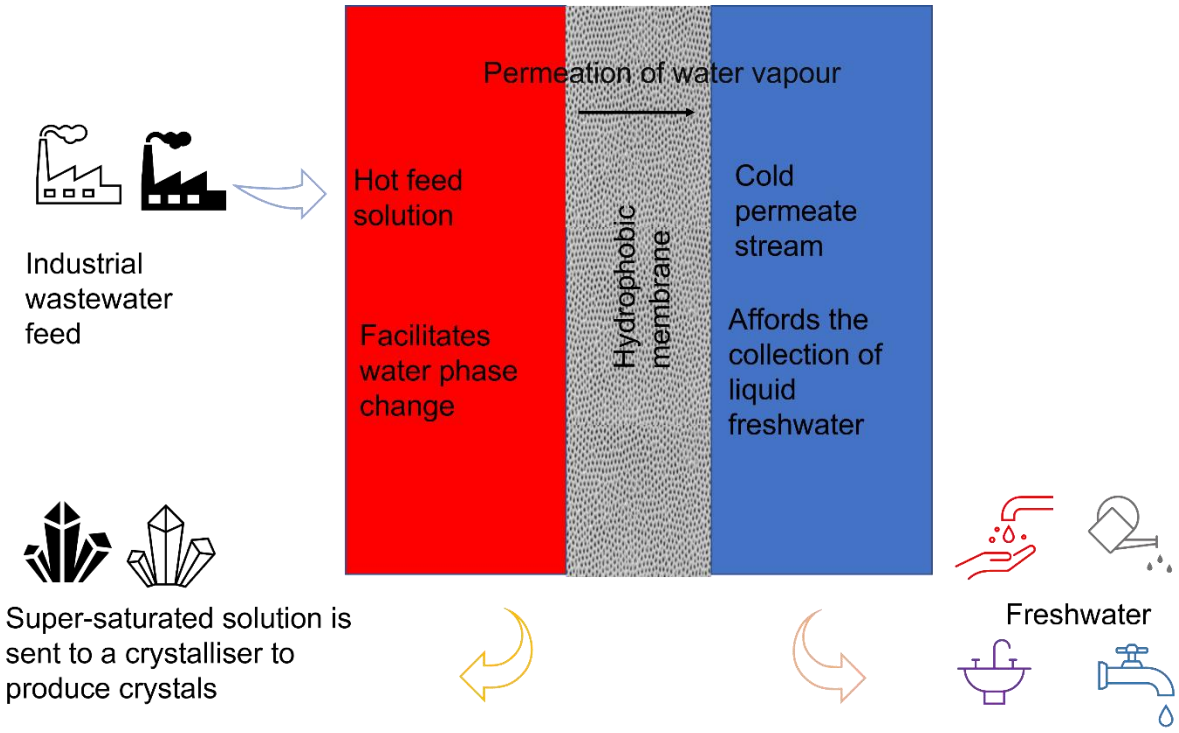

Figure 2.1: Schematic representation of MDC for recovery of freshwater and minerals from industrial wastewater.

Table 2.1: Summary of the advantages and disadvantages associated with MDC.

Advantages	**Disadvantages**	**Reference**
Independent of the feed concentration. Not affected by osmotic pressures from concentrated brines	Membranes are susceptible to fouling due to the contaminant deposition in membrane pores, resulting in clogging among other consequences	(Drioli, Di Profio and Curcio, 2012; Pramanik *et al.*, 2016; Ali *et al.*, 2018)
Can be utilized for salt separation processes to circumvent salt co-crystallization. Also, crystal growth and nucleation are controlled	May suffer from scaling which is due to the collection of inorganic salts on the membrane surface	(Drioli, Di Profio and Curcio, 2012; Bouchrit *et al.*, 2017; Ruiz Salmón and Luis, 2018)
Lower energy consumption and can make use of alternative energy sources such as solar power	Membrane performance may deteriorate due to membrane wetting	(Ruiz Salmón and Luis, 2018; Das, Dutta and Singh, 2021)

Provides sustainable and simultaneous water and mineral salt recovery	-	(Pramanik *et al.*, 2016)

2.3 Parameter optimization to enhance membrane distillation crystallization.

The development of a viable MDC process requires optimization to prevent undesired crystallization inside the module and tubing. For this reason, the selection of appropriate MD and crystallization operating conditions are imperative. These parameters include process temperature, solution supersaturation, flow rates and duration of crystallization. Moreover, the temperatures and flow rates affect the crystal size distribution. Therefore, analysis of these parameters provides a better understanding of the MDC process and requirements to realize the maximum performance while ensuring zero discharge to the environment.

2.3.1 Process temperature

The effect of process temperature on permeate flux is best described by Antoine equation, where α, β, and γ are constants relating to the specific substance and P_i is the vapour pressure (Pa) and T is the temperature (K).

$$P_i(T) = e^{(\alpha - \frac{\beta}{\gamma + T})}$$

According to the Antoine equation, vapour pressure exponentially increases with temperature (Choudhury *et al.*, 2019). Furthermore, water flux is directly proportional to feed temperature (Banat and Simandl, 1998). However, flux increments are limited by the process temperature and declines once an optimum has been attained (Banat and Simandl, 1998). Moreover, Attia et al. (2017) evaluated the effect of temperature using synthetic electrospun PVDF, superhydrophobic alumina, and commercial PVDF membranes in a comparative AGMD process. A direct relationship between permeate flux and feed temperature was established (Attia *et al.*, 2017). Liu et al. (2022) assessed the effect of temperature and flow velocity to obtain lithium chloride from air-conditioning systems via DCMD. Reportedly, an increase in feed temperature improved solute generation although the membrane's hydrophobicity was altered. However, the increase in solute concentration reduced the water flux due to a decreased partial vapour pressure (Liu *et al.*, 2022). Although high water fluxes are obtained at higher

temperatures, the water recovery factor is reduced due to salt precipitation (Zhu *et al.*, 2021). The effect of feed temperature on process operation is summarized in **Table 2.2**.

Table 2.2: Summary of the effect of varying the feed temperature on the permeate flux.

Membrane type	**MD process type**	**Feed temperature variation (℃)**	**Flow rate (L min^{-1})**	**Permeate flux (L m^{-2} h^{-1})**	**Ref.**
Electrospun PVDF	AGMD	30 – 70	1.5	Increased from 9.17 to 26.22,	(Attia *et al.*, 2017)
Flat sheet PVDF membrane	ADMD	25 - 80	5.5	Increased from 0.5 to 9.1	(Banat and Simandl, 1998)
Commercial polypropylene (PP) membrane	Integrated FO – MD process	40 - 70	0.4	Increased from 8.1 to 35.4	(Husnain *et al.*, 2015)
PTFE	DCMD	55 -65	0.4 – 1.0	Significant increase in flux.	(Liu *et al.*, 2022)
PTFE	AGMD	50 – 80	0.03 – 0.06	3.06	(Kargari and Yousefi, 2021)
Polyimide fibrous membrane (PI FM)	DCMD	30 - 50	0.24	Increased from 26.12 to 64.15	(Zhu *et al.*, 2021)
Commercial PTFE	DCMD	40 - 60	1.0	Increased from 4 to12	(Ramos *et al.*, 2022)

2.3.2 Solution supersaturation

The capability of the MD technology to progressively concentrate a feed solution to supersaturation gave rise to MDC (Yadav *et al.,* 2022). The gradual passage of water vapor from the feed stream to the distillate results in the eventual concentration of the feed solution to its critical saturation. Further increase in feed supersaturation enables the recovery of crystal salts from the crystallization reactor (Das *et al.,* 2021). Importantly, this process facilitates the recovery of higher quality mineral crystals in terms of size and purity. Other benefits include controlled rate of supersaturation and nucleation (Yadav *et.al.,* 2022). However, the increase in feed concentration towards solution supersaturation induces temperature and concentration polarization, thus reducing the permeate flux (Martínez, 2004). Moreover, pore blockage

occurs due to the formation of crystals on the surface of membrane (Yadav *et al.,* 2022). Martínez (2004) investigated the effect of feed concentration on the permeate flux using a flat sheet PTFE membrane and feed solutions of pure water, sodium chloride, and sucrose. Notably, the pure water flux remained stable towards supersaturation. However, the deposition of sodium chloride and sucrose crystal on the membrane surface resulted in a decrease in the permeate flux (Martínez, 2004). When supersaturation is attained in the bulk feed solution, nucleation is then induced which is succeeded by crystallization (Yadav *et.al.,* 2022). Moreover, a higher feed temperature increases rate of solvent evaporation, thus facilitating an increased rate of supersaturation compared to that experienced at low feed temperatures (Edwie and Chung, 2013).

2.3.3 Duration of crystallization

The formation and crystal growth are influenced by the solubility of the salt, rate of water recovery and process temperature. For instance, feed solutions with a low concentration containing extremely soluble solutes requires a lengthy period to form crystals (Rudolph, 2010; Liu *et al.*, 2021). Additionally, slow crystal growth rate facilitates formation of large crystals. Therefore, longer crystallization periods give rise to larger crystals (Alvarez *et al.*, 2020). In their study, Wagstaff et al. (1964) evaluated the impact of crystallization duration to the size of cristobalite. Based on their findings, the size of the crystals increased quadratically upon increase in duration of process crystallization (Wagstaff, Brown and Cutler, 1964). Essentially, the rate of crystal growth is governed by the various factors including flow of latent heat from the growing crystal, diffusion and reactions occurring at the crystal interface (Rudolph, 2010). In MDC processes, the inclusion of the membrane provides a site for heterogeneous nucleation. The Gibbs free energy is lower at the membrane-solution interface, thus favoring heterogeneous nucleation rather than homogenous nucleation (Ruiz Salmón and Luis, 2018). According to Edwie and Chung (2013), a high feed temperature encourages a higher rate of evaporation resulting in a lower average crystal size. Once nucleation has been established, the nuclei begin to grow until the critical cluster size has been achieved. Thereafter, crystals form and grow in saturation zones (i.e. metastable and unstable growth zones) (Yadav *et al.*, 2022). Technically, rate of supersaturation and nucleation affect crystal network growth, consequently the duration of crystallization (Das *et al.*, 2021).

2.3.4 Recirculation rate

High recovery rates of MDC processes are realized at higher recirculation rates (Swaminathan and Lienhard, 2018). For an efficient and high performing MDC process, the overall recovery factor should be greater than that of a single pass process (Lokare *et al.*, 2018). To achieve high recovery factors, the retentate is mixed with the new feed solution prior to crystallization (Lokare *et al.*, 2018). In addition to high recoveries, an increase in the recirculation rate enhances the heat transfer coefficient. Consequently, this minimizes the boundary layer thus improving the permeate flux (Srisurichan, Jiraratananon and Fane, 2006). Due to the improvement of water turbulence, a high recirculation rate reduces temperature polarization and membrane fouling, thus ensuring the stable water flux (Lokare *et al.*, 2018).

2.4 Fouling of MDC membranes

Occurrence of fouling in MDC is a common problem affecting process performance. To minimize fouling, its developments and successions should be established. Briefly, fouling occurs due to the deposition of microbial, colloidal, organic, or inorganic constituents on the surface or inner pores of the membrane, thus causing blockages (Choudhury *et al.*, 2019; Mpala *et al.*, 2022). Due to changes in the membrane physicochemical properties, fouling reduces permeate water flux, salt rejections and also increases the operating expenditure (OPEX) of the process (Nthunya *et al.*, 2022). Additionally, fouling reduces membrane hydrophobicity leading to membrane wetting (Wang and Lin, 2017). Reduced membrane hydrophobicity encourages the passage of water in liquid state, thus reducing mineral salt rejection (Wang and Lin, 2017; Choudhury *et al.*, 2019). Moreover, fouling is not limited to the membrane surface, but can also occur within the membrane pores. This was evident in a study conducted by Kim, Kim and Hong (2018) reporting deposition of foulants within the membrane pores in conjunction with reduced water recoveries and permeate flux. Usually, permeate flux reduction is caused by partial and complete wetting while the latter is true for water quality deterioration (**Figure 2.2**) (Yao *et al.*, 2020). Technically, the membrane is partially wetted by process conditions with limited passage of water in both liquid and vapour state. However, during full pore wetting, the water carrying salt ions passes through the membrane in liquid state, thus reducing the quality of the distillate.

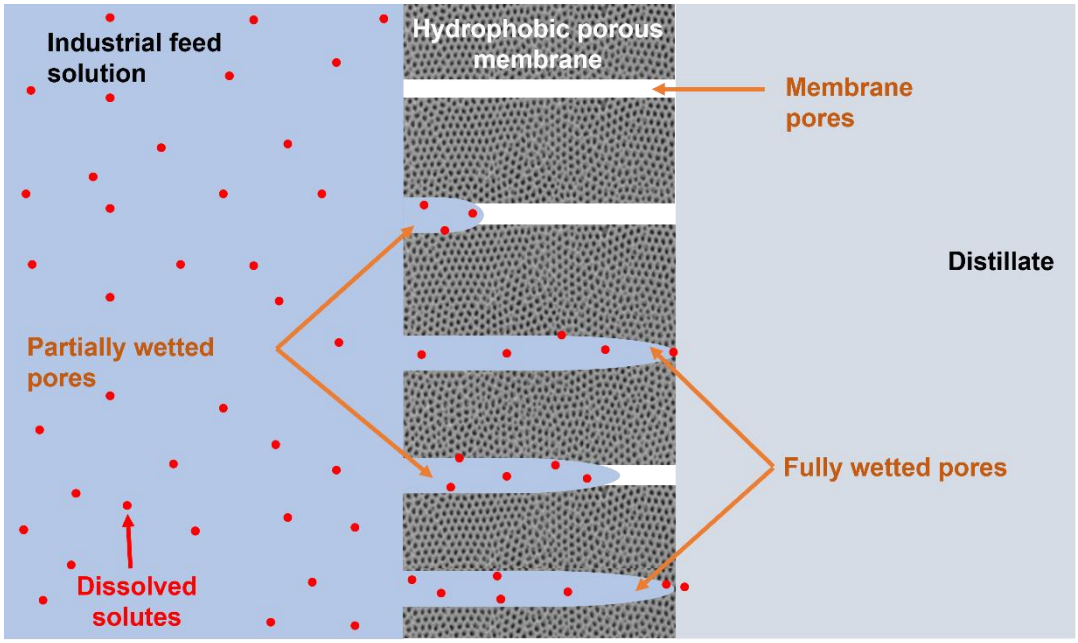

Figure 2.2: Graphical representation of membrane pore wetting experienced in MDC.

Common factors influencing fouling include feed solution properties, hydrodynamic conditions, and membrane characteristics (Yao *et al.*, 2020). The most prevalent form of fouling in MDC is scaling caused by sparingly soluble salts (Pramanik *et al.*, 2016; Charfi *et al.*, 2021). Inorganic scaling occurs via two mechanisms, namely; 1) nucleation and precipitate growth on the surface or pores of the membrane and 2) the build-up of precipitates materializing in the bulk solution (Horseman *et al.*, 2021). Common scalants causing membrane damage include calcium sulphate and calcium carbonate (Alkhatib, Ayari and Hawari, 2021). Fouling can be classified into porous and non-porous where the former causes thermal resistance and the latter results in both thermal and hydraulic resistance (Abdel-Karim *et al.*, 2021; Alkhatib, Ayari and Hawari, 2021). Therefore, to maintain high MDC process performance, operational challenges associated with a high concentration of salts and a complex feed solution should be overcome. Fouling and its implications are presented in **Table 2.3** below.

Table 2.3: Implications of fouling during experimental procedures.

Membrane type	**Fouling classification**	**Implications**	**Reference**
Commercial PP hollow-fiber	Calcium carbonate and sodium scaling	Reduced water recovery and permeate flux	(Kim, Kim and Hong, 2018)

Synthesised PVDF hollow-fiber	Organic fouling (dyes)	Decreased flux with long term operation	(Shi *et al.*, 2022)
Commercial PVDF	Scaling	Rapid flux decline	(Choi *et al.*, 2020)
PTFE/PP	Calcium sulphate scaling	Permeate flux decreased almost to zero	(Nghiem and Cath, 2011)
PTFE and PE	Organic fouling (from petrochemical wastewater) and scaling	Decreased permeate flux	(Venzke *et al.*, 2021)
Commercial PTFE	Organic fouling	Reduced water recovery rate and permeate flux	(Ramos *et al.*, 2022)
Synthesised PVDF/PSF hollow fiber	Organic (ginseng) and inorganic fouling	Reduced overall flux and rejection factor	(Zou *et al.*, 2022)
Commercial PP	Organic and inorganic fouling	40 % flux decline	(Gryta, 2020)

2.5 Fouling control

Membrane fouling is inevitable and therefore requires strategic measures to minimize its effects on process performance. Fouling control increases the membrane lifespan and maintains the performance of MDC processes (Laqbaqbi *et al.*, 2017). Membrane fouling is controlled through several measures including pre-treatments, backwashing, and chemical cleaning. These processes lengthen membrane longevity. Chemical cleaning and backwashing are employed post membrane fouling to recover flux and salt rejection. To increase water recoveries, fouling control is optimized to minimize cost and damage of membranes.

2.6 Pre-treatment

Flux decline caused by membrane fouling requires frequent membrane cleaning and possibly replacement, consequently increasing operating and maintenance costs (OPEX). Therefore, wastewater pre-treatment integrated to MDC improves process performance. Primarily, pre-treatment strategies limit fouling by reducing foulants concentration in the feed water. The choice of pre-treatment depends on the feed water. Typically, a combination of pre-treatment strategies is required to improve efficiency of foulant removal from the feed solution. These combinations involve physical and chemical processes such as low-pressure membrane

filtration, coagulation and flocculation, adsorption, pH adjustments, and the addition of anti-scalants.

Mechanical pre-treatments consist of membrane processes such as microfiltration (MF), ultrafiltration (UF), and nanofiltration (NF). Particularly, NF is used for water softening and reduction of natural organic matter (NOM). The UF and MF reduces colloidal, suspended and biological matter (Alkhatib, Ayari and Hawari, 2021). These pre-treatment methods have been evaluated in water processing of various complexities (Nthunya, Mbakop and Mhlanga, 2021). El-Abbassi et al. (2013) studied coagulation-flocculation and MF pre-treatment of olive mill wastewater in DCMD. Coagulation-flocculation pre-treatment reduced the concentration of TDS and phenolic compounds by 23% and 18%, respectively. The TDS removal was improved to 30% while that of phenolic compounds was reduced to 4.8% upon the MF treatment (El-Abbassi *et al.*, 2013). In another study, Karakulski & Gryta (2005) investigated NF pre-treatment of tap water for use in MD. Reportedly, untreated feed water caused membrane scaling leading to rapid flux decay. However, NF pre-treatment removed scalants thus ensuring high process performance (Karakulski and Gryta, 2005). Additionally, adsorption has been proven to effectively remove organic matter prior to MD water purification. Nthunya et al. (2019) reported removal of phenolic compounds from feed wastewater using a candle filter (pore size ~100 µm) equipped with polyethyleneimine-functionalized polyacrylonitrile nanofibre membranes. The membranes presented 39.9 $mg \cdot g^{-1}$ adsorption capacity (Lebea N Nthunya, Gutierrez, Derese and Mamba, 2019). Notably, MD process performance remained relatively stable upon feeding with pre-treated wastewater. Coagulation-flocculation is another process proven to effectively remove foulants prior to MD water processing. In this process, foulant particles are converted into larger flocs, thus reducing their adhesive interaction with the membranes. Moreover, coagulation-flocculation coupled with conventional treatment or membrane filtration processes remove the flocs from the feed water (Alkhatib, Ayari and Hawari, 2021). Li et al. (2016) investigated the purification of biologically treated coking wastewater using MD coupled with coagulation pre-treatment. A poly-aluminium chloride (PACl) flocculant reduced the foulants thus promoting the stable performance in MD (Li *et al.*, 2016). Lastly, pH-adjustments have been extensively used to treat feed solutions in membrane processes. The increase in feed pH promotes formation of metal precipitates which are removed as insoluble metal hydroxides prior to MDC. Similarly, the feed solution is acidified to dissolve the foulant, thus impeding their interaction with the membranes (Karakulski and Gryta, 2005). A summary of MDC pre-treatment processes is presented in **Figure 2.3**.

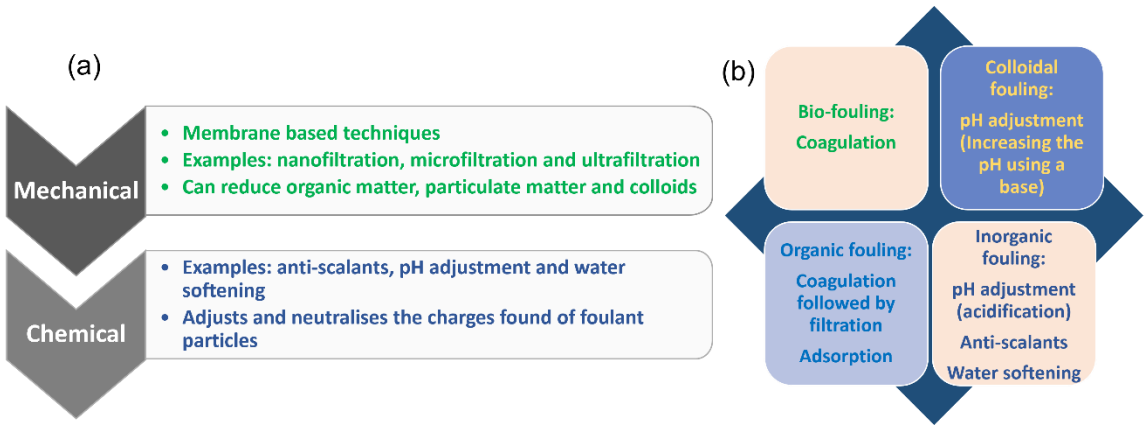

Figure 2.3: A summary of pre-treatment processes in MDC **(a)** pre-treatment classifications and **(b)** process selection for specific foulant.

2.5.1 Use of anti-scalants

Anti-scalants are precipitation-inhibiting chemicals impeding nucleation or crystal growth of scalants on membrane surfaces. Anti-scalants adsorb on the nuclei surface to obstruct the rate of crystal growth and agglomeration (Lin and Singer, 2005; Gloede and Melin, 2008; Abdel-Karim *et al.*, 2021). The anti-scaling mechanism of action takes place through ligand exchange or electrostatic interactions (Horseman *et al.*, 2021). Commonly used anti-scalants include organophosphates, polyelectrolytes and polyphosphates (Ketrane *et al.*, 2009). Yin et al. (2021) evaluated gypsum anti-scaling in reverse osmosis (RO) coupled with MD using Poly(acrylic) acid (PAA). A 1300 min test recorded 95% water flux decay in the absence of an antiscalant. However, the decay was reduced by 30% upon addition of anti-scalant, thus corresponding to 40% water recovery (Yin *et al.*, 2021). Lin & Singer (2005) utilized polyphosphates to minimize calcite crystal growth in MD. The process performance remained stable with minimal flux decay recorded. Though anti-scalants improve MDC processes, their addition beyond maximum threshold promote membrane biofouling (Tijing *et al.*, 2015). Therefore, the anti-scalant dosage should be optimized to meet the process requirement upon treatment of a specific feed solution.

2.5.2 Membrane flushing and gas bubbling

Membrane flushing and gas bubbling are classified as physical fouling mitigation strategies. Flushing is often carried out to remove adsorbed solutes from the membrane surface using deionized water. Nonetheless, flushing fails to remove solutes within the membrane pores (Alkhatib, Ayari and Hawari, 2021). Flushing is often operated in two modes namely, forward and backwashing. Technically, deionized water is pumped in a forward direction during forward flushing while the reverse is true for backflushing (Alkhatib, Ayari and Hawari, 2021). Gas bubbling enhances shear rate and fluid dynamics thus reducing temperature and concentration polarization (Alkhatib, Ayari and Hawari, 2021). Reportedly, finely dispersed bubbles are more efficient compared to course bubbles (Lu *et al.*, 2008). Choi et al. (2020) assessed the recovery of sodium sulfate from seawater brine using a hollow fiber PVDF membrane in fractionally submerged MD crystallization. Two cleaning procedures were used, namely air backwashing and deionized water flushing in the presence of ammonium sulfate. Air backwashing enabled 90% flux recovery. Similarly, flushing recovered 82% water flux from the original level. However, multiple air backwashing caused progressive permeate flux decline (Choi *et al.*, 2020). To reduce scaling of a commercial PTFE membrane supported on polypropylene (PP), Nghiem & Cath (2011) used MilliQ water. Five cycles of membrane flushing recovered 30% of the original flux (Nghiem and Cath, 2011). Though flushing is more efficient for removal of inorganic foulants, it can also be used for removal of organic foulants upon treatment of an oil-contaminated feed (Gryta, 2020).

2.5.3 Temperature adjustments and backflow

Temperature and flow reversal (backflow) techniques are novel methods used to mitigate fouling in MD/MDC. This experimental procedure was evaluated by Hickenbottom & Cath (2014) to minimize scaling while ensuring stable process performance. The temperature swap between the feed and distillate effectively reversed the driving force across the membrane, thus reducing the surface interactions between the membrane and scalants. Water flux and rejection efficiencies were recovered to 95%. Remarkably, both methods minimized scaling, thus ensuring stable fluxes and maintaining high salt rejection (Hickenbottom and Cath, 2014). Notably, these mitigation strategies avoid the use of expensive and toxic chemicals. Therefore, temperature and flow reversal are attractive alternative measures to control membrane fouling. However, extensive research is required to ascertain their sustainability at an industrial scale.

2.5.4 Chemical cleaning

Chemical cleaning is the most evaluated reactive measure used to control membrane fouling. The mechanism of action involves breaking foulant-membrane interactions (Alkhatib, Ayari and Hawari, 2021). Chemical reagents include acids, bases, surfactants, chelating agents, enzymes, and oxidants (Al-Amoudi and Lovitt, 2007; Porcelli and Judd, 2010). Typically, bases and surfactants are used to address organic and biofouling (Alkhatib, Ayari and Hawari, 2021; Charfi *et al.*, 2021) while acids and chelating agents are true for inorganic fouling (Alkhatib, Ayari and Hawari, 2021; Gryta, 2021). To ensure a synergistic cleaning process, a combination of chemicals is generally used during the treatment of complex feed solutions characterized by various foulants (Alkhatib, Ayari and Hawari, 2021). Charfi et al. (2021) optimized cleaning procedures of the MD process during treatment of anaerobic digestate. Reportedly, deionized water flushing was followed by 0.2% NaOCl and 3% citric acid for 60 min. NaOCl and citric acid were effective for organic and inorganic foulant removal, respectively thus ensuring 75.5% flux recovery. Furthermore, the cleaning process recovered 87% of membrane hydrophobicity with minimal membrane wetting (Charfi *et al.*, 2021). In another study Guillen-Burrieza et al. (2014) evaluated a variety of cleaning agents in long-term scaling control in MD processes. As per reported findings, a combination of 0.1 wt% oxalic acid and 0.8 wt% citric acid recovered 97% of the membrane WCA. Furthermore, formic, and sulfuric acid recovered 96.7% and 94.6% of the membrane WCA respectively. Although these processes restored WCA, the integrity and mechanical strength of the membranes were affected (Guillen-Burrieza *et al.*, 2014). The destruction of membrane integrity depends on cleaning conditions including the concentration of reagents, duration, and cleaning frequency. To understand the impact of chemical cleaning pertaining to physicochemical properties, various characterization techniques should be employed. These include chemical, morphological, topological, hydrophobic/hydrophilic, and mechanical analysis of the membrane. Puspitasari et al. (2010) investigated the cleaning and ageing of PVDF membranes using oxidative sodium hypochlorite (NaOCl). The effect of chemical concentration on the cleaning and ageing of the membrane is presented in **Figure 2.4a**. The cleaning efficiency improved with an increase in NaOCl. The same trend was observed for cyclical membrane cleaning. However, following the cleaning protocol, SEM micrographs showed presence of foulants on the membrane surface. Moreover, FTIR results presented changes in the chemical functional groups of membrane, thus alluding to an ageing effect. Furthermore, higher concentrations NaOCl damaged the integrity of the membrane (**Figure 2.4b)** (Puspitasari *et al.*, 2010). To minimize the damage, a

combination of cleaning reagents and anti-scalants is commonly used. This was evaluated by Peng et al. (2015) during the MD treatment of RO concentrated brine. A series of chemicals namely, NaCl, NaOH, KCOOH, citric acid, and EDTA-4Na were used. While operating at elevated temperatures, EDTA-4Na enabled highest flux recovery. Improved recovery was associated to chelation of calcium ions, thus reducing their interactions with the membranes (Peng *et al.*, 2015). In another study, Zhang et al. (2021) used a combination of organic phosphoric acid and hexamethylene diamine tetra(methylene phosphonic acid) (HDTMPA) during treatment of landfill leachate in FO/MD system. A combination of these chemicals reduced the foulant-membrane interactions, thus improving the process performance. Although 90% of flux was recovered in the first cycle, continuous cleaning did not show significant increase in performance recovery (Zhang *et al.*, 2021).

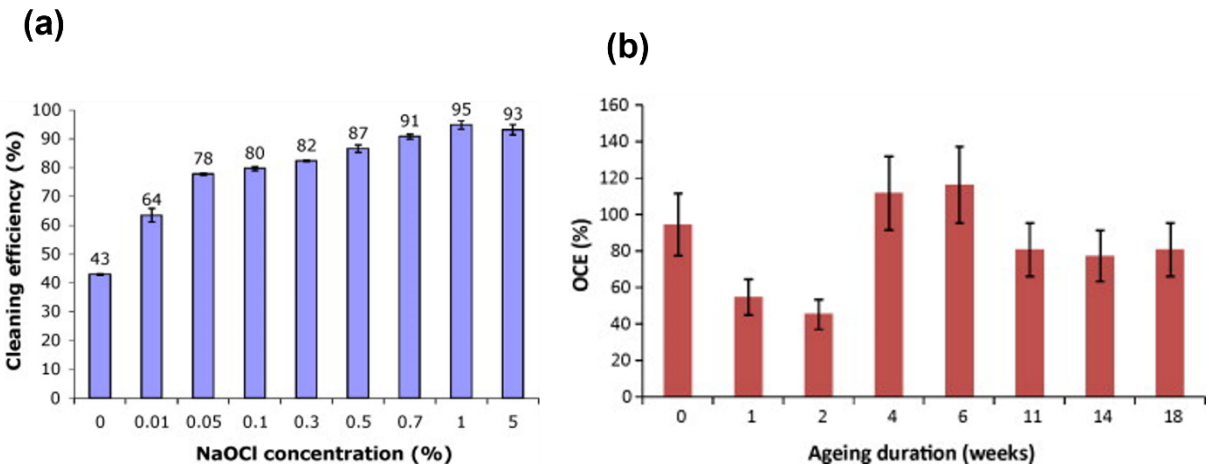

Figure 2.4: **(a)** Average cleaning efficiencies as a function of varying NaOCl concentrations, **(b)** overall cleaning efficiencies (OCE) observed for aged, fouled membranes (Puspitasari *et al.*, 2010).

Some foulants bind strongly on membrane surfaces, thus causing irreversible fouling. This phenomenon was reported by Naidu et al. (2015) upon NaOH cleaning MD membranes fouled by humic substances. Partial regeneration of the membrane with 19% hydrophobicity recovery was reported (Naidu, Jeong and Vigneswaran, 2015). Further improvements in chemical cleaning involves the use of 3D spacers. Spacers amplify flow turbulence, thus reducing foulant-membrane interaction. In their study, Castillo et al. (2019) investigated a step-wise cleaning of MD membrane using citric acid and water in the presence of spacers. Upon

cleaning, 87% of membrane WCA was recovered (Castillo *et al.*, 2019). The effect of various cleaning strategies is presented in **Table 2.4**.

Table 2.4: Summary of the cleaning strategies used in various studies.

Cleaning strategy	Cleaning duration	Frequency	Effect on Flux	Effect on WCA	Comments	Ref.
60 min rinsing with deionized water followed by 0.2 % NaOCl and 3 % citric acid		Every two days	87% water flux was recovered	75.5 % WCA was restored	Membrane was resistant to wetting	(Charfi *et al.*, 2021)
30 min rinsing with deionized water followed by 0.1 wt% oxalic acid and 0.8 wt% citric acid		-	-	126.4° compared to 129° for the unused membrane	Mechanical integrity of the membrane was reduced	(Guillen-Burrieza *et al.*, 2014)
1% NaOCl followed by 10 min rinsing with deionized		-	-	-	95% cleaning efficiency was recorded	(Puspitasari *et al.*, 2010)
60 min washing with NaOH, absolute ethanol, and pure water		-	-	-	Combined cleaning strategy was effective	(Shi *et al.*, 2022)
EDTA-4Na	-	-	-	-	Higher flux recoveries achieved at higher temperatures	(Peng *et al.* 2015)
2.5 wt% HCl	30 – 70 hrs	-	-	-	100% flux recovery was recorded	(Gryta, 2007)
Deionized water rinsing and NaOH	-	-	-	Average hydrophobicity was reduced by 19 %	Fouling was irreversible	(Naidu *et al.*, 2015)

Membrane modification using SiO_2-PNIPAM particles, and thermal actuation	5 and 10 min	-	-		Membrane surface free energy was reduced, thus restoring hydrophobicity	(Lyly *et al.*, 2021)
Hydraulic rinsing	-		Flux recovery of > 90 %	-	HDTMPA facilitated antiscaling	(Zhang *et al.*, 2021)
0.1 wt% citric acid and deionized wate. Also, 3D Gyroid spacer was used	24 hrs,	-	-	WCA of membranes was reduced by 13%	Acid improved cleaning process	(Castillo *et al.*, 2019)

2.5.5 Membrane modification

Membrane modification improves resistance to fouling and wetting. Typically, modification is achieved through systematic manipulation. Currently, superhydrophobic membranes characterized by self-cleaning properties are explored with low success rate. To improve membrane resistance to fouling while retaining high salt rejection, omniphobic and Janus membranes are also reported (Wang and Lin, 2017; Yao *et al.*, 2020; Tjale *et al.*, 2022). These membranes are characterized by asymmetric wettability to minimize fouling while retaining process stability (Afsari, Shon and Tijing, 2021). Xiao et al. (2020) prepared omniphobic membranes through incorporation of silica nanoparticles (SiNPs)-coated micropillars (MP) to PVDF. Reportedly, SiNPs-MP-PVDF membrane reduced scaling and fouling, thus maintaining the process performance over a longer period. **Figures 2.5 (a) and (b)** present the role of membrane modification towards preventing flux decay.

In another study, Toh et al. (2019) modified PVDF-co-hexafluropropylene membranes using silica nanoparticles to improve their resistance to wetting and fouling. The modified membranes were characterized by high WCA and low surface energy (Toh *et al.*, 2019). Zhang et al. (2021) reported hydrophilic surface modification of PVDF hollow fibre membrane through co-deposition of polydopamine (PDA) and poly(MPC-co-2-aminoethyl methacrylate hydrochloride) (MPC-co-AEMA). The smooth hydrophilic thin layer reduced the foulant-membrane interaction (Zhang *et al.*, 2021). In addition to hydrophilic coating, antimicrobial nanoparticles are embedded on hydrophobic membranes to combat organic, inorganic and biofouling. These additives include silver nanoparticles, cellulose nanocrystals and carbon nanotubes (Nthunya *et al.*, 2019; Nthunya *et al.*, 2020). Membrane modifications processes addressing fouling are presented in **Table 2.5**.

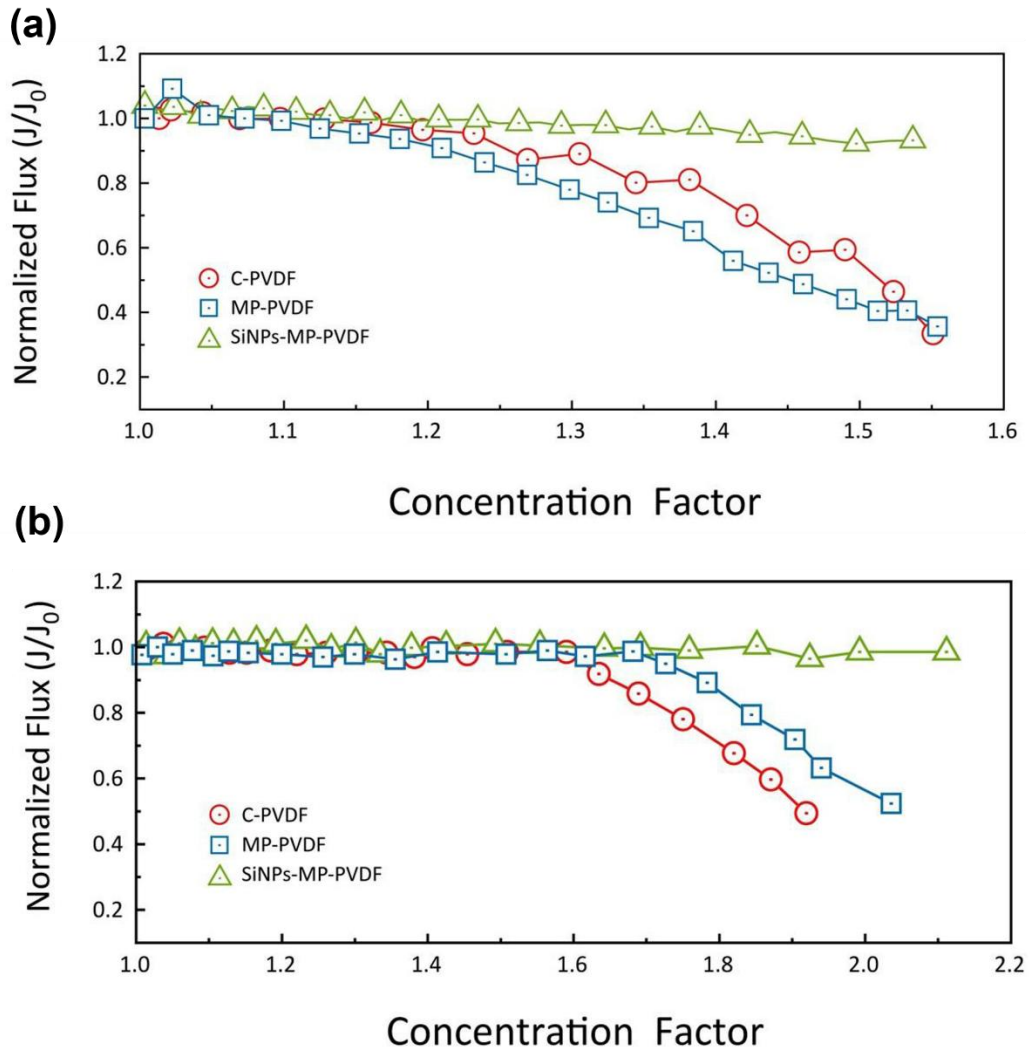

Figure 2.5: Normalized water flux (J/J_o) vs concentration factor for the individual membranes upon evaluation of **(a)** $CaSO_4$ scaling, **(b)** casein protein organic fouling (Xiao *et al.*, 2020).

Table 2.5: Summary of various membrane modification strategies and their effects on membrane properties.

Membrane type	**Membrane modification**	**Physical properties**			**Findings**	**Ref.**
		WCA (°)	**LEP (Bar)**	**Flux (kg m^{-2} hr^{-1})**		
Omniphobic PVDF membrane	Incorporation of silica nanoparticles	Improved from 130.1 to 175.6	-	-	Fouling resistant	(Xiao *et al*., 2020)
Superhydroph-obic PVDF-HFP)	Incorporation of silica nanoparticles	Improved from 135 to 151	-	-		(Toh *et al*., 2019)
PVDF hollow fiber membrane	Modified with PDA and AEMA-HCl	-	Improved from 1.13 to 1.15	-	Improved fouling resistance	(Zhang *et al*., 2021)
Two-layer superhydroph-obic PVDF membrane	Surface fluorination coating	Increased from 123.1 to 154.5	-	18% flux increase	Fouling resistant	(Kharraz & An, 2020)
Superhydroph-obic electrospun PVDF membrane	Electrosprayed with PDMS and silica fumes	170	-	-	Anti-abrasive and fouling resistant	(Liao *et al*., 2020)
PFPE/PVDF	Prepared by UV-curing	162.6	-	34.2	No flux and salt rejection decay	(Pan *et al*., 2022)
PVDF-PDMS Janus membrane	AgNP deposition on membrane surface	Top surface: 85.62, and bottom surface: 119.7	-	Flux increased from 11.5 to 20	Improved vaporiz-ation and flux	(Yue *et al*., 2021)
PVDF membrane	Modified with TNTs	-	-	Water flux increased by 38.7%	Improved porosity, thermal and mechanical properties	(Rahmaniyan *et al*., 2021)
PVDF	Blended with Hyflon and PFPE	Hyflon/PV: 138.4 and PFPE/PV: 157.7	-	Hyflon/PVDF: > 28 L PFPE/PVDF: 21	Improved permeate quality and resistant to flux decay	(Pan *et al*., 2022)
PVDF/PSF hollow fiber	Fluorinated	132	-	~ 6.0	Improved mechanical strength, anti-wettability,	(Zou *et al*., 2022)

	and water permeability

2.6 Application in wastewater treatment

Membrane distillation crystallization (MDC) emerged as a promising innovation in response to the global shortage of fresh water and mineral resources. Owing to the challenges associated with industrial application, MDC is extensively tested at laboratory-scale. Various applications of MDC are summarized in **Table 2.6**. Nonetheless, process optimization with sound findings has motivated its industrial use for treatment of wastewater. For instance, Hamzah *et al*. (2019) reported a flux of 11.0 $kg \cdot m^{-2} \cdot hr^{-1}$ during the treatment of a phenolic-rich feed solution using a PVDF/TiO_2/SiO_2 composite membrane. Remarkably, TiO_2-modification improved process resistance to organic fouling (Hamzah *et al.* 2019). Although fouling is minimized to some extent, it remains critically challenging (Kim *et al.*, 2017). Notably, fouled membranes attract scaling and wetting (Kim *et al.*, 2017). Despite all these challenges, MDC is relatively versatile towards treatment of complex feed solutions. In their study, Lu *et al.* (2017), reported 99% water purity recovered from oil-processing wastewater. Moreover, MDC is used as a finishing process to recover minerals and freshwater (90% water recovery and 99% salt rejection) from the RO concentrate (Venzke *et al.*, 2021). Nonetheless, treatment of the RO concentrate causes concentration polarization and scaling (Venzke *et al.*, 2021). Interestingly, MDC does not only treat industrial wastewater but also biological waste including human urine (Zhao *et al.*, 2013). During this treatment, 31.9 – 48.6 % water recovery was reported along with ammonia-nitrogen recovery and COD reduction (Zhao *et al.*, 2013). Among other factors related to the economics of the process, MDC is driven by renewable energy sources. The use of solar energy was evaluated by Li *et al.* (2020) in a pilot-scale where photothermal membrane was used. Although high flux (21.99 $kg \cdot m^{-2} \cdot hr^{-1}$) was reported, water recovery factors were low and production of photothermal membrane was costly (Li *et al.*, 2020). The successes achieved at lab scale supports the implementation of this technology toward pilot and industrial scale. Memstill ® reported first pilot testing of MD technology implemented at an incineration plant in Singapore in 2006 (Dotremont *et al.*, 2010). Other pilot studies were established at BASF in Antwerp, Belgium in 2011 (Camacho *et al.*, 2013).

Table 2.6: Various application of MDC towards treatment of wastewater and mineral recovery.

Membrane type	Mode of application	Feed solution used	Process temperature (Feed/ permeate/ crystallizer) (℃)	Process flow rates	Permeate flux	Products	Ref.
Commercial hollow fiber PVDF	Fractional submerged MDC	RO brine	50.0/ 20.1/ -	0.8 L min^{-1}	-	72% water recovery, 223.73 g Na_2SO_4	(Choi *et al.*, 2020)
Commercial hollow fiber PP	MDC	Shale gas produced water	60/ 20/ -	-	-	84% water recovery, salt production 2.72 $kg \cdot m^{-2} \cdot day^{-1}$	(Kim, Kim and Hong, 2018)
Hollow fiber PP	VMD-crystallization	Wastewater from oil extraction.	55 - 75/ 10/ -	-	-	99% water purity, NaCl and ethylene glycol	(Lu *et al.*, 2017)
Commercial PVDF	DCMD - MDC	2 M concentrated Na_2SO_4	40 – 70/ 25/ variable	2 L hr^{-1}	-	80% water recovery, 100 kg m^{-3} Na_2SO_4	(Bouchrit *et al.*, 2017)
PTFE	MD/MDC	Synthetic shale gas produced water	60/ 20/ 40	25 cm s^{-1}	-	62.5% water recovery and NaCl, $BaCl_2$, and $CaCO_3$	(Kim *et al.*, 2017)

Microporous PTFE plate membrane	VMD	Human urine	50 – 70/ -/ -	30 L hr^{-1}	-	31.9 – 48.6% water recovery	(Zhao *et al.*, 2013)
Fe_3O_4 – PVDF – co-hexafluoropropylene nanofibers	Solar driven MD	Synthetic NaCl solution	-/ 20/ -	20 ml min^{-1}	0.97 kg m^{-2} h^{-1}	Salt rejection of 99.99 %	(Li *et al.*, 2020)
Cloisite 15 - modified PVDF hollow fiber membrane	MDC	26.4 wt% NaCl solution	70/ -/ 25	-	-	34 kg NaCl was produced per m^3 of feed	(Edwie and Chung, 2013)
PTFE, standard PE (PE – S) and oleophobic PE (PE – O)	DCMD	RO concentrates from petrochemical wastewater	60/ 20	-	PE – O = 5.0 $kg{\cdot}m^{-2}{\cdot}h^{-1}$, PE – S = 2.1 $kg{\cdot}m^{-2}{\cdot}h^{-1}$ and PTFE reduced by 30% of initial flux after 250 hrs	Recoveries close to 90% and rejection rates > 99.5%	(Venzke *et al.*, 2021)
PVDF blended with multi-walled carbon nanotubes	DCMD	35 $g{\cdot}L^{-1}$ synthetic NaCl solution	82/ 20/ -	48 ml min^{-1}	9.5 x 10^{-3} kg m^{-2} s^{-1}	Salt rejection of 100 % after 60 min	(Silva *et al.*, 2015)
PVDF/TiO_2/SiO_2	DCMD	A phenolic-rich solution containing surfactant	40/20/-	300 ml min^{-1}	11.0 $kg{\cdot}m^{-2}{\cdot}h^{-1}$ after 8 hrs	99.9% gallic acid rejection with a flux decay resistance	(Hamzah, Leo and Ooi, 2019)

Commercial PP and hollow fiber PVDF	DCMD	Wastewater produced from oil and gas production	35,45,55/10/-	Feed: 150 $ml \cdot min^{-1}$ and permeate: 70 $ml \cdot min^{-1}$	Increased flux as a function of temperature	NaCl purity: > 99.9%, water and NaCl recovery: 37% and 16 $kg \cdot m^{-3}$ respectively	(Ali et al., 2015)

2.7 Conclusion and future perspectives

MDC addresses financial challenges affecting developing countries. Various literature reports have documented the successes of this technique in effectively recovering freshwater and mineral salts from a myriad of wastewater feed sources (Quist-Jensen *et al.*, 2016, 2017; Kim *et al.*, 2017; Choi *et al.*, 2020). In conjunction to emerging laboratory-scale studies, implementation of pilot studies at an industrial platform provides a promising trajectory for the future of this technology. Nevertheless, membrane fouling, and wetting requires special attention. Membrane fouling can be classified into organic, inorganic (i.e., scaling), biofouling, and/or colloidal fouling. In some circumstances, a combination of foulants may exist in the feed solutions thus resulting in more complex membrane fouling scenarios. To circumvent these issues, various fouling control measures have been registered including mechanical pre-treatment options such as microfiltration (MF) and nanofiltration (NF). Other pre-treatment strategies include anti-scalants, temperature adjustments, and membrane flushing. Moreover, chemical cleaning has been extensively evaluated to restore MDC performance. While commercial membranes have be used for MDC processes, further research has been directed towards synthesis and modification of various fouling resistant membranes. This includes incorporation of nanoparticles to induce self-cleaning through superhydrophicity enhancement (i.e. improving the lotus effect of the membrane). Similarly, Janus membranes characterized by asymmetric wettability have been evaluated to mitigate membrane fouling. The steady development in this technique and its accompanying components has probed further interest into its applicative potential. Promising feedback established with the use of this technique pave the way towards further implementation in an industrial setting for mineral and water recycling. Future perspectives include, though not limited to:

- Production of membranes using environmentally friendly reagents in addressing membrane fouling and wetting.
- Optimization of membrane cleaning strategies towards a feasible industrial application.
- Further research and implementation of pilot-scale studies to provide a realistic MDC suitability in industrial application.
- Further research establishing fouling mechanism is required to understand membrane longevity and process performance.

References

Abdel-Karim, A. *et al.* (2021) 'Membrane cleaning and pretreatments in membrane distillation – a review', *Chemical Engineering Journal*, 422(April), p. 129696. doi: 10.1016/j.cej.2021.129696.

Afsari, M., Shon, H. K. and Tijing, L. D. (2021) 'Janus membranes for membrane distillation : Recent advances and challenges', *Advances in Colloid and Interface Science*, 289, p. 102362. doi: 10.1016/j.cis.2021.102362.

Ahmed, F. E., Hashaikeh, R. and Hilal, N. (2020) 'Hybrid technologies: The future of energy efficient desalination – A review', *Desalination*, 495(August), p. 114659. doi: 10.1016/j.desal.2020.114659.

Al-Amoudi, A. and Lovitt, R. W. (2007) 'Fouling strategies and the cleaning system of NF membranes and factors affecting cleaning efficiency', *Journal of Membrane Science*, 303(1–2), pp. 4–28. doi: 10.1016/j.memsci.2007.06.002.

Alanezi, A. A. *et al.* (2021) 'Theoretical Investigation of Vapor Transport Mechanism Using Tubular Membrane Distillation Module'.

Ali, A. *et al.* (2015) 'Application of membrane crystallization for minerals' recovery from produced water', *Membranes*, 5(4), pp. 772–792. doi: 10.3390/membranes5040772.

Ali, A. *et al.* (2018) 'Evaluation of integrated microfiltration and membrane distillation/crystallization processes for produced water treatment', *Desalination*, 434(May 2017), pp. 161–168. doi: 10.1016/j.desal.2017.11.035.

Ali, A. *et al.* (2019) 'Treatment of Wastewater Solutions from Anodizing Industry by Membrane Distillation and Membrane Crystallization', *Applied Sciences*, 9(2), pp. 1–15. doi: 10.3390/app9020287.

Alibakhshi, S. *et al.* (2019) 'Tuning morphology and transport in ultrafiltration membranes derived from polyethersulfone through exploration of dope formulation and characteristics', *Materials Research Express*, 6(12), pp. 1–14. doi: 10.1088/2053-1591/ab56c3.

Alkhatib, A., Ayari, M. A. and Hawari, A. H. (2021) 'Fouling mitigation strategies for different foulants in membrane distillation', *Chemical Engineering and Processing - Process Intensification*, 167(June), p. 108517. doi: 10.1016/j.cep.2021.108517.

Alvarez, R. *et al.* (2020) 'Single crystal growth of water-soluble metal complexes with the help of the nano-crystallization method', *Dalton Transactions*, 49(28), pp. 9632–9640. doi: 10.1039/d0dt01236j.

Ametek, S. (2023) *SPECTRO - The performance benchmark for ICP-OES/ICP-AES spectrometers*. Available at: https://www.spectro.com/products/icp-oes-aes-spectrometers?sf_campaign_id=7013V000000AcgW&google_ad=icp+resource-library(subs) (Accessed: 9 January 2023).

Ardeshiri, F. *et al.* (2018) 'PVDF membrane assisted by modified hydrophobic ZnO

nanoparticle for membrane distillation', *Asia-Pacific Journal of Chemical Engineering*, 13(3), pp. 1–12. doi: 10.1002/apj.2196.

Ashoor, B. B. *et al.* (2016) 'Principles and applications of direct contact membrane distillation (DCMD): A comprehensive review', *Desalination*, 398, pp. 222–246. doi: 10.1016/j.desal.2016.07.043.

Attia, H. *et al.* (2017) 'Modelling of air gap membrane distillation and its application in heavy metals removal', *Desalination*, 424(September), pp. 27–36. doi: 10.1016/j.desal.2017.09.027.

Balis, E., Griffin, J. C. and Hiibel, S. R. (2022) 'Membrane Distillation-Crystallization for inland desalination brine treatment', *Separation and Purification Technology*, 290(January), p. 120788. doi: 10.1016/j.seppur.2022.120788.

Banat, F. A. and Simandl, J. (1998) 'Desalination by Membrane Distillation: A Parametric Study', *Separation Science and Technology*, 33(2), pp. 201–226. doi: 10.1080/01496399808544764.

Bouchrit, R. *et al.* (2017) 'Membrane crystallization for mineral recovery from saline solution: Study case Na2SO4 crystals', *Desalination*, 412, pp. 1–12. doi: 10.1016/j.desal.2017.02.021.

Calvo, G. and Valero, A. (2022) 'Strategic mineral resources: Availability and future estimations for the renewable energy sector', *Environmental Development*, 41(April 2021), p. 100640. doi: 10.1016/j.envdev.2021.100640.

Camacho, L. M. *et al.* (2013) 'Advances in membrane distillation for water desalination and purification applications', *Water (Switzerland)*, 5(1), pp. 94–196. doi: 10.3390/w5010094.

Castillo, E. H. C. *et al.* (2019) '3D printed spacers for organic fouling mitigation in membrane distillation', *Journal of Membrane Science*, 581(March), pp. 331–343. doi: 10.1016/j.memsci.2019.03.040.

Charfi, A. *et al.* (2021) 'Optimal cleaning strategy to alleviate fouling in membrane distillation process to treat anaerobic digestate', 279. doi: 10.1016/j.chemosphere.2021.130524.

Chimanlal, I. *et al.* (2022) 'Membrane distillation crystallization for water and mineral recovery : The occurrence of fouling and its control during wastewater treatment', *Frontiers in Chemical Engineering*, (November), pp. 1–14. doi: 10.3389/fceng.2022.1066027.

Choi, Y. *et al.* (2020) 'Recovery of sodium sulfate from seawater brine using fractional submerged membrane distillation crystallizer', *Chemosphere*, 238, p. 124641. doi: 10.1016/j.chemosphere.2019.124641.

Choudhury, M. R. *et al.* (2019) 'Fouling and wetting in the membrane distillation driven wastewater reclamation process – A review', *Advances in Colloid and Interface Science*, 269, pp. 370–399. doi: 10.1016/j.cis.2019.04.008.

Curcio, E., Criscuoli, A. and Drioli, E. (2001) 'Membrane crystallizers', *Industrial and Engineering Chemistry Research*, 40(12), pp. 2679–2684. doi: 10.1021/ie000906d.

Das, P., Dutta, S. and Singh, K. K. (2021) 'Insights into membrane crystallization: A

sustainable tool for value added product recovery from effluent streams', *Separation and Purification Technology*, 257(August 2020), p. 117666. doi: 10.1016/j.seppur.2020.117666.

Ding, Z., Liu, Z. and Xiao, C. (2021) 'Excellent performance of novel superhydrophobic composite hollow membrane in the vacuum membrane distillation', *Separation and Purification Technology*, 268(October 2020), p. 118603. doi: 10.1016/j.seppur.2021.118603.

Dong, Z. Q. *et al.* (2014) 'Superhydrophobic PVDF-PTFE electrospun nanofibrous membranes for desalination by vacuum membrane distillation', *Desalination*, 347, pp. 175–183. doi: 10.1016/j.desal.2014.05.015.

Dotremont, C. *et al.* (2010) 'Seawater desalination with memstill technology - a sustainable solution for the industry', *Water Practice and Technology*, 5(2), p. wpt2010026. doi: 10.2166/wpt.2010.026.

Dow, N. *et al.* (2022) 'Pilot demonstration of nitrogen removal from municipal wastewater by vacuum membrane distillation', *Journal of Water Process Engineering*, 47(January), p. 102726. doi: 10.1016/j.jwpe.2022.102726.

Drioli, E., Ali, A. and Macedonio, F. (2015) 'Membrane distillation: Recent developments and perspectives', *Desalination*, 356, pp. 56–84. doi: 10.1016/j.desal.2014.10.028.

Drioli, E., Di Profio, G. and Curcio, E. (2012) 'Progress in membrane crystallization', *Current Opinion in Chemical Engineering*, 1(2), pp. 178–182. doi: 10.1016/j.coche.2012.03.005.

Edwie, F. and Chung, T.-S. (2013) 'Development of simultaneous membrane distillation–crystallization (SMDC) technology for treatment of saturated brine', *Chemical Engineering Science*, 98, pp. 160–172. doi: 10.1016/j.ces.2013.05.008.

El-Abbassi, A. *et al.* (2013) 'Integrated direct contact membrane distillation for olive mill wastewater treatment', *Desalination*, 323, pp. 31–38. doi: 10.1016/j.desal.2012.06.014.

El-Bourawi, M. S. *et al.* (2006) 'A framework for better understanding membrane distillation separation process', *Journal of Membrane Science*, 285(1–2), pp. 4–29. doi: 10.1016/j.memsci.2006.08.002.

Elhenawy, Y. *et al.* (2022) 'Performance enhancement of a hybrid multi effect evaporation / membrane distillation system driven by solar energy for desalination', *Journal of Environmental Chemical Engineering*, 10(6), p. 108855. doi: 10.1016/j.jece.2022.108855.

Eykens, L. *et al.* (2016) 'How to optimize the membrane properties for membrane distillation: A review', *Industrial and Engineering Chemistry Research*, 55(35), pp. 9333–9343. doi: 10.1021/acs.iecr.6b02226.

Eykens, L. *et al.* (2017) 'Membrane synthesis for membrane distillation: A review', *Separation and Purification Technology*, 182, pp. 36–51. doi: 10.1016/j.seppur.2017.03.035.

Farmani, R. *et al.* (2021) 'Intermittent water supply systems and their resilience to COVID-19: IWA IWS SG survey', *Aqua Water Infrastructure, Ecosystems and Society*, 70(4), pp. 507–520. doi: 10.2166/aqua.2021.009.

Fernandes, C. S. *et al.* (2021) 'Explication of hydrophobic silica as effective pore former for membrane fabrication', *Applied Surface Science Advances*, 3, p. 100051. doi: 10.1016/j.apsadv.2020.100051.

Fontananova, E. (2020) 'Encyclopedia of Membranes', *Encyclopedia of Membranes*, pp. 1–3. doi: 10.1007/978-3-642-40872-4.

Gao, C. *et al.* (2020) 'Superhydrophobic Electrospun PVDF Membranes with Silanization and Fluorosilanization Co-Functionalized CNTs for Improved Direct Contact Membrane Distillation', pp. 35–43. doi: 10.30919/es8d905.

Gloede, M. and Melin, T. (2008) 'Physical aspects of membrane scaling', *Desalination*, 224(1–3), pp. 71–75. doi: 10.1016/j.desal.2007.02.081.

Goh, S. *et al.* (2015) 'Membrane Distillation Bioreactor (MDBR) - A lower Green-House-Gas (GHG) option for industrial wastewater reclamation', *Chemosphere*. doi: 10.1016/j.chemosphere.2014.09.003.

Gryta, M. (2007) 'Influence of polypropylene membrane surface porosity on the performance of membrane distillation process', *Journal of Membrane Science*, 287(1), pp. 67–78. doi: 10.1016/j.memsci.2006.10.011.

Gryta, M. (2020) 'Separation of saline oily wastewater by membrane distillation', *Chemical Papers*, 74(7), pp. 2277–2286. doi: 10.1007/s11696-020-01071-y.

Gryta, M. (2021) 'Surface modification of polypropylene membrane by helium plasma treatment for membrane distillation', *Journal of Membrane Science*, 628(February). doi: 10.1016/j.memsci.2021.119265.

Guillen-Burrieza, E. *et al.* (2014) 'Membrane fouling and cleaning in long term plant-scale membrane distillation operations', *Journal of Membrane Science*, 468, pp. 360–372. doi: 10.1016/j.memsci.2014.05.064.

Guo, J. L. *et al.* (2014) 'Investigation of polyvinylidene fluoride membranes prepared by using surfactant OP-10 alone or with a second component, as additives, via the Non-Solvent-Induced Phase Separation (NIPS) process', *Journal of Macromolecular Science, Part B: Physics*, 53(8), pp. 1319–1334. doi: 10.1080/00222348.2014.928163.

El Haj Assad, M. *et al.* (2020) 'Applications of nanotechnology in membrane distillation: A review study', *Desalination and Water Treatment*, 192(March 2019), pp. 61–77. doi: 10.5004/dwt.2020.25821.

Hamzah, N., Leo, C. P. and Ooi, B. S. (2019) 'Superhydrophobic PVDF/TiO 2 -SiO 2 Membrane with Hierarchical Roughness in Membrane Distillation for Water Recovery from Phenolic Rich Solution Containing Surfactant', *Chinese Journal of Polymer Science (English Edition)*. doi: 10.1007/s10118-019-2235-y.

Hernández-Aguirre, O. A. *et al.* (2016) 'Surface Modification of Polypropylene Membrane Using Biopolymers with Potential Applications for Metal Ion Removal', *Journal of Chemistry*, 2016. doi: 10.1155/2016/2742013.

Hickenbottom, K. L. and Cath, T. Y. (2014) 'Sustainable operation of membrane distillation for enhancement of mineral recovery from hypersaline solutions', *Journal of Membrane Science*, 454, pp. 426–435. doi: 10.1016/j.memsci.2013.12.043.

Horseman, T. *et al.* (2021) 'Wetting, Scaling, and Fouling in Membrane Distillation: State-of-the-Art Insights on Fundamental Mechanisms and Mitigation Strategies', *ACS ES&T Engineering*, 1(1), pp. 117–140. doi: 10.1021/acsestengg.0c00025.

Husnain, T. *et al.* (2015) 'Integration of forward osmosis and membrane distillation for sustainable wastewater reuse', *Separation and Purification Technology*, 156, pp. 424–431. doi: 10.1016/j.seppur.2015.10.031.

Jung, J. T. *et al.* (2016) 'Understanding the non-solvent induced phase separation (NIPS) effect during the fabrication of microporous PVDF membranes via thermally induced phase separation (TIPS)', *Journal of Membrane Science*, 514, pp. 250–263. doi: 10.1016/j.memsci.2016.04.069.

Kang, G. dong and Cao, Y. ming (2014) 'Application and modification of poly(vinylidene fluoride) (PVDF) membranes - A review', *Journal of Membrane Science*, 463, pp. 145–165. doi: 10.1016/j.memsci.2014.03.055.

Karakulski, K. and Gryta, M. (2005) 'Water demineralisation by NF/MD integrated processes', *Desalination*, 177(1–3), pp. 109–119. doi: 10.1016/j.desal.2004.11.018.

Kargari, A. and Yousefi, A. (2021) 'Process intensification through magnetic treatment of seawater for production of drinking water by membrane distillation process: A novel approach for commercialization membrane distillation process', *Chemical Engineering and Processing - Process Intensification*, 167(April), p. 108543. doi: 10.1016/j.cep.2021.108543.

Ketrane, R. *et al.* (2009) 'Efficiency of five scale inhibitors on calcium carbonate precipitation from hard water: Effect of temperature and concentration', *Desalination*, 249(3), pp. 1397–1404. doi: 10.1016/j.desal.2009.06.013.

Khalid, A. *et al.* (2017) 'Fabrication of polysulfone nanocomposite membranes with silver-doped carbon nanotubes and their antifouling performance', *Journal of Applied Polymer Science*, 134(15), pp. 1–12. doi: 10.1002/app.44688.

Kharraz, J. A. *et al.* (2022) 'Membrane distillation bioreactor (MDBR) for wastewater treatment, water reuse, and resource recovery: A review', *Journal of Water Process Engineering*, 47(February), p. 102687. doi: 10.1016/j.jwpe.2022.102687.

Kharraz, J. A. and An, A. K. (2020) 'Patterned superhydrophobic polyvinylidene fluoride (PVDF) membranes for membrane distillation: Enhanced flux with improved fouling and wetting resistance', *Journal of Membrane Science*, 595(July 2019), p. 117596. doi: 10.1016/j.memsci.2019.117596.

Kim, J. *et al.* (2017) 'Membrane distillation (MD) integrated with crystallization (MDC) for shale gas produced water (SGPW) treatment', *Desalination*, 403, pp. 172–178. doi: 10.1016/j.desal.2016.07.045.

Kim, Junghyun, Kim, Jungwon and Hong, S. (2018) 'Recovery of water and minerals from shale gas produced water by membrane distillation crystallization', *Water Research*, 129, pp. 447–459. doi: 10.1016/j.watres.2017.11.017.

Kiss, A. A. and Kattan Readi, O. M. (2018) 'An industrial perspective on membrane distillation processes', *Journal of Chemical Technology and Biotechnology*, 93(8), pp. 2047–2055. doi: 10.1002/jctb.5674.

Kong, X. *et al.* (2020) 'Manipulating membrane surface porosity via deep insight into surfactants during nonsolvent induced phase separation', *Journal of Membrane Science*, 611(May), p. 118358. doi: 10.1016/j.memsci.2020.118358.

Laqbaqbi, M. *et al.* (2017) 'Fouling in membrane distillation, osmotic distillation and osmotic membrane distillation', *Applied Sciences (Switzerland)*, 7(4). doi: 10.3390/app7040334.

Lee, M. (2017) *X-Ray diffraction for materials research: from fundamentals to applications*. CRC Press.

Li, J. *et al.* (2016) 'Advanced treatment of biologically treated coking wastewater by membrane distillation coupled with pre-coagulation', *Desalination*, 380, pp. 43–51. doi: 10.1016/j.desal.2015.11.020.

Li, W. *et al.* (2020) 'Fe3O4/PVDF-HFP photothermal membrane with in-situ heating for sustainable, stable and efficient pilot-scale solar-driven membrane distillation', *Desalination*, 478(September 2019), p. 114288. doi: 10.1016/j.desal.2019.114288.

Liao, Y. *et al.* (2020) 'Development of robust and superhydrophobic membranes to mitigate membrane scaling and fouling in membrane distillation', *Journal of Membrane Science*, 601(December 2019), p. 117962. doi: 10.1016/j.memsci.2020.117962.

Lin, Y. P. and Singer, P. C. (2005) 'Inhibition of calcite crystal growth by polyphosphates', *Water Research*, 39(19), pp. 4835–4843. doi: 10.1016/j.watres.2005.10.003.

Liu, G. *et al.* (2021) 'Directional Crystallization from the Melt of an Organic p-Type and n-Type Semiconductor Blend', *Crystal Growth and Design*, 21(9), pp. 5231–5239. doi: 10.1021/acs.cgd.1c00570.

Liu, J. *et al.* (2022) 'Membrane fouling in direct contact membrane distillation for liquid desiccant regeneration: Effects of feed temperature and flow velocity', *Journal of Membrane Science*, 642(September 2021), p. 119936. doi: 10.1016/j.memsci.2021.119936.

Loh, C. H. *et al.* (2011) 'Fabrication of high performance polyethersulfone UF hollow fiber membranes using amphiphilic Pluronic block copolymers as pore-forming additives', *Journal of Membrane Science*, 380(1–2), pp. 114–123. doi: 10.1016/j.memsci.2011.06.041.

Lokare, O. R. *et al.* (2018) 'Importance of feed recirculation for the overall energy consumption in membrane distillation systems', *Desalination*, 428(September 2017), pp. 250–254. doi: 10.1016/j.desal.2017.11.037.

Loubser, C., Chimbanga, B. M. and Jacobs, H. (2021) 'Intermittent water supply: A South

African perspective', *Water SA*, 47(1), pp. 1–9. doi: 10.17159/wsa/2021.v47.i1.9440.

Lu, D. *et al.* (2017) 'Simultaneous Recovery and Crystallization Control of Saline Organic Wastewater by Membrane Distillation Crystallization', *AlChE Journal*, 63(6). doi: 10.1002/aic.

Lu, Y. *et al.* (2008) 'The influence of bubble characteristics on the performance of submerged hollow fiber membrane module used in microfiltration', 61, pp. 89–95. doi: 10.1016/j.seppur.2007.09.019.

Lyly, L. H. T. *et al.* (2021) 'Development of membrane distillation by dosing SiO2-PNIPAM with thermal cleaning properties via surface energy actuation', *Journal of Membrane Science*, 636(February). doi: 10.1016/j.memsci.2021.119193.

Macedonio, F. *et al.* (2014) 'Direct contact membrane distillation for treatment of oilfield produced water', *Separation and Purification Technology*, 126, pp. 69–81. doi: 10.1016/j.seppur.2014.02.004.

Makgabutlane, B. *et al.* (2020) 'Microwave Irradiation-Assisted Synthesis of Zeolites from Coal Fly Ash: An Optimization Study for a Sustainable and Efficient Production Process', *ACS Omega*, 5(39), pp. 25000–25008. doi: 10.1021/acsomega.0c00931.

Makgabutlane, B. *et al.* (2021) 'Green synthesis of carbon nanotubes to address the water-energy-food nexus: A critical review', *Journal of Environmental Chemical Engineering*, 9(1), p. 104736. doi: 10.1016/j.jece.2020.104736.

Manawi, Y. M. *et al.* (2018) 'Engineering the surface and mechanical properties of water desalination membranes using ultralong carbon nanotubes', *Membranes*, 8(4). doi: 10.3390/membranes8040106.

Martínez, L. (2004) 'Comparison of membrane distillation performance using different feeds', *Desalination*, 168(1–3), pp. 359–365. doi: 10.1016/j.desal.2004.07.022.

Mekonnen, M. M. and Hoekstra, A. Y. (2016) 'Four billion people facing severe water scarcity', (February), pp. 1–7.

Mericq, J.-P., Laborie, S. and Cabassud, C. (2010) 'Vacuum membrane distillation of seawater reverse osmosis brines', *Water Research*, 44(18), pp. 5260–5273. doi: 10.1016/j.watres.2010.06.052.

Mpala, T. J. *et al.* (2022) 'Biofouling phenomena in membrane distillation : mechanisms and mitigation strategies', *Environmental Science: Advances*. doi: 10.1039/d2va00161f.

Naidu, G., Jeong, S. and Vigneswaran, S. (2015) 'Interaction of humic substances on fouling in membrane distillation for seawater desalination', *Chemical Engineering Journal*, 262, pp. 946–957. doi: 10.1016/j.cej.2014.10.060.

Nghiem, L. D. and Cath, T. (2011) 'A scaling mitigation approach during direct contact membrane distillation', *Separation and Purification Technology*, 80(2), pp. 315–322. doi: 10.1016/j.seppur.2011.05.013.

Nitodas, S. F., Das, M. and Shah, R. (2022) 'Applications of Polymeric Membranes with Carbon Nanotubes: A Review', *Membranes*, 12(454), pp. 1–17. doi: 10.3390/membranes12050454.

Nthunya, Lebea N, Gutierrez, L., Derese, S., Edward, N., *et al.* (2019) 'A review of nanoparticle-enhanced membrane distillation membranes : membrane synthesis and applications in water treatment', *Chemical Technology and Biotechnology*, 94(9), pp. 2757–2771. doi: 10.1002/jctb.5977.

Nthunya, Lebea N, Gutierrez, L., Derese, S. and Mamba, B. B. (2019) 'Adsorption of phenolic compounds by polyacrylonitrile nano fibre membranes : A pretreatment for the removal of hydrophobic bearing compounds from water', *Journal of Environmental Chemical Engineering*, 7, p. 103254. doi: 10.1016/j.jece.2019.103254.

Nthunya, Lebea N, Gutierrez, L., Lapeire, L., *et al.* (2019) 'Fouling resistant PVDF nanofibre membranes for the desalination of brackish water in membrane distillation', *Separation and Purification Technology*, 228, p. 115793. doi: 10.1016/j.seppur.2019.115793.

Nthunya, Lebea N. *et al.* (2019) 'Removal of Fe and Mn from polluted water sources in Lesotho using modified clays', *Journal of Water Chemistry and Technology*, 41(2), pp. 81–86. doi: 10.3103/S1063455X19020036.

Nthunya, L. N. *et al.* (2020) 'f-MWCNTs / AgNPs-coated superhydrophobic PVDF nanofibre membrane for organic, colloidal, and biofouling mitigation in direct contact membrane distillation', *Journal of Environmental Chemical Engineering*, 8(2), p. 103654. doi: 10.1016/j.jece.2020.103654.

Nthunya, L. N. *et al.* (2022) 'Fouling, performance and cost analysis of membrane-based water desalination technologies: A critical review', *Journal of Environmental Management*, 301(July 2021), p. 113922. doi: 10.1016/j.jenvman.2021.113922.

Nthunya, L. N., Mbakop, S. and Mhlanga, S. D. (2021) 'Emerging nanoenhanced membrane-based hybrid processes for complex industrial wastewater treatment', in *Membrane-based hybrid processes for wastewater treatment*. Netherlands: Elsevier B.V, pp. 633–656. doi: 10.1016/B978-0-12-823804-2.00024-0 633.

Pan, J., Chen, M., *et al.* (2022) 'Enhanced anti-wetted PVDF membrane for pulping RO brine treatment by vacuum membrane distillation', *Desalination*, 526(December 2021), p. 115533. doi: 10.1016/j.desal.2021.115533.

Pan, J., Zhang, F., *et al.* (2022) 'Enhanced anti-wetting and anti-fouling properties of composite PFPE/PVDF membrane in vacuum membrane distillation', *Separation and Purification Technology*, 282(PB), p. 120084. doi: 10.1016/j.seppur.2021.120084.

Peng, Y. *et al.* (2015) 'Effects of anti-scaling and cleaning chemicals on membrane scale in direct contact membrane distillation process for RO brine concentrate', *Separation and Purification Technology*, 154, pp. 22–26. doi: 10.1016/j.seppur.2015.09.007.

Phattaranawik, J. *et al.* (2008) 'A novel membrane bioreactor based on membrane distillation',

Desalination, 223, pp. 386–395. doi: 10.1016/j.desal.2007.02.075.

Porcelli, N. and Judd, S. (2010) 'Chemical cleaning of potable water membranes: A review', *Separation and Purification Technology*, 71(2), pp. 137–143. doi: 10.1016/j.seppur.2009.12.007.

Pramanik, B. K. *et al.* (2016) 'A critical review of membrane crystallization for the purification of water and recovery of minerals', *Reviews in Environmental Science and Biotechnology*, 15(3), pp. 411–439. doi: 10.1007/s11157-016-9403-0.

Pramanik, B. K., Shu, L. and Jegatheesan, V. (2017) 'A review of the management and treatment of brine solutions', *Environmental Science: Water Research and Technology*, 3(4), pp. 625–658. doi: 10.1039/c6ew00339g.

Pramono, E. *et al.* (2017) 'Effects of PVDF concentration on the properties of PVDF membranes', *IOP Conference Series: Earth and Environmental Science*, 75(1). doi: 10.1088/1755-1315/75/1/012027.

Puspitasari, V. *et al.* (2010) 'Cleaning and ageing effect of sodium hypochlorite on polyvinylidene fluoride (PVDF) membrane', *Separation and Purification Technology*, 72(3), pp. 301–308. doi: 10.1016/j.seppur.2010.03.001.

Quist-Jensen, C. A. *et al.* (2016) 'A study of membrane distillation and crystallization for lithium recovery from high-concentrated aqueous solutions', *Journal of Membrane Science*, 505, pp. 167–173. doi: 10.1016/j.memsci.2016.01.033.

Quist-Jensen, C. A. *et al.* (2017) 'Reclamation of sodium sulfate from industrial wastewater by using membrane distillation and membrane crystallization', *Desalination*, 401, pp. 112–119. doi: 10.1016/j.desal.2016.05.007.

Quist-Jensen, C. A. *et al.* (2019) 'Perspectives on mining from sea and other alternative strategies for minerals and water recovery – The development of novel membrane operations', *Journal of the Taiwan Institute of Chemical Engineers*, 94, pp. 129–134. doi: 10.1016/j.jtice.2018.02.002.

Rahimpour, M. R. and Esmaeilbeig, M. A. (2019) 'Chapter 6 - Membrane Wetting in Membrane Distillation', in Angelo Basile, Efrem Curcio, I. (ed.) *Current Trends and Future Developments on (Bio-) Membranes*. Elsevier, pp. 143–174. doi: https://doi.org/10.1016/B978-0-12-813551-8.00006-1.

Rahmaniyan, B., Mohammadi, T. and Tofighy, M. A. (2021) 'Development of high flux PVDF/modified TNTs membrane with improved properties for desalination by vacuum membrane distillation', *Journal of Environmental Chemical Engineering*, 9(6), p. 106730. doi: 10.1016/j.jece.2021.106730.

Ramos, R. L. *et al.* (2022) 'Direct contact membrane distillation as an approach for water treatment with phenolic compounds', *Journal of Environmental Management*, 303(June 2021), p. 114117. doi: 10.1016/j.jenvman.2021.114117.

Reifenberger, R. G. (2015) *Fundamentals of Atomic Force Microscopy-Part I: Foundations*.

World Scientific.

Rudolph, P. (2010) ‘Defect Formation During Crystal Growth from the Melt’, in *Springer Handbook of Crystal Growth*. 1st edn. Berlin: Springer, pp. 159–201. doi: 10.1007/978-3-540-74761-1_6.

Ruiz Salmón, I. and Luis, P. (2018) ‘Membrane crystallization via membrane distillation’, *Chemical Engineering and Processing: Process Intensification*, 123(June 2017), pp. 258–271. doi: 10.1016/j.cep.2017.11.017.

Salehi, M. (2022) ‘Global water shortage and potable water safety; Today’s concern and tomorrow’s crisis’, *Environment International*, 158, p. 106936. doi: 10.1016/j.envint.2021.106936.

Schmidt, M. (2019) ‘Scarcity and environmental impact of mineral resources-an old and never-ending discussion’, *Resources*, 8(1), pp. 1–12. doi: 10.3390/resources8010002.

Selvarajan, V., Obuobi, S. and Ee, P. L. R. (2020) ‘Silica Nanoparticles—A Versatile Tool for the Treatment of Bacterial Infections’, *Frontiers in Chemistry*, 8(July), pp. 1–16. doi: 10.3389/fchem.2020.00602.

Sershen *et al.* (2016) ‘Water security in South Africa: Perceptions on public expectations and municipal obligations, governance and water re-use’, *Water SA*, 42(3), pp. 456–465. doi: 10.4314/wsa.v42i3.11.

Shi, W. *et al.* (2022) ‘An innovative hollow fiber vacuum membrane distillation-crystallization (VMDC) coupling process for dye house effluent separation to reclaim fresh water and salts’, *Journal of Cleaner Production*, 337(January), p. 130586. doi: 10.1016/j.jclepro.2022.130586.

Silva, T. L. S. *et al.* (2015) ‘Multi-walled carbon nanotube/PVDF blended membranes with sponge- and finger-like pores for direct contact membrane distillation’, *Desalination*, 357, pp. 233–245. doi: 10.1016/j.desal.2014.11.025.

Smith, B. . (2011) *Fundamentals of Fourier transform infrared spectroscopy*. Second edi. CRC press.

Sparenberg, M. C., Ruiz Salmón, I. and Luis, P. (2020) ‘Economic evaluation of salt recovery from wastewater via membrane distillation-crystallization’, *Separation and Purification Technology*, 235(April 2019), p. 116075. doi: 10.1016/j.seppur.2019.116075.

Srisurichan, S., Jiraratananon, R. and Fane, A. G. (2006) ‘Mass transfer mechanisms and transport resistances in direct contact membrane distillation process’, *Journal of Membrane Science*, 277(1–2), pp. 186–194. doi: 10.1016/j.memsci.2005.10.028.

Swaminathan, J. and Lienhard, J. H. (2018) ‘Design and operation of membrane distillation with feed recirculation for high recovery brine concentration’, *Desalination*, 445(August), pp. 51–62. doi: 10.1016/j.desal.2018.07.018.

Tan, H. F. *et al.* (2021) ‘Superhydrophobic PVDF/micro fibrillated cellulose membrane for membrane distillation crystallization of struvite’, *Chemical Engineering Research and Design*,

170, pp. 54–68. doi: 10.1016/j.cherd.2021.03.027.

Tijing, L. D. *et al.* (2015) 'Fouling and its control in membrane distillation-A review', *Journal of Membrane Science*, 475, pp. 215–244. doi: 10.1016/j.memsci.2014.09.042.

Tjale, L. *et al.* (2022) 'Silica nanoparticle modified polysulfone/polypropylene membrane for separation of oil-water emulsions', *Results in Engineering*, 16, p. 100623. doi: 10.1016/j.rineng.2022.100623.

Toh, M. J. *et al.* (2019) 'Antiwettability enhancement of PVDF-HFP membrane via superhydrophobic modification by SiO2 nanoparticles', *Comptes Rendus Chimie*, 22(5), pp. 369–372. doi: 10.1016/j.crci.2019.05.004.

UNICEF (2019) *Progress on drinking water, sanitation and hygiene: 2000 - 2017*. Available at: https://data.unicef.org/resources/progress-drinking-water-sanitation-hygiene-2019/ (Accessed: 4 July 2022).

Venzke, C. D. *et al.* (2021) 'Membrane distillation treating a real petrochemical reverse osmosis concentrate: Influence of membrane characteristics on the process performance', *Journal of Water Process Engineering*, 39(June 2020). doi: 10.1016/j.jwpe.2020.101722.

Vernon-Parry, K. D. (2000) 'Scanning electron microscopy: an introduction', *III-Vs Review*, 13(4), pp. 40–44. doi: https://doi.org/10.1016/S0961-1290(00)80006-X.

Vernon-Parry, K. D. and Wright, A. C. (2001) 'TEM: An introduction — part 2', *III-Vs Review*, 14(1), pp. 48–51. doi: https://doi.org/10.1016/S0961-1290(01)89008-6.

Vineis, P., Chan, Q. and Khan, A. (2011) 'Climate change impacts on water salinity and health', *Journal of Epidemiology and Global Health*, 1(1), pp. 5–10. doi: 10.1016/j.jegh.2011.09.001.

Wae AbdulKadir, W. A. F., Ahmad, A. L. and Ooi, B. S. (2022) 'Hydrophobic PVDF-HNT membrane for oxytetracycline removal via DCMD: The influence of fabrication parameters on permeability, selectivity and antifouling properties', *Journal of Water Process Engineering*, 49(June), p. 102960. doi: 10.1016/j.jwpe.2022.102960.

Wagstaff, F. E., Brown, S. D. and Cutler, I. . (1964) 'The influence of H2O and O2 atmospheres on the crystallisation of vitreous silica.', *Physics and Chemistry of Glasses*, 5(3), pp. 76–81.

Wang, Z. and Lin, S. (2017) 'Membrane fouling and wetting in membrane distillation and their mitigation by novel membranes with special wettability', *Water Research*, 112, pp. 38–47. doi: 10.1016/j.watres.2017.01.022.

Xiao, Z. *et al.* (2020) 'Unprecedented scaling/fouling resistance of omniphobic polyvinylidene fluoride membrane with silica nanoparticle coated micropillars in direct contact membrane distillation', *Journal of Membrane Science*, 599(January), p. 117819. doi: 10.1016/j.memsci.2020.117819.

Yadav, A., Labhasetwar, P. K. and Shahi, V. K. (2022) 'Science of the Total Environment Membrane distillation crystallization technology for zero liquid discharge and resource

recovery : Opportunities , challenges and futuristic perspectives', *Science of the Total Environment*, 806, p. 150692. doi: 10.1016/j.scitotenv.2021.150692.

Yao, M. *et al.* (2020) 'A review of membrane wettability for the treatment of saline water deploying membrane distillation', *Desalination*, 479(January), p. 114312. doi: 10.1016/j.desal.2020.114312.

Yin, Y. *et al.* (2021) 'The use of anti-scalants in gypsum scaling mitigation: Comparison with membrane surface modification and efficiency in combined reverse osmosis and membrane distillation', *Journal of Membrane Science*, 643(August 2021), p. 120077. doi: 10.1016/j.memsci.2021.120077.

Yue, D. *et al.* (2021) 'A novel silver / activated - polyvinylidene fluoride - polydimethyl siloxane hydrophilic-hydrophobic Janus membrane for vacuum membrane distillation and its anti-oil-fouling ability', *Journal of Membrane Science*, 638(April), p. 119718. doi: 10.1016/j.memsci.2021.119718.

Zakaria, M. *et al.* (2022) 'Water Desalination Using Solar Thermal Collectors Enhanced by Nanofluids', *Chemical Engineering and Technology*, 45(1), pp. 15–25. doi: 10.1002/ceat.202100339.

Zhang, J. *et al.* (2021) 'Scaling control of forward osmosis-membrane distillation (FO-MD) integrated process for pre-treated landfill leachate treatment', *Desalination*, 520(June), p. 115342. doi: 10.1016/j.desal.2021.115342.

Zhang, P. *et al.* (2021) 'Modification of PVDF hollow fiber membrane by co-deposition of PDA/MPC-co-AEMA for membrane distillation application with anti-fouling and anti-scaling properties', *Journal of Membrane Science*, 636(July), p. 119596. doi: 10.1016/j.memsci.2021.119596.

Zhao, Z. P. *et al.* (2013) 'Water regeneration from human urine by vacuum membrane distillation and analysis of membrane fouling characteristics', *Separation and Purification Technology*, 118, pp. 369–376. doi: 10.1016/j.seppur.2013.07.021.

Zhu, Z. *et al.* (2021) 'Omniphobic membrane with process optimization for advancing flux and durability toward concentrating reverse-osmosis concentrated seawater with membrane distillation', *Journal of Membrane Science*, 639(July), p. 119763. doi: 10.1016/j.memsci.2021.119763.

Zou, D. *et al.* (2022) 'Fabrication and modification of PVDF/PSF hollow-fiber membranes for ginseng extract and saline water separations via direct contact membrane distillation', *Journal of Membrane Science*, 644(October 2021), p. 120101. doi: 10.1016/j.memsci.2021.120101.

CHAPTER THREE – RESEARCH OBJECTIVES

This chapter unpacks the key aim of this project as previously discussed in Chapter One, and further elaborates on the specific objectives undertaken to realise the aim of the project.

3.1 Research significance and study objective

Membrane distillation crystallization (MDC) is a technology offering a myriad of advantages such as the 1) ability to function with renewable or waste energy sources, 2) the ability to treat concentrated wastewater without reducing the process performance, and 3) it affords green process tailoring of membranes. For these reasons, MDC is a promising cost-effective and sustainable technology towards treatment of industrially discharged brines. Remarkably, This technology affords the simultaneous recovery of freshwater and mineral salts from wastewater, thus ensuring sustainable solutions and circular economy. MDC is a new emerging technology with few current reports of the pilot studies. Therefore, process improvements is a key requirement for its industrial testing, particularly in South Africa, where treatment of wastewater remains a problem. The aim of this study was to synthesise various hydrophobic polymeric membranes and modify them using hydrophobic nanoparticles such as functionalised carbon nanotubes (fCNTs) and functionalised silica nanoparticles (fSiO_2NPs). Thereafter, the prepared membranes' performance was assessed through membrane distillation crystallisation (MDC) studies for the recovery of freshwater and mineral salts from wastewater.

3.2 Specific research objectives

3.2.1 Chemical characterisation of selected high saline wastewater samples obtained from wastewater sources using analytical techniques such as ion chromatography (IC) and inductively coupled plasma optical emission spectroscopy (ICP-OES).

3.2.2 Preparation and characterisation of nanoparticles and subsequently, modified PVDF membranes for use in MDC recovery of water and mineral salts. Synthesised and functionalised nanoparticles such as fSiO_2NPS and fCNTs were embedded into a PVDF polymeric matrix to improve its hydrophobicity, mechanical and tensile strength properties.

3.2.3 Evaluate the performance of the membranes using direct contact membrane distillation (DCMD) and thereafter evaluate the performance of the best-performing membranes using MDC.

3.2.4 Investigate the occurrence of membrane fouling and characterise the crystal product obtained from MDC experiments.

3.3 Hypothesis

Membrane distillation crystallisation (MDC) in conjunction with hydrophobic polymeric membranes can be used to effectively recover salt minerals and freshwater from industrially discharged wastewater. Additionally, MDC performance and process longevity can be improved with hydrophobic membranes to control membrane wetting and process efficiency. Lastly, the success rate of the MDC technique may allude to its suitability towards treatment of various water sources and thus provide an avenue for sustainable wastewater treatment.

CHAPTER FOUR – METHOLOGY

This chapter provides an overview of the experimental procedures carried out in this research project. All performed experimental procedures were carried out with the aim of attaining the set goals and objectives as outlined previously. A brief outline of the experimental methods undertaken in this study is presented below:

- **i.** Environmental sampling of high saline wastewater samples required for the application studies. Multiple samples were collected from various sampling locations.
- **ii.** Saline wastewater (leachate) samples were then pre-treated to remove organic contaminants and other contaminants such as oil and grease. All wastewater samples were subsequently characterised using ion chromatography (IC) and inductively coupled plasma – optical emission spectrometry (ICP-OES).
- **iii.** Silica nanoparticles were synthesised and functionalised using a fluorinated silane reagent to improve its characteristic hydrophobicity. Multiwalled carbon nanotubes (MWCNTS) were functionalised using a fluorinated silane reagent to increase their hydrophobicity.
- **iv.** Hydrophobic membranes were synthesised using polyvinylidene fluoride (PVDF) as the base polymer. Multiple membranes were prepared to conduct a comparative study to determine the optimal membrane needed for satisfactory MCr process performance. Modified NPs were incorporated into the membrane matrix to achieve hydrophobic and mechanically strong membranes.
- **v.** Prepared NPs and membranes were characterised using transmission electron microscopy (TEM), fourier transform infrared (FTIR) spectroscopy, gravimetric porosity, liquid entry pressure (LEP), pore size, scanning electron microscopy (SEM), water contact angle (WCA), tensile strength, atomic force microscopy (AFM). Fouled membranes were evaluated by means of scanning electron microscopy coupled with energy-dispersive x-ray spectroscopy (SEM/EDX).
- **vi.** The prepared membranes along with their commercial counterparts were evaluated in direct contact membrane distillation (DCMD) and membrane crystallization (MCr) studies. Furthermore, temperature profiles (deltaT profiles) and permeate conductivity profiles were established.
- **vii.** Obtained crystalline product from MCr studies were characterised by means of optical microscopy, single crystal x-ray diffraction (SXRD), and powder x-ray diffraction (PXRD).

The following serves as a designation of which methods related to specific chapters included in this dissertation which serve to address the aim of this project.

Chapter Five: Briefly, this chapter focussed on membrane preparation and its subsequent characterization, Thereafter, the membrane performance was evaluated through a series of DCMD experiments conducted at three different feed temperatures (40 – 60 ℃). Additionally, to investigate the driving force, temperature profiles were produced (deltaT profiles), and to monitor the permeate quality output the permeate conductivity was evaluated. In the DCMD studies, various process parameters were investigated such as the flow rate, optimal feed and permeate temperatures, and module configuration. Detailed explanations of the respective methods are provided in Chapter Five.

Chapter Six: Following the results produced in Chapter Five, the best-performing membranes were selected for MDC application. These included two fabricated membranes and one commercial membrane used as a benchmark. However, further modifications were carried out on one of the synthesized membranes to improve its overall performance (M5). Thus, its synthesis and characterization were documented. Moreover, MDC application studies were carried out using the three membranes of interest. In conjunction, water sampling analysis was included which formed the basis for the MDC feed solution. Following these experiments, the characterization of the solid product was conducted, and membrane surface deposition was investigated.

4.1 Instrumentation

4.1.1 Inductively coupled plasma optical emission spectroscopy (ICP-OES)

The concentration of alkali metals was measured using the ICP-OES, Spectro Genesis Spectro Analytical Instrument GmbH (Kleve, Germany). This information detailed the assortment of cationic analytes and their respective concentrations in the various wastewater samples. Principally, this technique calculates analyte concentration by measuring the amount of light emitted at various wavelengths as the analyte atoms become excited to higher energy levels (Ametek, 2023). The analysis was undertaken using the parameters described below.

System parameter	Instrumental setting
Replicates	3
Cooling water	7.10 Imp/s
Main argon pressure	6.5 bar

Nebulizer pressure	2.5 bar
Optic temperature	29.76 ℃

4.1.2 Ion chromatography (IC)

Anion concentrations were evaluated using IC, Eco IC, Metrohm (Herisau, Switzerland). This technique characterised the various anionic analytes and their respective concentrations in the wastewater samples. The IC analysis was best suited to characterise anionic analytes as it separated the analytes based upon their retention times in the packed column. Thereafter, the analytes were eluted in terms of analyte size and charge, where lighter and singly-charged analytes were eluted in preference to heavier analytes. The analysis was undertaken using the following parameters as shown below:

System parameter	**Instrumental setting**
Eluent composition	5 mM Na_2CO_3 and 16 mM $NaHCO_3$
Pressure	13.75 MPa
Flow rate	1.000 mL/min
Recording time	12.0 min
Column type	Metrosep A Supp 17 – 150/4.0

4.1.3 Fourier transform infrared spectroscopy (FTIR)

Fourier transform infrared spectroscopy (FTIR) was used to characterise the NPs and membranes synthesized in this study to gain insight into the functional groups present in the materials. In this technique, infrared radiation is passed through a sample, after which some radiation will be absorbed by the sample, and some will be transmitted. Moreover, FTIR spectroscopy detects the change in dipole moments in a sample which correspond to a particular vibrational energy (Smith, 2011).

4.1.4 Scanning electron microscopy and energy dispersive x-ray spectroscopy (SEM/EDX)

Scanning electron microscopy (SEM) was used to study the morphology and pore formations on the surface and cross-sections of the membranes. Briefly, an electron beam is released from an electron gun which is then condensed through the interaction with a series of condenser lenses. The electron beam is then allowed to interact with the sample surface in a raster pattern.

The interaction between the electron beam and the sample may produce back-scattered, Auger, and secondary electrons, x-rays and light which are picked up by the detector (Vernon-Parry, 2000). When analysing the fouled membranes in this study, the membranes underwent SEM/EDX analysis to view the fouled caking layer atop the active membrane surface. Elemental analysis (EDX) assisted in identifying the composition of the foulants present on the membrane.

4.1.5 Transmission electron microscopy (TEM)

Transmission electron microscopy (TEM) was used to evaluate the morphology and particle size of pristine silica nanoparticles (SiO_2NPs), functionalised silica nanoparticles (fSiO_2NPs), carbon nanotubes (CNTs), and carbon nanotubes (fCNTs). All micrographs were recorded using FEI Tecnai T12 TEM at 120 kV (Oregon, USA). Similar to the SEM, this technique employs an electron gun which produces an electron beam which is then made to pass through a series of condenser lenses. The electron beam is then allowed to penetrate a thin sample (Vernon-Parry and Wright, 2001).

4.1.6 Atomic force microscopy (AFM)

Atomic force microscopy (AFM) was employed in this study to provide insight into the surface roughness of the polymeric membrane materials. The roughness of the membranes alludes to the hydrophobicity of the material; therefore, it describes its wetting resistance. This information is relevant when applying membranes in processes such as membrane distillation crystallisation (MDC). In principle, this technique uses a probe which is in contact with the sample. The probe scans the sample in vertical and lateral motions and its movement is recorded by means of a laser beam reflected off the probe (Reifenberger, 2015).

4.1.7 Tensile strength

Mechanical properties of each of the membranes were evaluated by means of tensile strength. This information provides insight into the durability of the membrane under an applied pressure during MDC application studies. Tensile strength is reported as the ultimate strength and by the Young's modulus. The ultimate strength is defined as the maximum stress that the membrane can endure prior to breaking (Fontananova, 2020). The Young's modulus of a material is found using slope of the curve in the elastic region on a stress-strain curve. This value provides a measure of a elasticity of the membrane, which is where the membrane can return to its original form without undergoing permanent deformation under an applied stress

(Fontananova, 2020). The rigidity of the membrane increases with an increasing Young's modulus.

4.1.8 Water contact angle (WCA)

In the MDC technology, a hydrophobic membrane was required to facilitate the transport of water vapor in preference to liquid water from the feed solution. For this purpose, water contact angle (WCA) was directly related to the hydrophobicity of the membrane as it measured the ability of the membrane to repel water droplets. A water droplet was deposited onto the surface of the membrane and the contact angle between the droplet and the membrane was measured. A material is classified as superhydrophobic if the contact angle is > 150 °, hydrophobic if the contact angle is > 90 °, and hydrophilic if the contact angle is < 90 °

4.1.9 Powder x-ray diffraction (PXRD) and single crystal x-ray diffraction (SXRD)

Following MDC experiments, crystalline samples were generated that were present in both crystalline and powder crystalline forms. In the instance of a crystalline sample, SXRD was employed, and for the latter, PXRD was used. This technique of characterisation was utilised for structural characterisation of the crystalline products produced. Hard x-rays with shorter wavelengths are used when characterising materials, thus making it suitable to investigate the internal structure of crystalline samples (Lee, 2017). Principally, a diffraction pattern is characteristic of the direction and intensity of the diffracted beams, and therefore is unique to a given material (Lee, 2017).

4.1.11 Optical microscopy

Optical microscopy was utilised in this study to monitor the onset and progression of crystal growth during MDC studies. This followed the establishment of supersaturation whereby samples were taken at 30 min intervals from the feed solution and observed under a microscope.

References

Ametek, S. (2023) *SPECTRO - The performance benchmark for ICP-OES/ICP-AES spectrometers*. Available at: https://www.spectro.com/products/icp-oes-aes-spectrometers?sf_campaign_id=7013V000000AcgW&google_ad=icp+resource-library(subs) (Accessed: 9 January 2023).

Fontananova, E. (2020) 'Encyclopedia of Membranes', *Encyclopedia of Membranes*, pp. 1–3. doi: 10.1007/978-3-642-40872-4.

Lee, M. (2017) *X-Ray diffraction for materials research: from fundamentals to applications*.

CRC Press.

Reifenberger, R. G. (2015) *Fundamentals of Atomic Force Microscopy-Part I: Foundations*. World Scientific.

Smith, B. . (2011) *Fundamentals of Fourier transform infrared spectroscopy*. Second edi. CRC press.

Vernon-Parry, K. D. (2000) 'Scanning electron microscopy: an introduction', *III-Vs Review*, 13(4), pp. 40–44. doi: https://doi.org/10.1016/S0961-1290(00)80006-X.

Vernon-Parry, K. D. and Wright, A. C. (2001) 'TEM: An introduction — part 2', *III-Vs Review*, 14(1), pp. 48–51. doi: https://doi.org/10.1016/S0961-1290(01)89008-6.

CHAPTER FIVE

5 Nanoparticle-Enhanced PVDF Flat-Sheet Membranes for Seawater Desalination in Direct Contact Membrane Distillation

This chapter encompasses work published in the Membranes journal, titled "Nanoparticle-Enhanced PVDF Flat-Sheet Membranes for Seawater Desalination in Direct Contact Membrane Distillation". This work was authored by Indira Chimanlal. Lebea N. Nthunya, Oranso T. Mahlangu, Bastian Kirkebæk, Aamer Ali, Cejna Anne Quist-Jensen, and Heidi Richards.

5.1 Introduction

According to published literature, 2.2 billion people lack access to safe drinking water (Vineis, Chan and Khan, 2011; UNICEF, 2019; Salehi, 2022). Moreover, a steady decline in the abundance of freshwater resources and deteriorating infrastructure exacerbate existing water demands, thus creating a worsening crisis (Salehi, 2022). Furthermore, developing countries particularly in the African continent experience intermittent water supply (Sershen *et al.*, 2016; Lebea N. Nthunya *et al.*, 2019; Loubser, Chimbanga and Jacobs, 2021). More often, consumers use potable water under restricted conditions where water rationing is implemented. Predominantly, access to safe drinking is affected by poor financial reserves and inadequate infrastructure (Farmani *et al.*, 2021; Loubser, Chimbanga and Jacobs, 2021). Rapid population growth, industrialization, and climate change threaten freshwater resources resulting in substantial water shortages.

In addition to water scarcity, mineral resources are depleting at an alarming rate (Makgabutlane *et al.*, 2020; Calvo and Valero, 2022). Among other factors the increasing use of renewable energy sources further intensifies this demand. This is exacerbated by a rising demand in mineral resources due to growing economic and industrial sectors (Schmidt, 2019). For example, production of solar panels require elements such as cadmium, silver, or indium (Zakaria *et al.*, 2022) while electric vehicle batteries require lithium, nickel, and cobalt (Calvo and Valero, 2022). These pressing issues motivate the need for improved and sustainable technology solutions to the current problems experienced. Among others, membrane distillation (MD) emerged as a promising technology to address these issues, albeit relatively novel (Mericq, Laborie and Cabassud, 2010; Kiss and Kattan Readi, 2018). Briefly, this technology utilizes a temperature difference between the two interfaces of the membrane, thus

generating a vapour pressure gradient to drive this process (Ashoor *et al.*, 2016; Nthunya *et al.*, 2022). Furthermore, a hydrophobic membrane is employed to exclusively retain mineralized feed water while extracting fresh water in the form of vapour (Eykens *et al.*, 2016, 2017). Additionally, this process is well suited for the treatment of industrial wastewater (Quist-Jensen *et al.*, 2017; Lebea N Nthunya, Gutierrez, Derese, Edward, *et al.*, 2019). Importantly, this technology relies on its capability to treat harmful industrial wastewaters and waste recycling through recovery of valuable constituents from feed streams (Phattaranawik *et al.*, 2008; Goh *et al.*, 2015; Ali *et al.*, 2019). Furthermore, MD is characterized by high permeate quality, simple operation configuration and process conditions, such as temperature and pressure. Interestingly, MD treats a variety of solutions independent of their concentration, thus producing fresh water from a myriad of feed streams (Zhao *et al.*, 2013; Macedonio *et al.*, 2014; Lu *et al.*, 2017; Quist-Jensen *et al.*, 2017). The MD can also be suited for resource recovery when coupled with crystallization, thus giving rise to membrane distillation crystallization (MDC). In this process, the feed solution is concentrated towards supersaturation thus retrieving minerals from a waste solution. The MDC can recover both minerals and water from shale gas where low energy consumption of 28.2 kWh m^{-3} is used (Kim, Kim and Hong, 2018). Previous studies have reported the recovery of minerals such as NaCl, $CaCO_3$, $BaCO_3$, and Na_2SO_4 (Kim *et al.*, 2017; Quist-Jensen *et al.*, 2017; Kim, Kim and Hong, 2018). Additionally, MD has demonstrated its compatibility in hybrid systems. Coupling of MD to various other techniques has been reported to improve process outcomes and performances. Scaling control was achieved through the integration of forward osmosis (FO) and MD. Another study reported a hybrid system composed of multi-effect evaporation and MD for solar energy desalination. The hybrid system presented improved process performance compared to a standalone evaporation system. Furthermore, a water production capacity was 159.84 m^3 yr^{-1} (Elhenawy *et al.*, 2022). However, these systems are costly. The MD advancement towards resource recovery (simultaneous recovery of fresh water and minerals) is imperative. However, existing MD membranes are prone to fouling and wetting leading to performance deterioration (El Haj Assad *et al.*, 2020). Accordingly, membrane cleaning protocols are employed however, performance restoration is not guaranteed (Chimanlal *et al.*, 2022). Membrane modification arose to address concerns surrounding fouling and wetting thereby exploring various additives. Moreover, modified membranes are characterized by improved structural integrity and selectivity, among other physical properties (El Haj Assad *et al.*, 2020). Membrane modification is also an avenue taken to achieve highly porous membranes. This is imperative because the mechanism for water vapour mass transport is

primarily through the membrane pores and is controlled by Knudsen molecular diffusion (Alanezi *et al.*, 2021).

In the current study, nanoparticle-enhanced PVDF membranes were fabricated and evaluated for the treatment of synthetic seawater. Previously, various additives were incorporated into hydrophobic polymeric membranes to enhance their resistance to fouling and wetting, thus improving the permeate flux and salt rejections (Toh *et al.*, 2019; Afsari, Shon and Tijing, 2021; P. Zhang *et al.*, 2021). Such modifications include the incorporation of silica nanoparticles into a PVDF polymeric matrix to impart resistance towards scaling (Xiao *et al.*, 2020), surface fluorination to improve fouling resistance (Kharraz and An, 2020), and silver coating to improve flux (Yue *et al.*, 2021). Different from previously reported literature, the current study explored fluorination of the CNTs using a fluorinated silane reagent, with a subsequent embedment into PVDF membranes. Moreover, this study explores the synergistic effect of modified CNTs and functionalized silica nanoparticles (SiO_2NPs). Metal oxide additives such as silica nanoparticles were used due to their advantages such as ease of functionalization and their ability to enhance physical properties of membranes. Silica nanoparticles improve the hydrophobicity of the membranes therefore increasing its wetting resistance (El Haj Assad *et al.*, 2020; Selvarajan, Obuobi and Ee, 2020). Similarly, the addition of CNTs offer durability and improved structural integrity (Silva *et al.*, 2015; Nitodas, Das and Shah, 2022). The modified membranes were evaluated towards desalination of 3.5 wt% synthetic seawater in direct contact membrane distillation (DCMD).

5.2 Materials and Methods

5.2.1 Chemicals and equipment

Tetraethyl orthosilicate (TEOS, reagent grade, 98.0%), ammonium hydroxide (NH_4OH, ACS reagent, 28.0-30.0% NH_3), absolute ethanol (ETOH, ACS reagent, 99.5%), toluene (anhydrous, 99.8%), sodium chloride (NaCl, ACS reagent, 99.0%), 1H,1H,2H,2H-perfluorooctyl triethoxysilane (POTS, MW = 610.38 $g \cdot mol^{-1}$, 97.0%), isopropanol (ACS reagent, 99.5%), nitric acid (HNO_3, puriss p.a., 65.0%), polyvinylidene fluoride (PVDF, MW = 534,000 $g \cdot mol^{-1}$), and polyvinylpyrrolidone (PVP, MW = 360,000 $g \cdot mol^{-1}$, dimethylformamide (DMF, ACS reagent, 99.8%) N,N-dimetheylacetamide (DMAc, puriss p.a., 99.5%), were acquired from Sigma-Aldrich (Germany). Multiwalled carbon nanotubes (MWCNTs, outer diameter = 10 nm, 98.0%) was obtained from SabiNano (Pty) Ltd (Johannesburg, South Africa). Two commercially PTFE membranes (pore sizes of 0.45 µm

and 0.20 µm) supported on non-woven polyester (LH0P) were procured from Pall Corporation (New York, USA). The membranes were termed as PTFE-20 (0.20 µm) and PTFE-45 (0.45 µm). Ultrapure water was obtained from our laboratory using Milli-Q-RO4 (Millipore, Bedford, MA, USA). Permeate conductivity was recorded using the Mettler Toledo conductivity probe (Columbus, Ohio, USA).

5.2.2 Synthesis and functionalisation of silica nanoparticles (SiO_2NPs)

The SiO_2NPS were synthesised using a modified StÖber method (Xiao *et al.*, 2020). Briefly, TEOS (10 ml) and ethanol (40 ml) were added to a mixture of de-ionized water (22.5 ml), NH_4OH (10 ml), and ethanol (16.5 ml). This was followed by vigorous stirring until a milky-white turbid mixture was produced. The resultant mixture was stirred for 5 hrs at a slower speed followed by centrifugation in Hettich Zentrifugen Rotofix 32A (Tuttlingen, Germany) and washed with ethanol. Subsequently, it was dried at 50 ℃ for 24 hrs. The resultant SiO_2NPS were dispersed in ethanol and bath sonicated (Eins Sci Profession ultrasonic cleaner, Johannesburg, South Africa) for 30 min to reduce particle aggregation. Furthermore, the nanoparticles (NPs) were filtered and dried. Prepared SiO_2NPS were functionalized using 1H,1H,2H,2H-perfluorooctyl triethoxysilane (POTS). Briefly, SiO_2NPS were dispersed in an appropriate volume of toluene followed by the slow addition of 40 wt% POTS using a syringe. The resultant material was stirred at room temperature for 5 hrs. The functionalized nanoparticles were washed with ethanol to ensure the removal of any excess reagent followed by drying for 24 hrs. Functionalized SiO_2NPS were termed as fSiO_2NPS.

5.2.3 Functionalisation of CNTs

Commercially acquired CNTs were functionalized to enhance their hydrophobic characteristics before dispersion into PVDF membranes. The functionalization was adopted from a modified method reported by Gao et al. (2020). The method was conducted in a two-step process, namely an acid treatment followed by fluorination using a fluorosilane reagent. While acidic modification of CNTs rendered the material hydrophilic due to the introduction of carboxyl functional groups, they provide a binding site for hydrophobic agents such as POTS. The flurosilanization step contributes to the overall hydrophobicity due to the presence of long chain and bulky alkyl groups (-CH_3-). Moreover, flurosilanization improved the dispersion of the material in addition to improving its hydrophobicity (Gao *et al*. 2020). Unmodified CNTs were added to a 65% HNO_3 and sonicated for 1 hr followed by constant stirring for 24 hrs at ≈ 80 ℃. The resultant mixture was cooled, centrifuged, and washed with deionized water. The

CNTs were dried and kept for further modification. Dried CNTs were added to 82 ml of toluene followed by sonication for 70 min to promote particle dispersion. Thereafter, a 0.5 wt% POTS solution containing toluene was added to the mixture containing a CNT-toluene and stirred for 24 hrs. The functionalized CNTs were centrifuged, washed using toluene and dried in an oven at 60 ℃ for 24 hrs. The functionalized CNTs were termed as fCNTs.

5.2.4 Membrane preparation

An appropriate amount of PVDF was dissolved in a mixed solvent system of DMAc and DMF at the ratio of 2:3. According to previously reported literature, DMac/DMF solvent combinations were explored due to their high affinity toward PVDF as evidenced by their solubility parameters (Shaliutina-Kolešová, 2018). Furthermore, the specific ratio was employed in this study due to the optimal solubility of the polymer in the solvent mixture as demonstrated by solvent ternary diagrams (Yeow, Liu and Li, 2003; Shaliutina-Kolešová, 2018).The solution was stirred for 24 hrs in the absence of heat followed by degassing. The resultant polymer solution was cast on a glass plate to an approximate height of 50 µm using Elcometer 4340 casting knife film applicator (England, United Kingdom). The cast solution was placed in a coagulation bath containing water (a non-solvent). To ensure complete phase separation, the membrane solution was kept in a coagulation bath for 2 days. A similar procedure was followed during the synthesis of M2, M3 and M4. The composition of each membrane is provided in **Table 5.1**. To prepare M3 and M4, the fCNTs and fSiO_2NPs were sonicated in the solvent to ensure particle dispersion before addition to polymer solution. The concentration of fSiO_2NPs was chosen based on findings from previously reported literature. Researchers demonstrated superior hydrophobicity attributed to silica nanoparticles at a loading of 3.5wt% as compared to lower concentrations (Toh *et al.*, 2019). Similarly, the concentration of the fCNTs used in this study was also chosen based on previously reported literature. According to Khalid et al. (2017), CNT loadings > 0.4 wt% cause agglomeration, thus resulting in poor dispersion. This was justified by the strong van der Waal's interactions between the lattice of the CNT (Khalid *et al.*, 2017).

Table 5.1: Composition of the as-synthesised membranes.

Membrane	**DMF**	**DMAc**	**PVDF (wt%)**	**PVP (wt%)**	**fCNTs (wt%)**	**fSiO_2NPS (wt%)**
M1	51.0	34.0	15.0	0.0	0.0	0.0
M2	50.9	34.0	15.0	0.1	0.0	0.0

M3	50.8	33.9	15.0	0.1	0.2	0.0
M4	48.7	32.5	15.0	0.1	0.2	3.5

5.2.5 Characterisation of the NPs and membranes

FTIR was used to understand the physicochemical characteristics of the synthesised NPs and membranes. Fourier transform infrared spectroscopy (FTIR) analysis was conducted using a Bruker Tensor 27 FTIR (Billercia, Massachusetts, USA). Spectra were obtained at a wavelength range of 3900 – 650 cm^{-1} (**Figure A1 and A2**). Transmission electron microscopy (TEM) was used to evaluate the morphological and particle size of pristine SiO_2NPs, and CNTs. All micrographs were recorded using FEI Tecnai T12 TEM at 120 kV (Oregon, USA). Surface and cross-sectional morphologies of each membrane were obtained from the Zeiss EVO 60 scanning electron microscope GmbH (Oberkochen, Germany). Samples were coated with Au prior to analysis. Membrane roughness and topography were evaluated using atomic force microscopy (AFM). The AFM analysis was conducted using the WITec Alpha 300A TS-150 (WITec Wissenschaftliche Instrumente und Technologie GmbH, Ulm, Germany). Mechanical properties of the membranes were acquired from stress-strain plots obtained from the AG-Plus Universal tester (Shimadzu Europa GmbH, Duisburg, Germany). The size of the membrane specimen was 25 x 25 mm^2 and the pulling speed was 0.5 mm min^{-1}. Membrane water contact angle (WCA) was analyzed through the sessile method using a drop shape analyzer (Biolin Scientific Attention Theta Line (Stockholm, Sweden) to understand their hydrophobicity. The measurements were conducted at room temperature using deionized water. A dead-end filtration cell was used to measure the liquid entry pressure (LEP) of the membranes. A circular piece of the dry membrane (diameter = 5 cm) was placed in a dead-end filtration cell. Afterwards, the cell was filled with ultrapure water. To determine the minimum pressure required to eject the water, pressure was gradually increased until the first water drop was produced. Membrane pore sizes were determined in POROLUX^{TM} 1000 using porefil as the wetting agent, and a membrane area of approximately 300 mm^2. Membrane porosity was determined using a modified gravimetric method (Silva *et al.*, 2015). A dry membrane (m_d) (1 cm^2) was immersed in an appropriate volume of isopropanol for 24 hrs to ensure complete solvent absorption into the membrane pores. Following this, the mass of the wetted membrane was measured (m_w). Each measurement was performed in triplicate. **Equation 1** was used to determine the porosity of the as-synthesised membranes.

$$\varepsilon = \frac{(m_w - m_d)/\rho_{solvent}}{\left(\frac{m_w - m_d}{\rho_{solvent}}\right) + \left(\frac{m_d}{\rho_{polymer}}\right)} \text{ x } 100 \quad \textbf{(1)}$$

Where m_w and m_d are the masses of wet and dry membranes respectively, $\rho_{solvent}$ and $\rho_{polymer}$ are the densities of isopropanol (0.786 g cm^{-3}), PVDF polymer (1.78 g cm^{-3}) and PTFE polymer (2.20 g cm^{-3}) respectively.

5.2.6 Membrane distillation

A laboratory-scale MD system was employed for all DCMD tests performed. All membranes were assessed in the DCMD set-up using deionized water (dH_2O) (**Figure A3)** and 3.5 wt% NaCl as feed solutions. These solutions were circulated at a feed temperature range of 40, 50, and 60 ℃. For the distillate, deionized water was circulated at a temperature of approximately 10.0 ℃. Across the flat sheet membrane module (3.3 x 8.0 mm), four temperature sensors were installed at the entrance and exit channels of both the feed and permeate. The feed and permeate were circulated in a co-current mode at the crossflow velocity of 601.0 ml·min^{-1}. Although counter-current solution configurations are typically employed, the small membrane area used in this study meant that a co-current configuration would have negligible effects on the system performance. The weight increment and conductivity of the permeate were measured continuously. To ensure continuous dissolution of the NaCl feed solution, the solution was stirred continuously. After each experiment, the membrane was rinsed with deionized water to wash away any precipitated salts from the surface. Permeate flux (J) was calculated using **Equation (2),** where Δm is the difference in the permeate mass (kg), Δt is the time difference (hr) and A is the membrane area (m^2).

$$J = \frac{\Delta m}{\Delta t * A} \quad \textbf{(2)}$$

Temperature gradient in DCMD was estimated using the log mean temperature obtained from **Equation (3)** where ΔT_1 and ΔT_2 are defined by **Equations (4)** and **(5),** respectively.

$$\Delta T_{ln} = \frac{\Delta T_1 - \Delta T_2}{\ln\left(\frac{\Delta T_1}{\Delta T_2}\right)} \quad \textbf{(3)}$$

$$\Delta T_1 = T_{retentate,in} - T_{permeate,in} \quad \textbf{(4)}$$

$$\Delta T_2 = T_{retentate,out} - T_{permeate,out} \quad \textbf{(5)}$$

5.3 Results and discussion

5.3.1 TEM analysis of the SiO_2NPs and CNTs

The TEM micrographs (**Figure 5.1**) were used to evaluate morphology, particle size and distribution of the SiO_2NPs (**A1-A2**), fSiO_2NPs (**B1-B2**), CNTs (**C1-C2**), and fCNTs **(D1-D2**). The SiO_2NPs and fSiO_2NPs were homogenous and spherical with minimal structural defects (**Figures 1 A1** and **B1**). The particle size of the SiO_2NPs and fSiO_2NPs were 588 ± 7.21 x 10^{-3} nm and 593 ± 7.49 x 10^{-1} nm respectively (**Figures 5.1 A2 and B2)**. Notably, a slight increase in the particle size was realized after silane modification of the SiO_2NPs. This increase was attributed to the coating effect of the silane reagent (i.e. POTS).

The CNTs were elongated, homogenous, and cylindrical tubes with minimal irregularities **(Figures 5.1 C1 and D1).** Their sizes before and after modification were 8.97 ± 0.0969 nm and 10.8 ± 0.296 nm respectively (**Figures 5.1 C2 and D2)**. Similarly, an increase in the particle size was realized following modification. The increase confirmed silane growth on the surface of the CNTs. Modification process was further verified from the FTIR analysis **(Figure A1).**

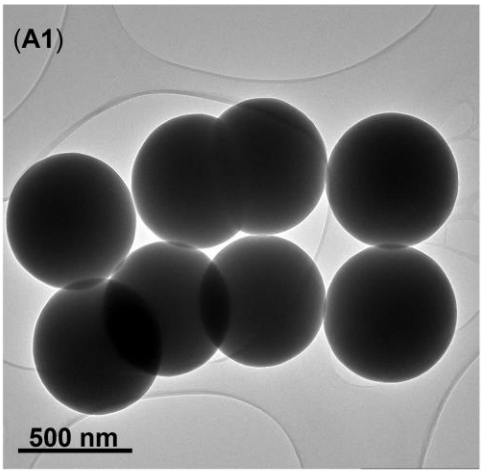

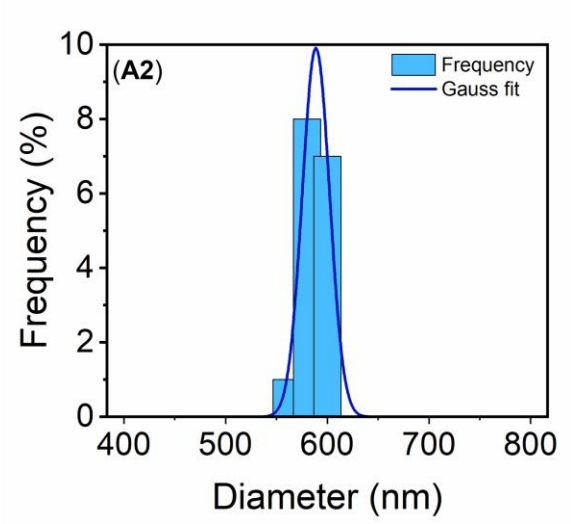

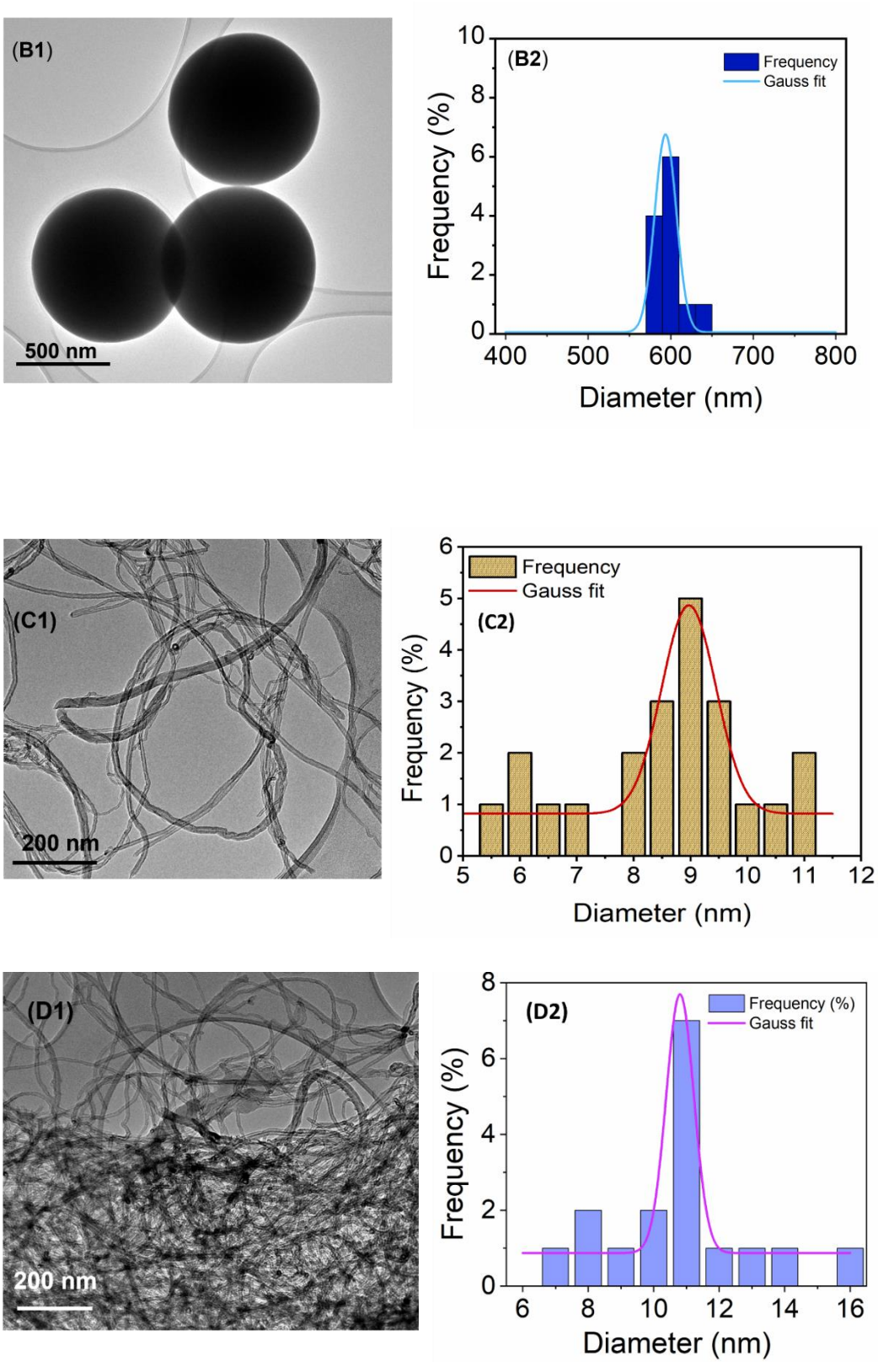

Figure 5.1: TEM micrographs and corresponding particle size distribution (A1-A2) SiO_2NPs, (B1-B2) fSiO_2NPs, (C1-C2) CNTs, and (D1-D2) fCNTs.

5.3.2 Membrane porosity, pore size, WCA, and LEP

The porosity measurements of M1, M2, M3, and M4 were 81.68%, 73.00%, 64.34%, and 63.61%, respectively **(Table 5.2**). Notably, M1 presented the highest porosity with a decreasing porosity upon incoporation of additives (M2-M4). The decreasing porosity following modification was substantiated by the reported literature (Pan, Chen, *et al.*, 2022). Furthermore, a decline in porosity of M3 and M4 was largely due to membrane pore blockage caused by additive cavity filling. The porosity of commercial PTFE-45 and PTFE-20 were 51.03% and 54.13%, respectively. These porosity values were lower than all the synthesised membranes. The discrepancy was associated to the difference in fabrication procedures and polymer types (Kong *et al.*, 2020). The pore size of M1 and M2 were 0.27 and 0.21 µm, respectively (**Table 5.2**). Upon incoporation of fCNTs (M3), the pore size decreased to 0.19 µm. A similar effect was realised for M4 (0.22 µm). Slight increase in pore size from M3 to M4 was caused by incorporation of fSiO_2NPs (Silva *et al.*, 2015; Tan *et al.*, 2021). According to Fernandes et al., (2021), hydrophobic SiO_2NPs increase solution viscosity caused by sudden polymer entanglement (Fernandes *et al.*, 2021). The polymer entanglement increases in the presence of water during phase inversion caused by low affinity between the hydrophobic NPs and water. As per ternary diagrams, Alibakhshi et al., (2019) reported an increase in membrane pore size due to reduced affinity of polymer to the non-solvent during phase inversion (Alibakhshi *et al.*, 2019). The presence of hydrophobic NPs enable steric hindrance of solvent and non-solvent exchange, leading to formation of abundant and large pore sizes (Fernandes *et al.*, 2021). These processes justify the slight increase in membrane pore size from M3 to M4. The inclusion of nanoparticle additives in the membrane matrix resulted in a physical interaction whereby the NP additives were dispersed into the polymeric matrix. This was corroborated by FTIR characterisation of the membranes which demonstrated no chemical changes to the polymeric structure indicating that a physical change was introduced (**Appendix A1.1 & A1.2).**

The WCA measurements of M1 was 116.52°, which decreased to 84.69° upon addition of PVP in the casting solution (**Table 5.2**). The decrease in membrane hydrophobicity was associated with the hydrophilic nature of the water-soluble pore former (PVP). However, upon addition of fSiO_2NPs and fCNTs, the WCA of M3 and M4 increased to 101.60° and 103.81°**,** respectively, implying an improvement in their hydrophobicity. Similar results were reported by Silva et al. (2015) upon incoporating multi-walled CNTs (MWCNTS) into a PVDF polymeric matrix. Though WCA increased upon the addition of fCNTs, membrane hydrophobicity remained relatively lower than prestine PVDF membrane, largely due to

minimal fluourination of the CNTs. Compared to M3, the WCA of M4 improved due to the addition of $fSiO_2$NPs. The WCA of PTFE-20 and PTFE-45 were 97.35° and 101.57°, respectively**,** thus comparable to modified M3 and M4. The WCA suggest the membrane's suitability for use in MD applications.

Liquid entry pressure (LEP) measurements were carried out to understand possible wettability of the membranes by the process liquids. The MD operating pressure should not exceed the LEP of the membranes to ensure their wetting resistance. The LEP of a membrane is governed by various factors including membrane pore size and hydrophobicity (El-Bourawi *et al.*, 2006; Dong *et al.*, 2014). The LEP of M1 was 393 ± 4.00 kPa (**Table 5.2**). Upon the addition of the pore former, the LEP of M2 decreased to 273 ± 37.7 kPa. The drop in LEP was caused by the decline in mass transfer resistance. This was explained by its low WCA therefore, it's hydrophilic properties and larger pore size established minimal resistance of mass transfer through the membrane. However, incorporation of the fCNTs and $fSiO_2$NPs increased the LEP of M3 and M4 to 500 ± 97.9 kPa and 590 ± 90.0 kPa, respectively. The increased LEP of M3 and M4 was associated with an increased mass transfer resistance caused by a decreased membrane pore size and improved hydrophobicity indicated by their WCA's. The reduced pore size and LEP was supported by previously reported studies (Tan *et al.*, 2021; Pan, Chen, *et al.*, 2022). The LEP of PTFE-20 and PTFE-45 was 603 ± 20.5 kPa and 200 ± 90.0 kPa, respectively. PTFE-45 was characterized by a larger pore size (i.e., 0.45µm) compared to PTFE-20 (0.20µm), thus enabling low mass transfer resistance. Also, membrane pore geometry is an important factor, as pore irregularities in axial and radial directions result in deviations from perfectly cylindrical pores thus affecting mass transfer (Rahimpour and Esmaeilbeig, 2019). Differences in LEP was correlated to SEM micrographs of these membranes (**Figures 5.2 C1 and F1**). Irregularly shaped pores were recorded with different circular, elongated and cylindrical structures.

Table 5.2: Physical characteristics of the as-synthesised PVDF and PTFE membranes.

Membrane	**Porosity (%)**	**WCA (°)**	**LEP (kPa)**	**Pore size (µm)**
M1	81.68 ± 3.00	116.52	393 ± 4.00	0.27
M2	73.00 ± 5.14	84.69	273 ± 37.7	0.21
M3	64.34 ± 0.13	101.60	500 ± 97.9	0.19
M4	63.61 ± 0.95	103.81	590 ± 90.0	0.22

PTFE-20	54.13 ± 1.94	97.35	603 ± 20.5	0.20
PTFE-45	51.03 ± 1.48	101.57	200 ± 90.0	0.45

5.3.3 SEM analysis of the membranes

The obtained SEM micrographs were used to evaluate the surface and cross-sectional morphology of the as-synthesised PVDF membranes (**Figure 5.2**). A surface view of M1 (**Figure 5.2 A1)**) presented a densely porous sponge-like surface. Based on the cross-sectional micrograph (**Figure 5.2 A2**), the membrane was characterized by smaller and round pores. Although M2 was densely porous, this membrane possessed a globule-like surface (**Figure 5.2 B1**). Based on cross-sectional analysis (**Figure 5.2 B2**), M2 was characterized by elongated, finger-like pore structures. This is a consequence of the addition of PVP into the membrane matrix (Silva *et al.*, 2015). Due to its high water solubility, PVP promoted the formation of elongated pores during phase separation (Kang and Cao, 2014). Nonetheless, SEM does not indicate an increase in membrane porosity from M1 to M2, thus supporting the previously reported information (**Table 5.2**). For the modified membrane, M3 showed a densely porous structure with varying pore sizes (**Figure 5.2 C1-C2**). The internal structure contained a complex mixture of small, round, spongy pores in addition to elongated pores (**Figure 5.2 C2**). Similar findings of sponge-like pores were reported by Silva et al. (2015). The pore elongation was linked to addition of fCNTs. Lastly, M4 (**Figure 5.2 D1)** revealed a densely porous surface with an irregular pattern, caused by the addition of fSiO_2NPS in the casting solution. Analysis of the corresponding cross-sectional view demonstrated a combination of elongated pores and small, dense pores induced by addition of PVP, fCNTs and fSiO_2NPS, respectively. Notably, the internal structure of M4 contained macrovoids induced by membrane additives (**Figure 5.2 D2**) (Jung *et al.*, 2016). PTFE-20 and PTFE-45 were characterized by rod-like structures with irregularly shaped pores (**Figures 5.2 E1 and F1**). Based on their cross-sectional views, these membranes were dense with an irregular porous structure.

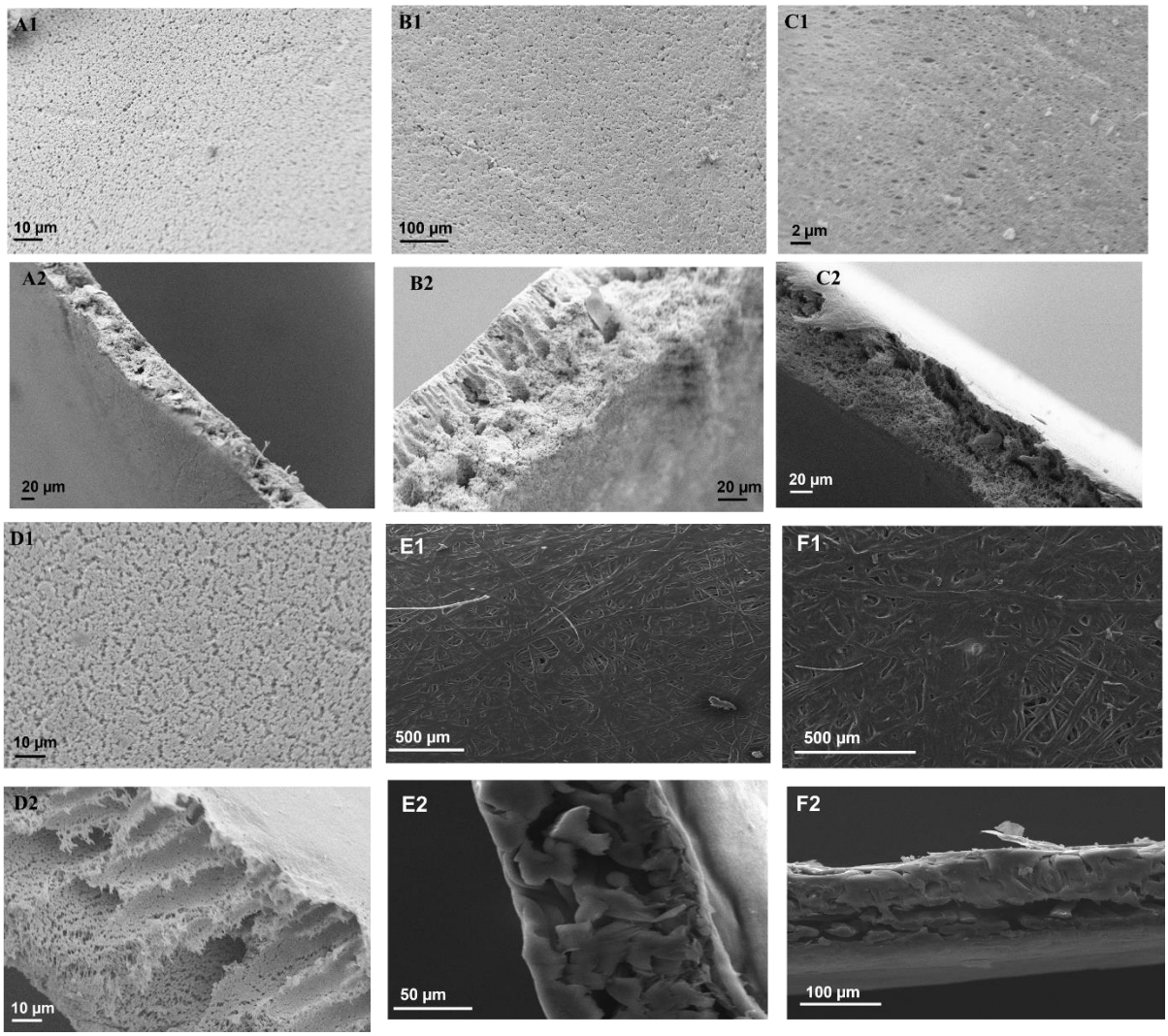

Figure 5.2: SEM micrographs of (A1-A2) M1, (B1-B2) M2, (C1-C2) M3, and (D1-D2) M4, (E1-E2) PTFE-20, and (F1-F2) PTFE-45: Surface and cross-sectional structures.

5.3.4 AFM analysis of the membranes

Owing to its effect on process performance, the membrane surface roughness was evaluated (**Figure 5.3**). The root-mean-square roughness (R_q) for M1, M2, M3, M4, PTFE-20, and PTFE-45 were 62.90 nm, 68.52 nm, 129.88 nm, 367.38 nm, 882.30 nm, and 1691.36 nm, respectively. Modified membranes (M2-M4) displayed a greater density of dark and light ridges indicating the deepest and highest regions on the membrane surface (**Figure 5.3 B – D**). Technically, these membranes presented greater surface roughness compared to M1 (**Figure 5.3 A)** (Hernández-Aguirre *et al.*, 2016). The R_q values increased upon incorporation of pore former and additives (PVP, fCNTs and fSiO_2NPS), suggesting increased surface roughness. The surface roughness of the commercial membranes PTFE-20 (882.3 nm) and PTFE-45 (1691.36 nm) exceeded that of the synthetic membranes. Based on the rough surface acting as air

pockets, the performance of these commercial membranes may supersede that the synthetic membranes. Comparably, increased membrane surface roughness caused by incorporation of NPs was reported in various studies (Hamzah, Leo and Ooi, 2019; Ding, Liu and Xiao, 2021).

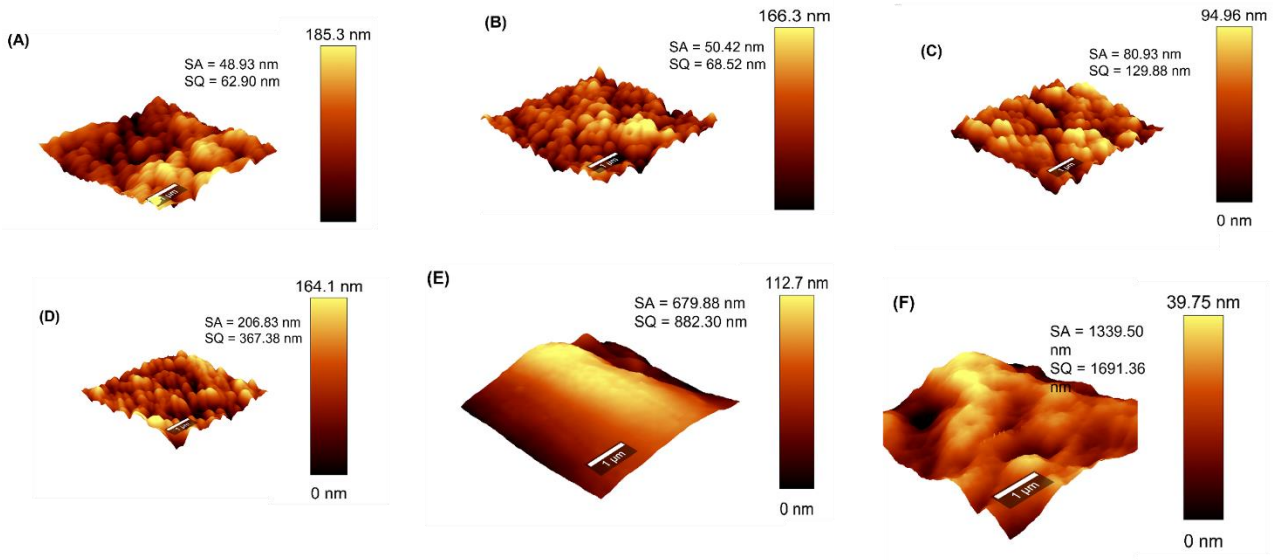

Figure 5.3: Topographical micrographs displaying surface roughness of (A) M1, (B) M2, (C) M3, (D) M4, (E) PTFE-20 and (F) PTFE-45.

5.3.5 Mechanical properties of the membranes

The mechanical properties of the fSiO_2NPs and fCNTs were determined using the Young's modulus estimated from the stress-strain plots (**Figures 5.4 A** and **B**). Mechanically strong membranes are required to sustain MD operating conditions (Pramono *et al.*, 2017). The tensile strength of the membranes was reported on the basis of Young's modulus (**Table 5.3).** The Young's modulus of M1 (0.45 MPa) was lower than that of M2 (1.06 MPa). This was attributed to the porous microstructure of M1 thus weakening its mechanical properties (Manawi *et al.*, 2018). Moreover, membrane pores act as stress absorbers thus increasing the tensile strength of M2. Similar findings were reported by Pramono et al. (2017). There was no significant difference in mechanical strength of M2 (1.06 MPa) and M3 (1.07 MPa). However, addition of fCNTs presented a slight increase in mechanical strength of the membrane. The carbon atoms present in single graphene of fCNTs are characterized by strong chemical bonds. These bonds increase elasticity of the fCNTs, ensuring full restoration of the particle size upon release of external force (Makgabutlane *et al.*, 2021). When incorporated into the polymer matrix, fCNTs increases membrane strength. However, the tensile strength of M4 decreased to 0.39 MPa upon incorporation of fSiO_2NPs. The decrease was a consequence of macrovoids causing

structural defects of the membrane **(Figure 5.2 D2)** (Loh *et al.*, 2011; Guo *et al.*, 2014; Jung *et al.*, 2016). Furthermore, nanoparticle aggregation cause skewed mechanical integrity of the modified membrane (Manawi *et al.*, 2018). Lastly, the mechanical properties of the commercial membranes, PTFE-20 (2.90 MPa) and PTFE-45 (6.96 MPa) were larger than that of the synthetic membranes. These differences were associated to mechanical integrity of the different polymers.

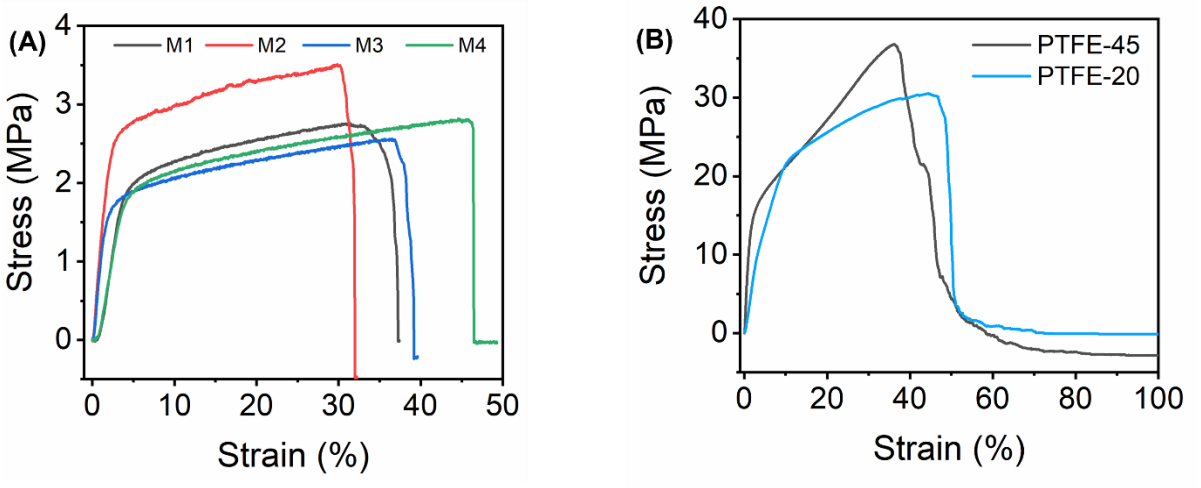

Figure 5.4: Stress-strain plots of (A) the as-synthesised membranes and (B) the commercial membranes.

Table 5.3: Young's modulus of the as-synthesised PVDF membranes and commercial PTFE membranes

Membrane	**Young's modulus**
M1	0.45 ± 0.24
M2	1.06 ± 0.42
M3	1.07 ± 0.25
M4	0.39 ± 0.30
PTFE-20	2.90 ± 0.88
PTFE-45	6.96 ± 4.63

5.3.6 Flux and salt rejection evaluation in DCMD using synthetic saltwater

The 3.5 wt% NaCl was used to assess the MD process performance of the membranes (**Figure 5.6**). Evaluations were performed at three different feed temperatures to assess their effect on process performance. The permeate flux increased with an increase in feed temperature. At

40 °C, the water flux of M1, M2, M3, M4, PTFE-20 and PTFE-45 were 7.58 kg m^{-2} hr^{-1}, 8.52 kg m^{-2} hr^{-1}, 11.36 kg m^{-2} hr^{-1}, 19.88 kg m^{-2} hr^{-1}, 25.68 kg m^{-2} hr^{-1}, and 27.46 kg m^{-2} hr^{-1},respectively. Upon increasing the feed temperature to 60 °C, the water flux increased to 14.20 kg m^{-2} hr^{-1} (M1), 22.72 kg m^{-2} hr^{-1} (M2), and 22.69 kg m^{-2} hr^{-1} (M3), and 39.77 kg m^{-2} hr^{-1} (M4), 62.5 kg m^{-2} hr^{-1} (PTFE-20), and 54.92 kg m^{-2} hr^{-1} (PTFE-45), respectively. The increase in feed temperature increased the vapour pressure gradient, thus improving the mass transfer (**Figures 5.6 A2-F2**). These findings were substantiated by previously reported studies (Attia *et al.*, 2017; Alanezi *et al.*, 2021; Zhu *et al.*, 2021). The permeate flux and deltaT remained stable for 3 hrs thus indicating process resistance to flux decays. Although the flux remained relatively stable, minimal fluctuations were recorded. For instance, the permeate flux of M4 was 38.83 kg m^{-2} hr^{-1} at t = 15 min. Though deltaT remained relatively constant at t = 180 min, the flux slightly decreased to 32.20 kg m^{-2} hr^{-1}. These variations caused by various parameters including pore wetting, and concentration polarization (Edwie and Chung, 2013). Similar results were recorded for M3 where the permeate flux decreased from 22.72 to 20.83 kg m^{-2} hr^{-1} at same time intervals. The membrane conductivity increased slightly as a function of time for all operating temperatures. This increase in conductivity implied the slight transfer of water in liquid state caused by membrane wetting. Interestingly, the rate of permeate conductivity increase was higher at high feed temperature. This was associated to an increased salt solubility. Although the membranes experienced slight wetting effects, the salt rejection remained relatively high (> 99%) for all membranes over the experimental time. Therefore, the increased permeate conductivity effects were negligible as the membranes demonstrated the capacity to produce high quality distillate. Comparatively, the salt rejections of the synthesized membranes were comparable to commercial membranes, thus motivating the successful incorporation of NPs in the membrane to improve process performance. Furthermore, the findings of this study were compared with the existing literature where PVDF membranes were modified with NPs for use in MD systems (**Table 5.4**). A comparative assessment elucidates the role of NPs towards process performance. Also, incorporation of NPs into the membrane matrix enhancing membranes properties and their structural integrity was substantiated. According to Ardeshiri et al., (2018), incoporation of ZnONPs improved porosity and surface roughness of PVDF membranes, thus ensuring high MD process performance (Ardeshiri *et al.*, 2018). Specifically, water flux (25 kg $m^{-2}{\cdot}hr^{-1}$) and a salt rejection (99%) were reported. Other studies used modified SiO_2NPs to improve membrane properties. Increased membrane porosity and WCA were reported (Hamzah, Leo and Ooi, 2019; Lebea N Nthunya, Gutierrez, Derese and Mamba, 2019). These properties were instrumental in ensuring high permeate flux and salt

rejection as seen in **Table 5.4**. In some instances, CNTs are used to modify PVDF membranes for DCMD, thus ensuring 100% salt rejection (Silva *et al.*, 2015). According to the existing findings, various operating conditions were evaluated to provide an overview of process versatility. These include process temperatures and flow rates. The water flux and salt rejection reported in the current study correspond to the existing literature at feed temperature of 60 °C. Therefore, manipulation of membrane properties for improved MD process performance is key.

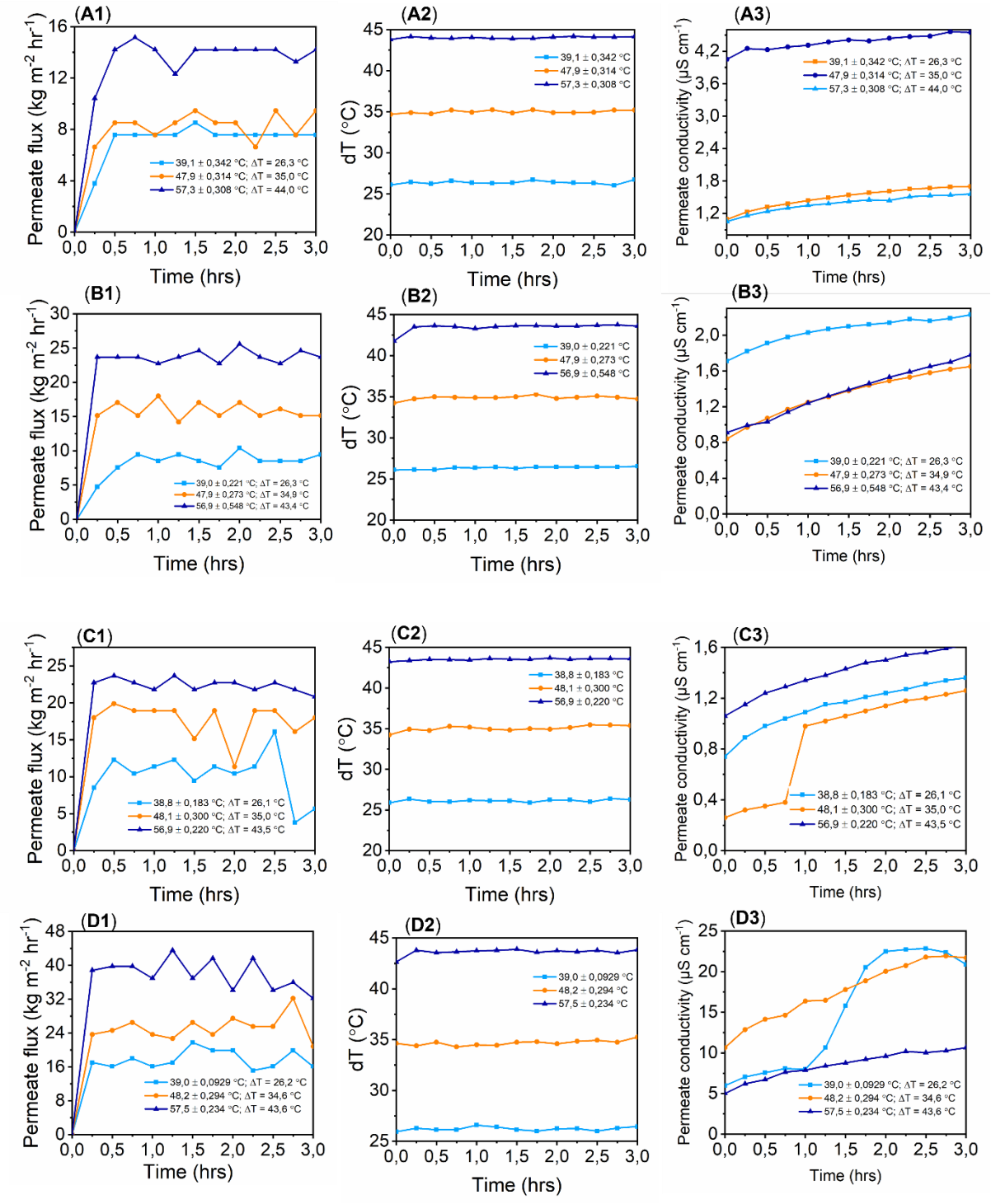

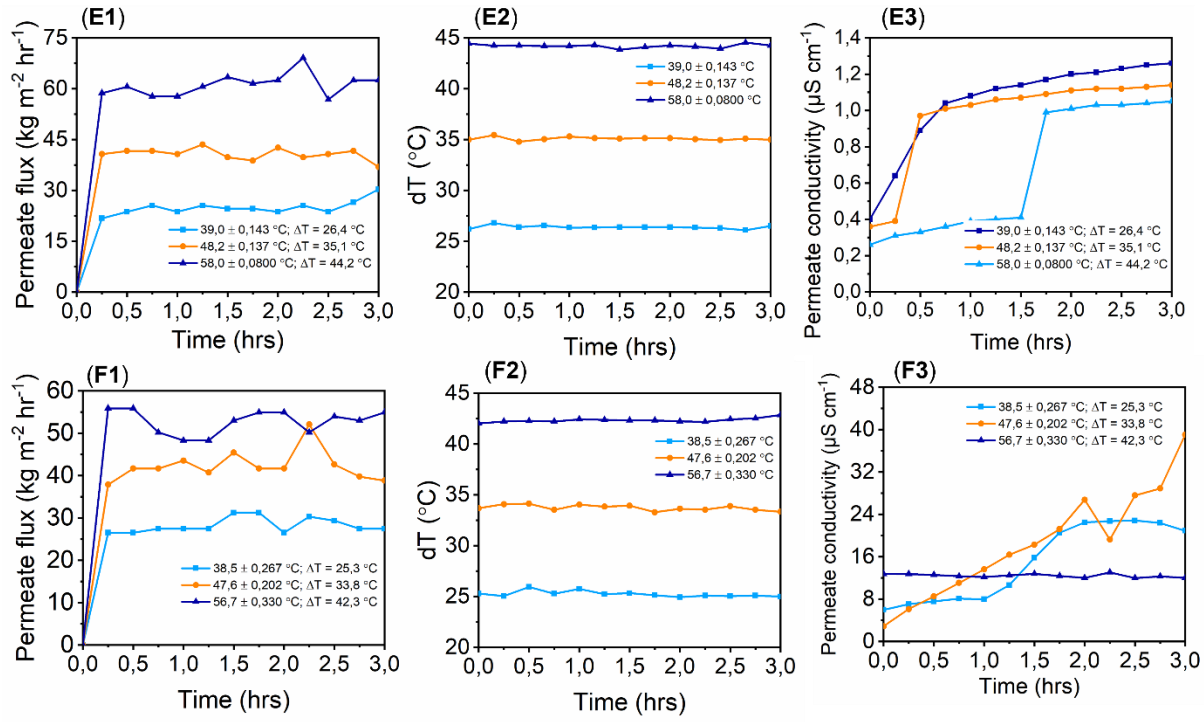

Figure 5.5: Permeate flux, deltaT, permeate conductivity vs time at various temperatures for NaCl separation in DCMD: (A1-A3) M1, (B1-B3) M2, (C1-C3) M3, (D1-D3) M4, (E1-E3) PTFE-20, and (F1-F3) PTFE-45.

Table 5.4: Comparison of nanoparticle modified PVDF membranes for water desalination in DCMD,

Membranes	**Modifying NPs**	**Operating conditions**			**Process performance**		**Ref.**
		Feed temperature (°C)	**Permeate temperature (°C)**	**Flow rate (ml min^{-1})**	**Flux (kg m^{-2} hr^{-1})**	**Rejection (%)**	
PVDF	ZnO	86	22	400.00	25.00	99	(Ardeshiri *et al.*, 2018)
PVDF	halloysite nanotubes	60	20	252.36	5.52	95	(Wae AbdulKadir, Ahmad and Ooi, 2022)
PVDF nanofiber	SiO_2NPs	20 - 80	20	750.00	34.2	99	(Lebea N Nthunya, Gutierrez, Derese and Mamba, 2019)
PVDF	TiO_2-SiO_2	40	20	300.00	11.00	99	(Hamzah, Leo and Ooi, 2019)

PVDF	CNTs	82	20	48.00	34.20	100	(Silva *et al.*, 2015)
PVDF	$fSiO_2NPs/fCNTs$	60	10	601.00	39.77	99	This study

5.4 Conclusion

This study explored membrane preparation and nanoparticle-modification to improve their performance in MD applications. Synthetic membranes, namely M1, M2, M3 and M4, were comparatively assessed against commercial membranes, PTFE-20 and PTFE-45. The membrane WCA decreased from 116.52° (M1) to 84.69° (M2) upon incorporation of pore former (PVP). However, WCA increased significantly to 101.60° and 103.61° upon further addition of fCNTs (M3) and fSiO_2NPs (M4), respectively. Furthermore, the LEP of the membranes decreased upon increased pore formation within the membrane surface. Interestingly, incorporation of fCNTs and fSiO_2NPs produced membranes of high LEP values > 500 kPa. Based on SEM analysis, these membranes were densely porous with irregular patterns of varying small, round, and spongy pores. The increased LEP after the addition of fCNTs in M3 was governed by its reduced pore size. In contrast, incorporation of fSiO_2NPs increased the size of the macrovoids and therefore indicating the dependence of M4 LEP on its hydrophobicity with slight dependence on pore size. As-synthesised membranes presented comparable properties to commercial membranes, thus demonstrating their potential applications in MD systems. However, further research is needed to investigate the synergistic effect of the additives towards improved performance at industrial level. This includes investigation into the fluorination of CNTs and their effect on process performance is also recommended. During separation experiments, the as-synthesised membrane achieved > 99.0 % salt rejection and produced relatively stable fluxes and deltaT profiles. Based on flux, salt rejection tests and physicochemical properties, fSiO_2NPs was the most favourable hydrophobic additive producing membranes of high performance. Curation of membrane properties and structural integrity through incorporation of fCNTs and fSiO_2NPs provided a clear path towards improved wetting resistance. As a result, the current study provided experimental evidence for the successful use of modified PVDF membranes in DCMD, thus opening further research directions towards improved process performance.

References

Afsari, M., Shon, H. K. and Tijing, L. D. (2021) ‘Janus membranes for membrane distillation : Recent advances and challenges’, *Advances in Colloid and Interface Science*, 289, p. 102362. doi: 10.1016/j.cis.2021.102362.

Alhathal Alanezi, A. *et al.* (2021) ‘Theoretical Investigation of Vapor Transport Mechanism Using Tubular Membrane Distillation Module’, *Membranes*. doi: 10.3390/membranes11080560.

Ali, A. *et al.* (2019) 'Treatment of Wastewater Solutions from Anodizing Industry by Membrane Distillation and Membrane Crystallization', *Applied Sciences*, 9(2), pp. 1–15. doi: 10.3390/app9020287.

Alibakhshi, S. *et al.* (2019) 'Tuning morphology and transport in ultrafiltration membranes derived from polyethersulfone through exploration of dope formulation and characteristics', *Materials Research Express*, 6(12), pp. 1–14. doi: 10.1088/2053-1591/ab56c3.

Ardeshiri, F. *et al.* (2018) 'PVDF membrane assisted by modified hydrophobic ZnO nanoparticle for membrane distillation', *Asia-Pacific Journal of Chemical Engineering*, 13(3), pp. 1–12. doi: 10.1002/apj.2196.

Ashoor, B. B. *et al.* (2016) 'Principles and applications of direct contact membrane distillation (DCMD): A comprehensive review', *Desalination*, 398, pp. 222–246. doi: 10.1016/j.desal.2016.07.043.

Attia, H. *et al.* (2017) 'Modelling of air gap membrane distillation and its application in heavy metals removal', *Desalination*, 424(September), pp. 27–36. doi: 10.1016/j.desal.2017.09.027.

Calvo, G. and Valero, A. (2022) 'Strategic mineral resources: Availability and future estimations for the renewable energy sector', *Environmental Development*, 41(April 2021), p. 100640. doi: 10.1016/j.envdev.2021.100640.

Chimanlal, I. *et al.* (2022) 'Membrane distillation crystallization for water and mineral recovery : The occurrence of fouling and its control during wastewater treatment', *Frontiers in Chemical Engineering*, (November), pp. 1–14. doi: 10.3389/fceng.2022.1066027.

Ding, Z., Liu, Z. and Xiao, C. (2021) 'Excellent performance of novel superhydrophobic composite hollow membrane in the vacuum membrane distillation', *Separation and Purification Technology*, 268(October 2020), p. 118603. doi: 10.1016/j.seppur.2021.118603.

Dong, Z. Q. *et al.* (2014) 'Superhydrophobic PVDF-PTFE electrospun nanofibrous membranes for desalination by vacuum membrane distillation', *Desalination*, 347, pp. 175–183. doi: 10.1016/j.desal.2014.05.015.

Edwie, F. and Chung, T.-S. (2013) 'Development of simultaneous membrane distillation–crystallization (SMDC) technology for treatment of saturated brine', *Chemical Engineering Science*, 98, pp. 160–172. doi: 10.1016/j.ces.2013.05.008.

El-Bourawi, M. S. *et al.* (2006) 'A framework for better understanding membrane distillation separation process', *Journal of Membrane Science*, 285(1–2), pp. 4–29. doi: 10.1016/j.memsci.2006.08.002.

Elhenawy, Y. *et al.* (2022) 'Performance enhancement of a hybrid multi effect evaporation / membrane distillation system driven by solar energy for desalination', *Journal of Environmental Chemical Engineering*, 10(6), p. 108855. doi: 10.1016/j.jece.2022.108855.

Eykens, L. *et al.* (2016) 'How to optimize the membrane properties for membrane distillation: A review', *Industrial and Engineering Chemistry Research*, 55(35), pp. 9333–9343. doi: 10.1021/acs.iecr.6b02226.

Eykens, L. *et al.* (2017) 'Membrane synthesis for membrane distillation: A review', *Separation and Purification Technology*, 182, pp. 36–51. doi: 10.1016/j.seppur.2017.03.035.

Farmani, R. *et al.* (2021) 'Intermittent water supply systems and their resilience to COVID-19: IWA IWS SG survey', *Aqua Water Infrastructure, Ecosystems and Society*, 70(4), pp. 507–520. doi: 10.2166/aqua.2021.009.

Fernandes, C. S. *et al.* (2021) 'Explication of hydrophobic silica as effective pore former for membrane fabrication', *Applied Surface Science Advances*, 3, p. 100051. doi: 10.1016/j.apsadv.2020.100051.

Gao, C. *et al.* (2020) 'Superhydrophobic Electrospun PVDF Membranes with Silanization and Fluorosilanization Co-Functionalized CNTs for Improved Direct Contact Membrane Distillation', pp. 35–43. doi: 10.30919/es8d905.

Goh, S. *et al.* (2015) 'Membrane Distillation Bioreactor (MDBR) - A lower Green-House-Gas (GHG) option for industrial wastewater reclamation', *Chemosphere*. doi: 10.1016/j.chemosphere.2014.09.003.

Guo, J. L. *et al.* (2014) 'Investigation of polyvinylidene fluoride membranes prepared by using surfactant OP-10 alone or with a second component, as additives, via the Non-Solvent-Induced Phase Separation (NIPS) process', *Journal of Macromolecular Science, Part B: Physics*, 53(8), pp. 1319–1334. doi: 10.1080/00222348.2014.928163.

El Haj Assad, M. *et al.* (2020) 'Applications of nanotechnology in membrane distillation: A review study', *Desalination and Water Treatment*, 192(March 2019), pp. 61–77. doi: 10.5004/dwt.2020.25821.

Hamzah, N., Leo, C. P. and Ooi, B. S. (2019) 'Superhydrophobic PVDF/TiO 2 -SiO 2 Membrane with Hierarchical Roughness in Membrane Distillation for Water Recovery from Phenolic Rich Solution Containing Surfactant', *Chinese Journal of Polymer Science (English Edition)*. doi: 10.1007/s10118-019-2235-y.

Hernández-Aguirre, O. A. *et al.* (2016) 'Surface Modification of Polypropylene Membrane Using Biopolymers with Potential Applications for Metal Ion Removal', *Journal of Chemistry*, 2016. doi: 10.1155/2016/2742013.

Jung, J. T. *et al.* (2016) 'Understanding the non-solvent induced phase separation (NIPS) effect during the fabrication of microporous PVDF membranes via thermally induced phase separation (TIPS)', *Journal of Membrane Science*, 514, pp. 250–263. doi: 10.1016/j.memsci.2016.04.069.

Kang, G. dong and Cao, Y. ming (2014) 'Application and modification of poly(vinylidene fluoride) (PVDF) membranes - A review', *Journal of Membrane Science*, 463, pp. 145–165. doi: 10.1016/j.memsci.2014.03.055.

Khalid, A. *et al.* (2017) 'Fabrication of polysulfone nanocomposite membranes with silver-doped carbon nanotubes and their antifouling performance', *Journal of Applied Polymer Science*, 134(15), pp. 1–12. doi: 10.1002/app.44688.

Kharraz, J. A. and An, A. K. (2020) 'Patterned superhydrophobic polyvinylidene fluoride (PVDF) membranes for membrane distillation: Enhanced flux with improved fouling and wetting resistance', *Journal of Membrane Science*, 595(July 2019), p. 117596. doi: 10.1016/j.memsci.2019.117596.

Kim, J. *et al.* (2017) 'Membrane distillation (MD) integrated with crystallization (MDC) for shale gas produced water (SGPW) treatment', *Desalination*, 403, pp. 172–178. doi: 10.1016/j.desal.2016.07.045.

Kim, Junghyun, Kim, Jungwon and Hong, S. (2018) 'Recovery of water and minerals from shale gas produced water by membrane distillation crystallization', *Water Research*, 129, pp. 447–459. doi: 10.1016/j.watres.2017.11.017.

Kiss, A. A. and Kattan Readi, O. M. (2018) 'An industrial perspective on membrane distillation processes', *Journal of Chemical Technology and Biotechnology*, 93(8), pp. 2047–2055. doi: 10.1002/jctb.5674.

Kong, X. *et al.* (2020) 'Manipulating membrane surface porosity via deep insight into surfactants during nonsolvent induced phase separation', *Journal of Membrane Science*, 611(May), p. 118358. doi: 10.1016/j.memsci.2020.118358.

Loh, C. H. *et al.* (2011) 'Fabrication of high performance polyethersulfone UF hollow fiber membranes using amphiphilic Pluronic block copolymers as pore-forming additives', *Journal of Membrane Science*, 380(1–2), pp. 114–123. doi: 10.1016/j.memsci.2011.06.041.

Loubser, C., Chimbanga, B. M. and Jacobs, H. (2021) 'Intermittent water supply: A South African perspective', *Water SA*, 47(1), pp. 1–9. doi: 10.17159/wsa/2021.v47.i1.9440.

Lu, D. *et al.* (2017) 'Simultaneous Recovery and Crystallization Control of Saline Organic Wastewater by Membrane Distillation Crystallization', *AlChE Journal*, 63(6). doi:

10.1002/aic.

Macedonio, F. *et al.* (2014) 'Direct contact membrane distillation for treatment of oilfield produced water', *Separation and Purification Technology*, 126, pp. 69–81. doi: 10.1016/j.seppur.2014.02.004.

Makgabutlane, B. *et al.* (2020) 'Microwave Irradiation-Assisted Synthesis of Zeolites from Coal Fly Ash: An Optimization Study for a Sustainable and Efficient Production Process', *ACS Omega*, 5(39), pp. 25000–25008. doi: 10.1021/acsomega.0c00931.

Makgabutlane, B. *et al.* (2021) 'Green synthesis of carbon nanotubes to address the water-energy-food nexus: A critical review', *Journal of Environmental Chemical Engineering*, 9(1), p. 104736. doi: 10.1016/j.jece.2020.104736.

Manawi, Y. M. *et al.* (2018) 'Engineering the surface and mechanical properties of water desalination membranes using ultralong carbon nanotubes', *Membranes*, 8(4). doi: 10.3390/membranes8040106.

Mericq, J.-P., Laborie, S. and Cabassud, C. (2010) 'Vacuum membrane distillation of seawater reverse osmosis brines', *Water Research*, 44(18), pp. 5260–5273. doi: 10.1016/j.watres.2010.06.052.

Toh, M. J. *et al.* (2019) 'Antiwettability enhancement of PVDF-HFP membrane via superhydrophobic modification by SiO2 nanoparticles', *Comptes Rendus Chimie*, 22(5), pp. 369–372. doi: 10.1016/j.crci.2019.05.004.

Nitodas, S. F., Das, M. and Shah, R. (2022) 'Applications of Polymeric Membranes with Carbon Nanotubes: A Review', *Membranes*, 12(454), pp. 1–17. doi: 10.3390/membranes12050454.

Nthunya, Lebea N, Gutierrez, L., Derese, S., Edward, N., *et al.* (2019) 'A review of nanoparticle-enhanced membrane distillation membranes : membrane synthesis and applications in water treatment', *Chemical Technology and Biotechnology*, 94(9), pp. 2757–2771. doi: 10.1002/jctb.5977.

Nthunya, Lebea N, Gutierrez, L., Derese, S. and Mamba, B. B. (2019) 'Adsorption of phenolic compounds by polyacrylonitrile nano fibre membranes : A pretreatment for the removal of hydrophobic bearing compounds from water', *Journal of Environmental Chemical Engineering*, 7, p. 103254. doi: 10.1016/j.jece.2019.103254.

Nthunya, Lebea N. *et al.* (2019) 'Removal of Fe and Mn from polluted water sources in Lesotho using modified clays', *Journal of Water Chemistry and Technology*, 41(2), pp. 81–86. doi: 10.3103/S1063455X19020036.

Nthunya, L. N. *et al.* (2022) 'Fouling, performance and cost analysis of membrane-based water desalination technologies: A critical review', *Journal of Environmental Management*, 301(July 2021), p. 113922. doi: 10.1016/j.jenvman.2021.113922.

Pan, J. *et al.* (2022) 'Enhanced anti-wetted PVDF membrane for pulping RO brine treatment by vacuum membrane distillation', *Desalination*, 526(December 2021), p. 115533. doi: 10.1016/j.desal.2021.115533.

Phattaranawik, J. *et al.* (2008) 'A novel membrane bioreactor based on membrane distillation', *Desalination*, 223, pp. 386–395. doi: 10.1016/j.desal.2007.02.075.

Pramono, E. *et al.* (2017) 'Effects of PVDF concentration on the properties of PVDF membranes', *IOP Conference Series: Earth and Environmental Science*, 75(1). doi: 10.1088/1755-1315/75/1/012027.

Quist-Jensen, C. A. *et al.* (2017) 'Reclamation of sodium sulfate from industrial wastewater by using membrane distillation and membrane crystallization', *Desalination*, 401, pp. 112–119. doi: 10.1016/j.desal.2016.05.007.

Rahimpour, M. R. and Esmaeilbeig, M. A. (2019) 'Chapter 6 - Membrane Wetting in Membrane Distillation', in Angelo Basile, Efrem Curcio, I. (ed.) *Current Trends and Future Developments on (Bio-) Membranes*. Elsevier, pp. 143–174. doi: https://doi.org/10.1016/B978-0-12-813551-8.00006-1.

Salehi, M. (2022) 'Global water shortage and potable water safety; Today's concern and tomorrow's crisis', *Environment International*, 158, p. 106936. doi: 10.1016/j.envint.2021.106936.

Schmidt, M. (2019) 'Scarcity and environmental impact of mineral resources-an old and never-ending discussion', *Resources*, 8(1), pp. 1–12. doi: 10.3390/resources8010002.

Selvarajan, V., Obuobi, S. and Ee, P. L. R. (2020) 'Silica Nanoparticles—A Versatile Tool for the Treatment of Bacterial Infections', *Frontiers in Chemistry*, 8(July), pp. 1–16. doi: 10.3389/fchem.2020.00602.

Sershen *et al.* (2016) 'Water security in South Africa: Perceptions on public expectations and municipal obligations, governance and water re-use', *Water SA*, 42(3), pp. 456–465. doi: 10.4314/wsa.v42i3.11.

Shaliutina-Kolešová, A. (2018) 'A fundamental study of Morphology Prediction for Nano and Microstructure of PVDF for Membrane Fabrication and Film Formation Applications', *International Journal of Advanced Engineering and Nano Technology (IJAENT)*, (9), pp. 2347–6389. Available at: https://www.researchgate.net/publication/342121695.

Silva, T. L. S. *et al.* (2015) 'Multi-walled carbon nanotube/PVDF blended membranes with sponge- and finger-like pores for direct contact membrane distillation', *Desalination*, 357, pp. 233–245. doi: 10.1016/j.desal.2014.11.025.

Tan, H. F. *et al.* (2021) 'Superhydrophobic PVDF/micro fibrillated cellulose membrane for membrane distillation crystallization of struvite', *Chemical Engineering Research and Design*, 170, pp. 54–68. doi: 10.1016/j.cherd.2021.03.027.

Toh, M. J. *et al.* (2019) 'Antiwettability enhancement of PVDF-HFP membrane via superhydrophobic modification by SiO2 nanoparticles', *Comptes Rendus Chimie*, 22(5), pp. 369–372. doi: 10.1016/j.crci.2019.05.004.

UNICEF (2019) *Progress on drinking water, sanitation and hygiene: 2000 - 2017*. Available at: https://data.unicef.org/resources/progress-drinking-water-sanitation-hygiene-2019/ (Accessed: 4 July 2022).

Vineis, P., Chan, Q. and Khan, A. (2011) 'Climate change impacts on water salinity and health', *Journal of Epidemiology and Global Health*, 1(1), pp. 5–10. doi: 10.1016/j.jegh.2011.09.001.

Wae AbdulKadir, W. A. F., Ahmad, A. L. and Ooi, B. S. (2022) 'Hydrophobic PVDF-HNT membrane for oxytetracycline removal via DCMD: The influence of fabrication parameters on permeability, selectivity and antifouling properties', *Journal of Water Process Engineering*, 49(June), p. 102960. doi: 10.1016/j.jwpe.2022.102960.

Xiao, Z. *et al.* (2020) 'Unprecedented scaling/fouling resistance of omniphobic polyvinylidene fluoride membrane with silica nanoparticle coated micropillars in direct contact membrane distillation', *Journal of Membrane Science*, 599(January), p. 117819. doi: 10.1016/j.memsci.2020.117819.

Yeow, M. L., Liu, Y. T. and Li, K. (2003) 'Isothermal Phase Diagrams and Phase-Inversion Behavior of Poly(vinylidene fluoride)/Solvents/Additives/Water Systems', *Journal of Applied Polymer Science*, 90(8), pp. 2150–2155. doi: 10.1002/app.12846.

Yue, D. *et al.* (2021) 'A novel silver / activated - polyvinylidene fluoride - polydimethyl siloxane hydrophilic-hydrophobic Janus membrane for vacuum membrane distillation and its anti-oil-fouling ability', *Journal of Membrane Science*, 638(April), p. 119718. doi: 10.1016/j.memsci.2021.119718.

Zakaria, M. *et al.* (2022) 'Water Desalination Using Solar Thermal Collectors Enhanced by Nanofluids', *Chemical Engineering and Technology*, 45(1), pp. 15–25. doi:

10.1002/ceat.202100339.

Zhang, P. *et al.* (2021) 'Modification of PVDF hollow fiber membrane by co-deposition of PDA/MPC-co-AEMA for membrane distillation application with anti-fouling and anti-scaling properties', *Journal of Membrane Science*, 636(July), p. 119596. doi: 10.1016/j.memsci.2021.119596.

Zhao, Z. P. *et al.* (2013) 'Water regeneration from human urine by vacuum membrane distillation and analysis of membrane fouling characteristics', *Separation and Purification Technology*, 118, pp. 369–376. doi: 10.1016/j.seppur.2013.07.021.

Zhu, Z. *et al.* (2021) 'Omniphobic membrane with process optimization for advancing flux and durability toward concentrating reverse-osmosis concentrated seawater with membrane distillation', *Journal of Membrane Science*, 639(July), p. 119763. doi: 10.1016/j.memsci.2021.119763.

CHAPTER SIX

6 The Evaluation of Modified Synthetic Flat-Sheet PVDF Membranes for Membrane Distillation Crystallization (MDC) Using Simulated Wastewater

The work reported herein is in preparation for submission and is titled "The Evaluation of Modified Synthetic Flat-Sheet PVDF Membranes for Membrane Distillation Crystallization (MDC) Using Synthetic Wastewater. This was authored by Indira Chimanlal, Lebea N. Nthunya, Cejna Anne Quist-Jensen, and Heidi Richards.

6.1 Introduction

An increased global population has caused rising demand for natural resources. This is propelled by mineral needs in the wake of evolving industries and economic sectors. Consequently, a larger amount of waste is generated in tandem with greater industrial output. Upon disposal without adequate treatment, wastewater discharged from industries cause disastrous implications on the environment and human health (Yadav, Labhasetwar and Shahi, 2022). Produced water from oil and gas extraction (Ali *et al.*, 2015), acid mine drainage (AMD), and brine introduce large volumes of salt into the environment. These polluted wastewaters are related to the incorporation of harmful materials which negatively impact humans, animals, and other microbes in the ecosystem (Anekwe and Isa, 2023). The consequences thereof include plant dehydration, nutrient and hormonal imbalances, and environmental toxicity, among many others (Ondrasek and Rengel, 2021; Stein, Michael and Dugan, 2021). Wastewater when left untreated can result in biomagnification in aquatic and

terrestrial environments (Dhamsaniya *et al.*, 2022). Accordingly, freshwater sources are declining due to progressive environmental contamination and exploitation (Greve *et al.*, 2018). Therefore, remedial technologies are required. The abundance of minerals found in these waste streams provides an opportunity for their recycling and reuse. This is vital as it encourages circular economies, reduces the quantity of waste introduced to the environment, and improves the quality of discharged water to save the environment. Conventional wastewater treatment methods such as nanofiltration (NF), ultrafiltration (UF), and reverse osmosis (RO) are mature technologies commonly used to treat waste. These technologies are used individually or integrated depending on the quality of water required. Importantly, these technologies have limitations such as high operating pressures leading to high treatment expenditures. (Ali *et al.*, 2015; Lu *et al.*, 2017). For these reasons, they are rarely exploited in developing countries. Furthermore, RO produces concentrated brines, causing disposal challenges.

Membrane distillation (MD) was introduced as a promising technology to address challenges facing pressure-driven water treatment technologies. When integrated to conventional crystallization, MD can recover freshwater and minerals from wastewater (a technology known as membrane distillation crystallization, MDC). MDC is a thermal process facilitating separation through a hydrophobic membrane. Technically, the water passes through the membrane in vapour form, exclusively retaining non-volatiles (Lu *et al.*, 2017). The hot and cold interfaces from different sites of the membrane establish a vapour pressure gradient acting as the driving force. In MDC, the feed solution is concentrated to supersaturation thus facilitating mineral recovery through crystallization. During MDC applications, the hydrophobic membrane in MDC applications play two roles, namely; 1) provision of a mass transfer interface to concentrate the feed solution through solvent evaporation, and 2) promotion of heterogeneous nucleation as the membrane (Edwie and Chung, 2013; Jiang *et al.*, 2016). This technology possesses various advantages including treatment of highly concentrated feed streams, utilization of renewable energy and is less energy intensive. Also, MDC affords well-controlled supersaturation rates, crystal nucleation, and growth (Sparenberg, Ruiz Salmón and Luis, 2020). Most interestingly, MDC can simultaneously recover minerals and freshwater in one process (Yadav, Labhasetwar and Shahi, 2022). Unfortunately, MDC is affected by fouling/scaling whereby contaminants in the feed solution (organic, inorganic, and/or colloidal) deposit onto the membrane surface or within its pores resulting in a deteriorated membrane performance (Gryta, 2008; Nthunya *et al.*, 2019).

Membrane wetting is another common challenge commonly affecting the quality of recovered water (Chimanlal *et al.*, 2022). To ensure high process performance, various hydrophobic membranes originating from a variety of sources (commercial or synthetic) are often used in MDC systems. This work evaluated the recovery of freshwater and minerals in MDC using synthesized PVDF hydrophobic membranes and a commercial PTFE reference membrane. This study also utilised simulated environmental wastewater. Wastewater samples were obtained at various pollution zones in Gauteng, South Africa. Wastewater samples such as landfill leachate and acid mine drainage (AMD) were collected. Leachate wastewater is defined as water that has percolated through waste and contains a high level of unwanted chemicals (Dhamsaniya *et al.*, 2022). AMD is typically generated when sulphide materials encounter oxygenated water and air. Moreover, this type of wastewater is detrimental for surrounding ecosystems due to the high levels of iron and sulphate in conjunction to its low pH (Alegbe *et al.*, 2019). Various treatment strategies are often employed to alleviate the environmental expense of these pollutants and examples include, though not limited to, electrodialysis (Akcil and Koldas, 2006), passive bio-reactors (Akcil and Koldas, 2006), adsorbents (Egashira, Tanabe and Habaki, 2012; Chimanlal, Lesaoana and Richards, 2022), and biological treatments (Dhamsaniya *et al.*, 2022). However, it has not yet been widely reported on the use of MDC for the treatment of such wastewater. The feed solution was prepared to simulated acid mine drainage (AMD).

6.2 Methods and Materials

6.2.1 Chemicals and equipment

Certified aqueous reference cation multi-element standard and anion reference standard solutions (1000 mg L^{-1}) were obtained from De Bruyn Ultraspec (Johannesburg, South Africa). Materials used for membrane fabrication included polyvinylidene fluoride (PVDF, MW = 534,000 mg·mol^{-1}), dimethylformamide (DMF, 90.0%), dimethylacetamide (DMac, 99.0%), and polyvinylpyrrolidone as the pore former (PVP MW = 360,000 mg·mol^{-1}). All reagents used in the membrane fabrication process were purchased from Sigma-Aldrich (Johannesburg, South Africa). Ultrasonication was performed using the Eins Sci Profession ultrasonic cleaner under the normal setting (Johannesburg, South Africa). For membrane casting, an Elcometer 4340 casting knife film applicator set to a height of 50 µm along with the Elcometer 4340 Automatic Film Applicator to a speed setting of 4 (Manchester, United Kingdom). A commercially acquired PTFE (8” x 10”) membrane with a pore size (0.20 µm) supported on non-woven polyester was provided by Pall Corporation (New York, USA). Materials used for

the functionalization of the CNTs and SiO_2NPs are documented elsewhere (**Chapter Five)**. Permeate conductivity for MDC was recorded using the Hanna benchtop multiparameter meter (Washington, USA).

6.2.2 Solution preparation

6.2.2.1 Working standards

Standard solutions for inductively coupled plasma-optical emission spectroscopy (ICP-OES) analysis were prepared through serial dilutions of a multi-element stock solution in the range of 0.1 – 20 mg L^{-1}. Samples were acidified with 5% HNO_3. All solutions were stored in the dark at 4 °C when not in use. Similarly, anion standard solutions were used for preparation of calibration standards required for ion chromatography (IC) analysis in the range of 0.5 mg L^{-1}-100 mg L^{-1}. All calibration standards were prepared using ultrapure Milli-Q-RO4 water (Millipore, Bedford, MA, USA).

6.2.2.2 Feed solutions

For MDC, the feed solution employed was a simulated version of AMD obtained 200 m from the mine dump. The AMD is a recurrent environmental source of pollution (Pinetown, Ward and van der Westhuizen, 2007), and due to the magnitude of mining activity it is a frequent issue in many countries. For example, in South Africa the volume of AMD produced from the Witwatersrand Gold Field can reach alarming levels of 350 ML day^{-1} (Alegbe *et al.*, 2019). For MDC application, it is preferred that a highly saline wastewater solution be employed as it encourages the formation of supersaturation to facilitate salt recovery **(Table 6.2)**. Therefore, the highly saline water samples were leachate and AMD samples. However, due to the complex nature of the leachate samples (high toxicity and organic content), AMD samples were utilised preferentially. Specifically, the sample obtained 200 m from mine dump sample was chosen based on lengthy migration of dissolved minerals from the mine tailings. The synthetic solution was prepared from a mixture of different salts namely: sodium chloride (NaCl), sodium fluoride (NaF), potassium sulfate (K_2SO_4), nickel sulfate ($NiSO_4{\cdot}6H_2O$), cobalt chloride ($CoCl_2{\cdot}6H_2O$), zinc sulfate ($ZnSO_4{\cdot}H_2O$), calcium nitrate ($Ca(NO_3)_2{\cdot}4H_2O$), ferric sulphate ($Fe_2(SO4)_{3\cdot x}H_2O$), and anhydrous magnesium sulfate ($MgSO_4$). All salts were obtained from Sigma Aldrich (Johannesburg, South Africa). To adjust for the pH of the solution as seen in **Table 6.2,** nitric acid (HNO_3) (10.09 mL) and 0.1 mol L^{-1} sodium hydroxide (NaOH) was used. The nitric acid used also contributed to the NO_3^- concentration required. As necessary,

ultrapure deionized water was used Milli-Q-RO4 (Millipore, Bedford, MA, USA). The composition of the salts is presented in **Table 6.1** below.

6.2.3 Wastewater sampling and analysis

Wastewater samples were obtained from various water sampling sites and collected via plastic containers and stored in the dark at 4 °C. All samples were acidified with HNO_3 to prevent metal precipitation. Physical parameters such as pH, conductivity, salinity, and temperature were measured onsite.

Due to the high concentration of organics present in the leachate samples, rigorous sample preparation was undertaken to remove all organic matter prior to ICP-OES and IC analysis. During photo-oxidation, approximately 80 ml of the leachate samples were transferred into glass bottles and placed on a magnetic stirring plate under a UV lamp. While stirring, drops of hydrogen peroxide were added to the samples. The oxidation was carried out for 2 hrs.

Based on literature reports (Uddin *et al.*, 2016), digestion is an important sample preparation step assisting in elemental analysis. It affords the detachment of bound or insoluble matrices for an accurate determination. To do so, 2.0 mL HNO_3 (55 %) and 1.0 mL of HCl (32 %) were added 100 mL of the samples followed by digestion to dryness at 95 °C ± 5 °C. Furthermore, deionized water was added to fill the beaker to the original sample volume. The individual samples were filtered and stored in the dark at 4 °C.

6.2.4 Membrane fabrication and characterisation

Membrane preparation and characterization for PTFE-20 and M3 were reported in previously (Chimanlal *et al.*, 2023). However, extending the work produced from M4 reported earlier, an investigation into an increased fSiO_2NPs content (M5) was carried out. The NP content was increased to 7% to improve membrane properties for MDC. The fabrication procedure was reported previously (**Chapter Five)**. This membrane was characterised using SEM, AFM, tensile strength, porosity, LEP, and WCA. The details thereof may be seen in **(A1.3).** After MDC process evaluation, used membranes were analysed to understand their interaction with the feed solutions. Morphological properties of the salt crystals and membranes were acquired from TESCAN Vega scanning electron microscopy (SEM) (Libušina, Czech Republic) at 30.0 kV. All samples were coated with a layer of carbon and Au/Pd before analysis. Elemental mapping of the used membranes was obtained from Energy Dispersive Spectroscopy (EDS) coupled with SEM.

6.2.5 Membrane crystallisation (MDC) tests

In **Chapter Five**, synthetic and commercial membranes were evaluated for salt rejection and rate of water recovery in DCMD. Accordingly, M3, M4, and PTFE-20 presented the highest performance and were therefore chosen for MDC evaluation. Extending the work reported in **Chapter Five**, MDC application was performed on M3, M5, and PTFE-20. A simulated feed solution resembling the characteristics of AMD (200 m from mine dump) was prepared (**Table 6.1**). The feed and permeate solutions were circulated in a co-current configuration at 60 ℃ and 10.0 ℃, respectively. A membrane area of 152 x 110 mm was employed, along with a cross-flow velocity of 524 ml·min^{-1}. The change in mass and conductivity of the permeate was measured continuously. The feed solutions were stirred continuously to ensure continuous dissolution. Upon supersaturation, the feed solution was placed into an ice bath, followed by filtration, and drying of collected crystals. Distillate flux (J) was calculated using **Equation (1),** where Δm is the difference in the permeate mass (kg), Δt is the time difference (hrs) and A is the membrane area (m^2).

$$J = \frac{\Delta m}{\Delta t * A} \quad \textbf{(1)}$$

Table 6.1: Composition of the synthetic AMD solution used for MDC.

Salt	**Concentration (mg L^{-1})**
NaCl	89.68
$CaSO_4$	301.6
$CoSO_4$	10.52
$ZnSO_4$	64.03
$Fe_2(SO_4)_3$	981.0
$MgSO_4$	1617.3
K_2SO_4	325.4
$NiSO_4$	17.67
NaF	10.83
$Al_2(SO_4)_3$	253.6

6.2.6 Crystal characterisation

To evaluate the crystal formation, samples were collected at 30 min intervals and analysed using the Nikon stereoscopic microscope SMZ745T equipped with NIS elements Imaging software (Tokyo, Japan). Produced crystals were analysed using powder x-ray diffraction (PXRD, Bruker D2 Phaser Diffractometer equipped with a non-monochromated Co-Kα source, λ = 1.785 Å). In preparation for the analysis, each sample was compacted onto a Si zero background sample holder. Single crystals generated with PTFE-20 and M5 were collected on a Bruker D8 Venture Bio PHOTON III 28-pixel array area detector (208 x 128 mm^2) diffractometer, coupled with a Mo Kα IμS DIAMOND source (50kV, 1.4 mA). The analysis was performed at 173 K. The unit cell and complete data set were obtained using *APEX4* (Bruker, 2021) and integrated using *SAINT*. The *SADABS* was used to evaluate empirical adsorption corrections and data scaling. Furthermore, using Olex2 (Dolomanov *et al.*, 2009), the respective crystal structures were resolved with *ShelXT* (Sheldrick, 2015b) and refined using *ShelXL* (Sheldrick, 2015a). All database files were retrieved from the ICSD crystal database. Furthermore, all PXRD refinements and database matching was performed using BRUKER DIFFRAC.TOPAS V7.20 software.

6.3 Results and discussions

6.3.1 Quantitative determinations of minerals present in wastewater samples

6.3.1.1 Physical parameters of all wastewater samples

Physical parameters such as conductivity, total dissolved solids (TDS), salinity and pH were measured and recorded in **Table 6.2**. Notably, conductivity and salinity of leachate and AMD were higher compared to other wastewater sources. The leachates and AMD are characterised by high concentration of inorganic salts and heavy metals, thus contributing to their high conductivities and salinity. Additionally, the leachates and AMD were highly acidic with pH lower than 4. During mining, highway construction, and other large-scale excavations and mining activity, sulphide is exposed to water and oxygen. The sulfides oxidize to sulfuric acid, thus lowering the water pH which contributes to AMD (Skousen, Ziemkiewicz and McDonald, 2019). Mine tailings have restructured the landscape of various townships since the inception of mining in South Africa. These tailing dumps are continuously discharging polluted water into various streams through diffuse pollution. The diffuse and point source pollution increases water salinity and other characteristics of water pollution. To mitigate challenges experienced by users at lower stream, the upper stream release unpolluted water enabling water dilution.

However, these challenges can critically be addressed through MDC water treatment processes where freshwater is recovered while minerals are recycled for economic purposes.

Table 6.2: Physical parameters of the various wastewater samples collected and measured at room temperature.

Sampling area		Physical parameters measured at room temperature			
		Conductivity (µS cm^{-1})	**TDS (mg L^{-1})**	**pH**	**Salinity (PSU)**
Leachate A		130 000 ± 243	14 830 ± 230	3.9 ± 0.2	33.5 ± 1.1
Leachate B		168 000 ± 346	12 130 ± 670	3.4 ± 0.4	18.3 ± 1.9
Co-produced water	Water treatment plant	3 062 ± 109	1 529 ± 102	6.0 ± 0.7	1.6 ± 0.2
	Station dirty dam	5 876 ± 209	2 950 ± 261	6.3 ± 0.1	3.2 ± 0.7
	Ash dump dam	3 894 ± 302	1 951 ± 83	5.7 ± 0.4	2.1 ± 0.1
	Holding dam	3 505 ± 80	1 760 ± 107	5.1 ± 0.6	1.9 ± 0.3
	FGD blow down	22 800 ± 243	1 141 ± 99	5.9 ± 0.3	13.8 ± 1.2
	Clean station dam	683 ± 72	342 ± 21	6.7 ± 0.3	0.3 ± 0.1
	PS dirty reclaim dam	1 808 ± 203	904 ± 53	6.9 ± 0.5	0.9 ± 0.1
	Ash pond	2 684 ± 112	1 340 ± 97	9.5 ± 0.3	1.4 ± 0.4
Acid mine drainage	100 m from mine dump	18 902 ± 1 689	9 502 ± 728	2.4 ± 0.1	23.1 ± 1.1
	200 m from mine dump	6 890 ± 1091	3 431 ± 89	2.7 ± 0.4	30.21 ± 1.2
	Discharge to Fleurhof dam	4 782 ± 608	2 452 ± 320	3.9 ± 0.2	30.89 ± 1.3

6.3.1.2 Wastewater analysis – ICP-OES and IC

Collected wastewater samples were characterized using ICP-OES and IC to ascertain their cationic and anionic properties, respectively (**Table 6.3**). Further information pertaining to the transition metals detected can be found in **Table A2.** Based on the findings, leachate samples contained the highest concentrations of nitrates and sulphates which explained the toxic nature of these samples. High levels of nitrate levels in leachates originate from organic matter such as amino acids and other proteins (Cossu *et al.*, 2018). Moreover, high sulphate levels may derive from industrial waste such as construction and mining waste (Kijjanapanich *et al.*, 2014). Hence, these samples required extensive pre-treatments prior to analysis. Moreover, the low pH of leachates was ascribed to fresh organic waste thus characterising it as young leachate samples (less than 5 years old) (Dhamsaniya *et al.*, 2022). Nonetheless, these leachate samples contained high levels of organic matter, dissolved solids, and salts which were consistent with previously reported literature (Dhamsaniya *et al.*, 2022). The co-produced water samples were obtained at various sampling points along the industrial plant. Notably, sampling points such

as the water treatment plant and the clean station dam contained the least pollution as represented by the lower analyte concentrations. Comparatively, the other sampling points contained higher levels of analyte pollution. The difference may be ascribed to various water treatment protocols employed in the plant operation. AMD samples were also obtained at various sampling points along the stream bed. The analyte concentrations varied from the different sites which was attributed to changes in geological composition, rate of oxidation, and chemical deposition, among other factors (Alegbe *et al.*, 2019). Notably, analyte concentrations decreased with an increasing distance from the mine dump with some exceptions. For instance, the sulphate concentration at 100 m from the mine dump was the highest (20166.3 ± 692.6 mg L^{-1}) compared to the discharge into the dam (1636.5 ± 96.7 mg L^{-1}). Therefore, analyte concentrations were highest closest to the pollution source. Additionally, the collected AMD samples were highly acidic with a high conductivity and salinity. These findings are similar to previously reported literature (Gaikwad and Gupta, 2008). Gitari *et al.* (2008) reported AMD samples with a low pH in conjunction with a myriad of analytes such as Al, Cu, Na, and Ca. Reportedly, the samples contained sulphate levels exceeding 24 000 mg L^{-1} (Gitari *et al.*, 2008). The results reported in **Table 6.2** and **Table 6.3** reveal the hazardous nature of these wastewater samples present in the environment. Furthermore, their acidity and complex characteristics indicate their leaching potential from surrounding environments such as rocks and soils. Therefore, these samples pose serious environmental concerns, thus motivating the need for waste remediation. Additionally, the treatment of these and similar wastewater solutions allows for resource recovery as these solutions provide a variety of analytes which could possibly be recovered.

Table 6.3: Concentrations of analytes contributing to water salinity using ICP-OES and IC.

Sampling area		Group I and group II metal concentrations (mg L^{-1})				Anion concentration (mg L^{-1})			
		Ca^{2+}	K^{+}	Mg^{2+}	Na^{+}	Cl^{-}	F^{-}	NO_3^{-}	SO_4^{2-}
Leachate A		152.7 ± 12.4	750.7 ± 43.9	152.7 ± 9.7	750. 7 ± 52.9	26.8 ± 1.2	BDL	69340 ± 193	63897 ± 201
Leachate B		3.2 ± 0.3	91.9 ± 1.6	100.4 ± 4.1	150.4 ± 12.4	17.5 ± 0.4	BDL	89750 ± 312	3139 ± 89
Co-produced water	Water treatment plant	2.7 ± 0.1	6.7 ± 0.2	1.6 ± 0.1	221.4 ± 2.9	58.8 ± 0.8	BDL	2460 ± 112	961 ± 23
	Station dirty dam	285.7 ± 23.1	7.2 ± 0.1	155.8 ± 15.9	93.4 ± 6.2	136.5 ± 21.5	8.7 ± 0.5	3256.7 ± 425.1	2216.4 ± 186.3
	Ash dump dam	293.3 ± 0.3	12.7 ± 0.1	506.1 ± 23.7	76.7 ± 0.8	91.7 ± 2.6	4.6 ± 0.4	2520.1± 220.7	1549.3 ± 100.1
	Holding dam	136.9 ± 2.3	5.1 ± 0.2	67.4 ± 0.1	69.5 ± 1.9	791.4 ± 34.5	74.5 ± 1.8	4358.9 ± 287.5	7947 ± 107
	FGD blow down	445.6 ± 1.6	28.6 ± 0.4	1044.6 ± 6.1	413.8 ± 2.9	2695.8 ± 162.3	15.8 ± 0.5	18487.1 ± 87.2	6026.7 ± 206.3
	Clean station dam	8.6 ± 0.2	8.4 ± 0.1	BDL	25.1 ± 0.3	83.4 ± 8.7	BDL	2034.5 ± 110.7	125.6 ± 5.9
	Dirty reclaim dam	30.5 ± 0.2	22.1 ± 0.1	2.6 ± 0.1	73.9 ± 0.4	2384.3 ± 167.4	22.3 ± 0.6	19859.6 ± 601.5	5395.3 ± 323.8
	Ash pond	372.7 ± 12.9	37.1 ± 0.5	198 ± 1.3	155.7 ± 1.9	391.9 ± 23.7	1.3 ± 0.1	2181.4 ± 117.5	BDL
Acid mine drainage	100 m from mine dump	175.4 ± 4.8	116.7 ± 7.7	147.5 ± 7.3	116.7 ± 7.7	105.1 ± 6.2	9.7 ± 0.4	7445.5 ± 323.9	20166.3 ± 692.6
	200 m from mine dump	88.8 ± 0.4	73.0 ± 6.3	326.5 ± 10.9	73.0 ± 6.3	54.4 ± 1.6	4.9 ± 0.2	5041.3 ± 220.1	4046.7 ± 326.4
	Discharge into Fleurhof dam	85.6 ± 0.5	212.9 ± 4.4	210.3 ± 5.3	212.9 ± 4.4	343.1 ± 21.6	BDL	4256.1 ± 321.8	1636.5± 96.7

6.3.2 Freshwater and mineral recovery in MDC

Membrane distillation crystallization (MDC) was evaluated towards the recovery of freshwater and minerals from synthetic AMD wherein three membranes (M3, M5 and PTFE-20) were assessed at 60 °C (**Figure 6.1)**. The average permeate flux of PTFE-20 and M5 was 2.426 and 1.459 kg m^{-2} hr^{-1}, respectively. Additionally, the salt rejection was 99.96 % and 97.52% for the respective membranes. The reference membrane (PTFE-20) produced the highest permeate flux, which could be attributed to its superior hydrophobicity achieved at a commercial scale. However, M3 presented the poorest performance (**Figure 6.1 A1**). Due to its poor performance, it was incapable of attaining supersaturation, and thus did not produce any crystal product. Moreover, membrane performance was affected by surface deposition as evidenced by SEM imagery (**Figure 6.5 B**). It is possible that membrane deposition may have reduced its structural integrity thereby leading to its poor performance (Choi *et al.*, 2020). Nonetheless, M5 was susceptible to flux decline over time which could have been attributed to factors such as the feed temperature increasing to a critical value, or the feed cross flow velocity decreasing to a critical value (Zhao *et al.*, 2011). Notably, a deposition layer **(Figure 6.5 C)** was observed for this membrane as well, although, the decline in its performance was not as severe as it was for M3.

Salt deposition near the membrane-feed interface diminished the liquid-vapor boundary leading to a swift flux and salt rejection decline (Edwie and Chung, 2013). Compounded to this, temperature polarization could be another contributing factor towards flux decay (Olatunji and Camacho, 2018). Moreover, a reduced temperature at the membrane interface reduces vapour pressure, thus causing a decay in distillate flux (Edwie and Chung, 2013). Interestingly, incorporation of fSiO_2NPs (i.e., M5) improved process performance considerably. This was evident in the higher average permeate flux produced for M5 compared to M3. However, due to low recovery rate compared to PTFE-20, M5 required lengthy duration to reach supersaturation. However, A gradual increase in the distillate conductivity experienced for M5 suggested the onset of membrane wetting (**Figure 6.1 A2)**. Nonetheless, a satisfactory salt rejection was recorded (97.52%).

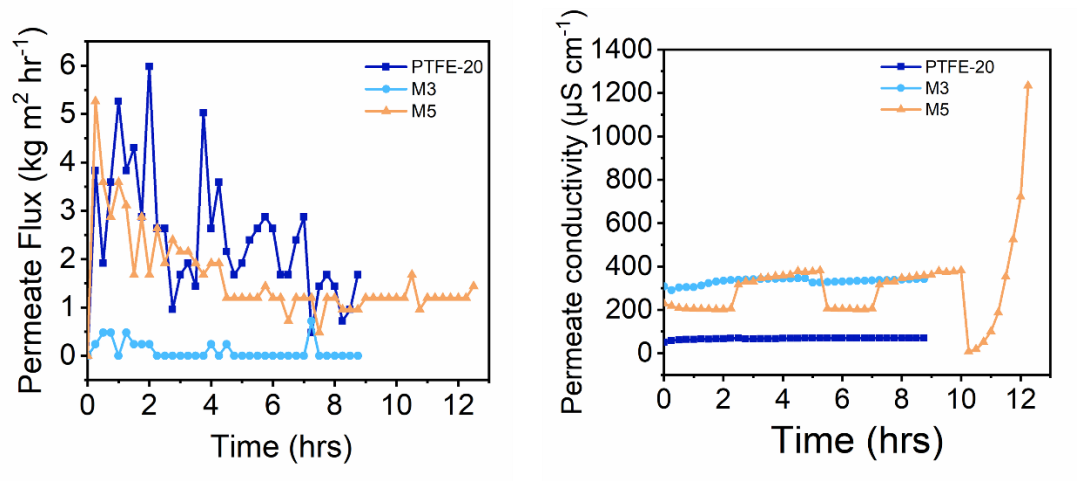

Figure 6.1: (**A1)** Permeate flux plots for all three membranes and (**A2)** their corresponding conductivity profiles.

6.3.3 Crystal analysis

6.3.3.1 Microscopic imagery

Upon saturation of the feed solution, crystal formation was assessed under the microscope (**Figures 6.2 A-C)**. Microscope imagery was employed to visualise the formation of crystals as the solution gradually reached supersaturation. Micrographs obtained using PTFE-20 (**Figure 6.2 A**) presented needle-like crystals with possible elongation with longer process duration (t = 4 hrs). Based on the microscope image, the number of crystals forming increased linearly with time (**Figures 6.2 B&C)**. Moreover, **Figure 6.2 B** provided evidence that although M3 exhibited poor MDC performance, it was still able to encourage some crystal formation in the initial stages of the experiment. Similarly, the crystals produced by M3 and M5 also appear to be elongated and needle-like in structure when compared to those produced by PTFE-20.

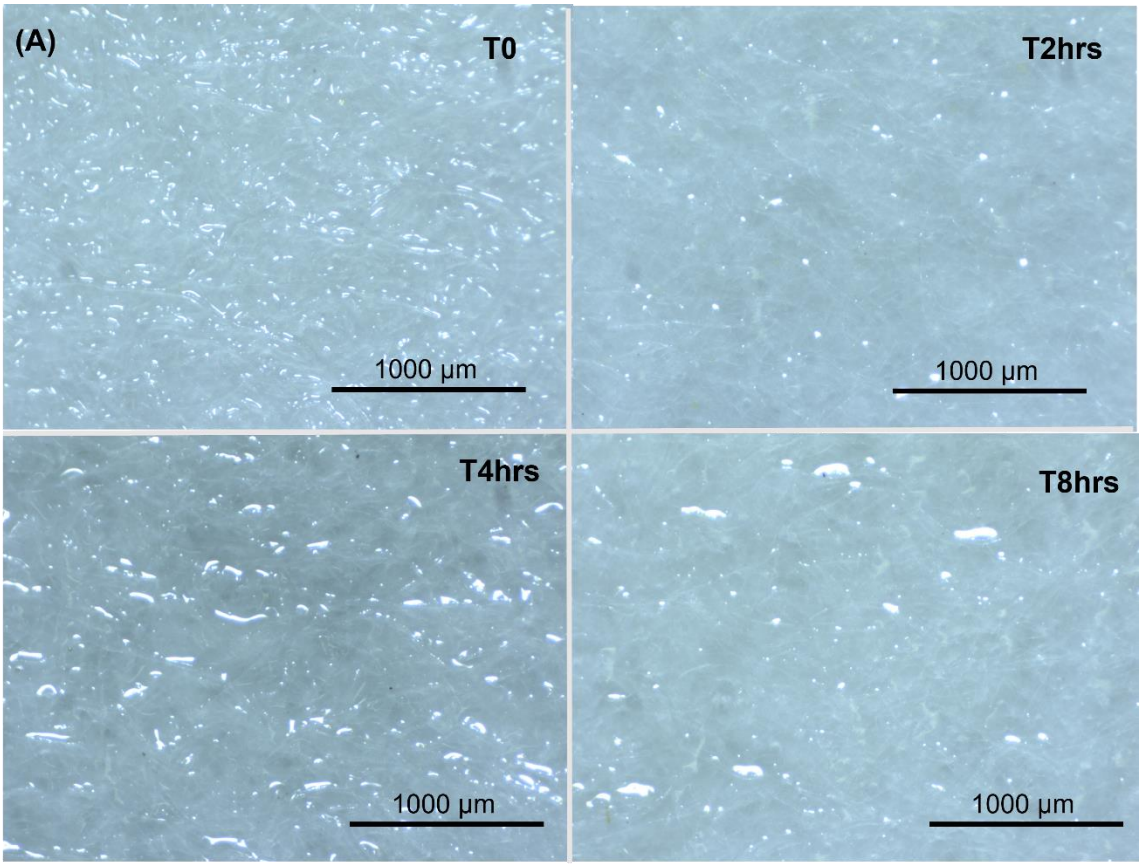
(A)
T0
1000 µm
T2hrs
1000 µm
T4hrs
1000 µm
T8hrs
1000 µm

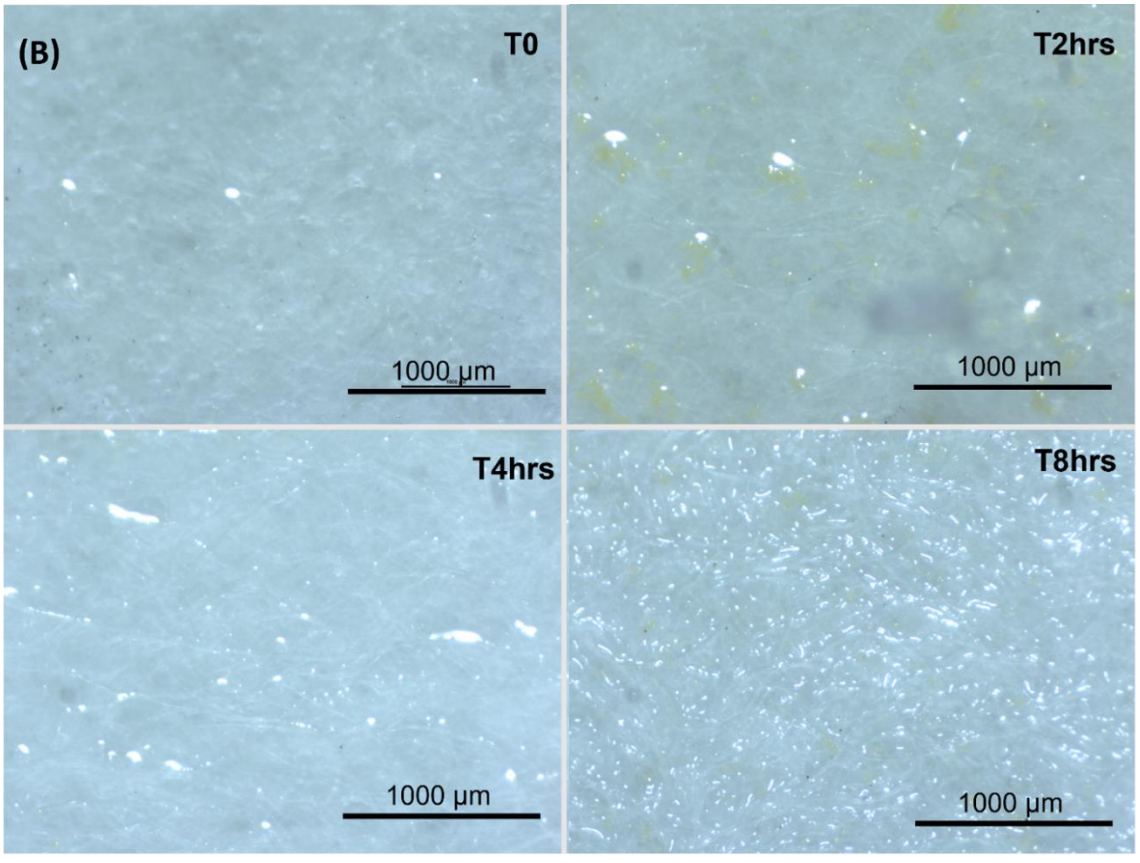
(B)
T0
1000 µm
T2hrs
1000 µm
T4hrs
1000 µm
T8hrs
1000 µm

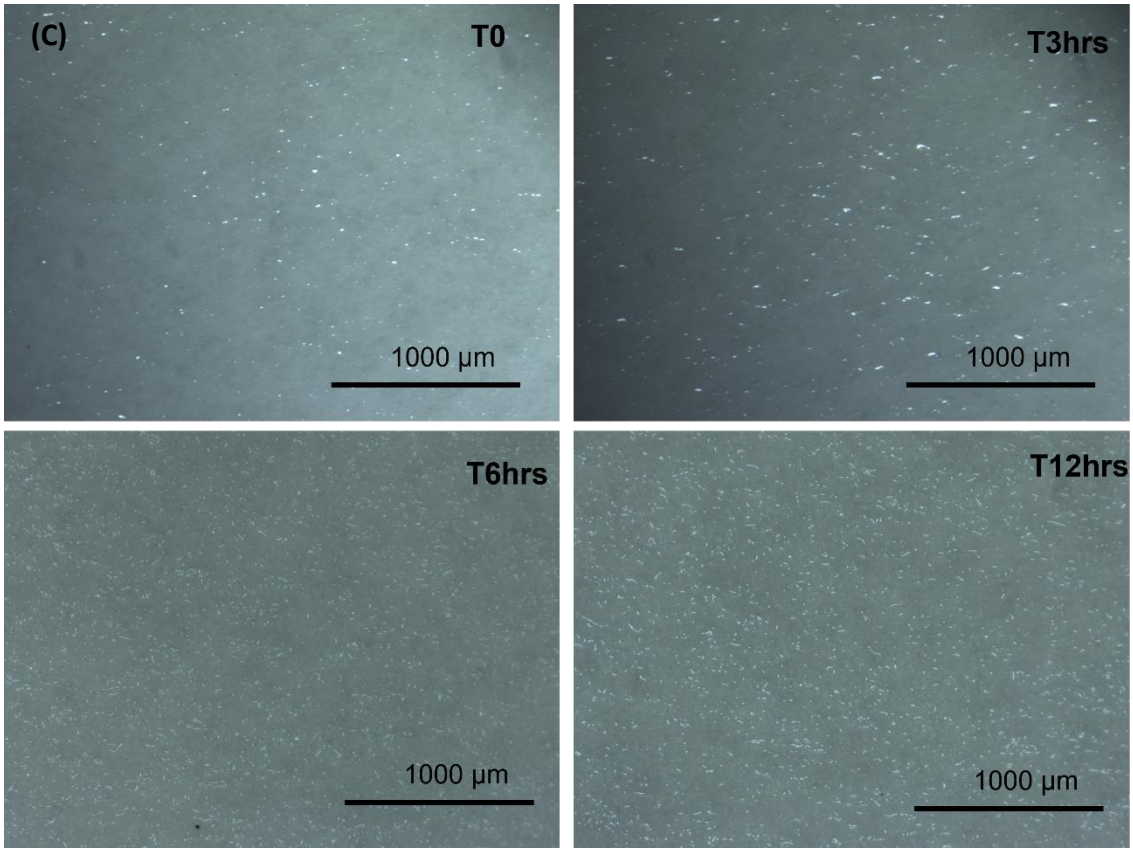

Figure 6.2: Micrographs depicting crystal development during MDC using membranes **(A)** PTFE-20, **(B)** M3, and **(C)** M5.

Figure 6.3 below presents SEM micrographs of the obtained crystals. The PTFE-20 and M4 membranes produced crystals of varying sizes with a cubic-like crystal structure. Similar findings were reported by Choi et al. (2018). However, XRD presented minor differences in crystallinity of the obtained minerals for M4 and PTFE-20 (**Table 6.5)**. Small changes in the morphology and crystal structure between the two products could be attributed to chemical reaction or physical factors (such as agitation speed) (Choi *et al.*, 2018). Notably, crystals were not formed upon use of M3. This confirmed that the solid product remaining when using M3 was undissolved salts and not the product of crystals formed at supersaturation.

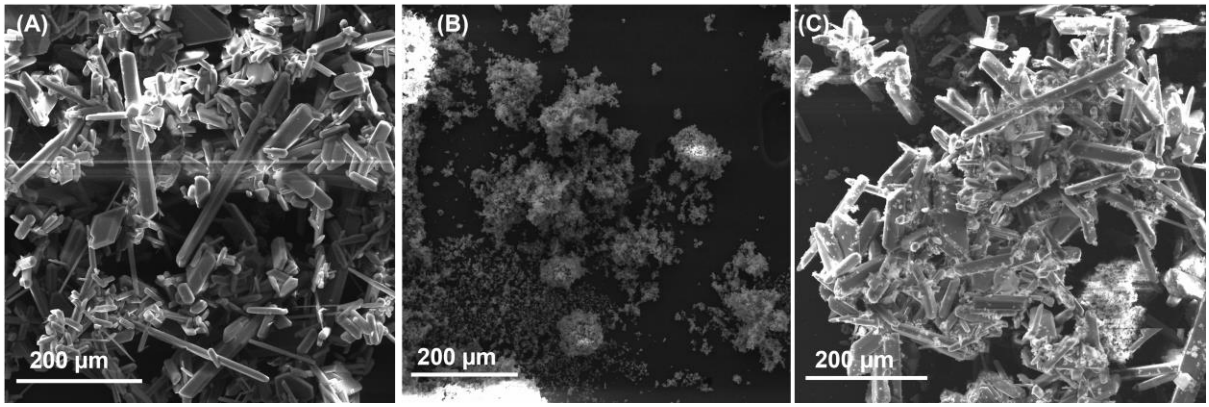

Figure 6.3: SEM micrographs showing crystal morphology following MDC tests using **(A)** PTFE-20, **(B)** M3, and **(C)** M5.

6.3.3.2 Crystal structure refinement and identification

Single crystal x-ray diffraction (XRD) was used to assess the type of minerals produced for each membrane. The solid products analysed were produced using PTFE-20 and M4. The dominating produced mineral was gypsum ($CaSO_4.2H_2O$). The crystal structures and crystallographic information of gypsum are presented in **Figure 6.4** and **Table 6.4**, respectively. Interestingly, gypsum produced from each membrane was monoclinic with the C2/c space group. Similar findings were reported by Nazzareni *et al.*, (2010). Additional experimental crystallographic information pertinent to this study may be found in the supplementary data **(Table A3).**

6.4: Crystallographic information for gypsum obtained with PTFE-20 and M5.

Crystal data	**PTFE-20**	**M5**
Empirical formula	CaH_4O_6S	CaH_4O_6S
Formula weight	172.17	172.17
Temperature (K)	173.00	173.00
Crystal system	monoclinic	monoclinic
Space group	C2/c	C2/c
a (Å)	6.2633 (3)	6.2626 (6)
b (Å)	15.1323 (8)	15.1313 (12)
c (Å)	5.6715 (3)	5.6692 (4)
α (°)	90	90
β (°)	490.25	114.201 (3)

γ (°)	90	90

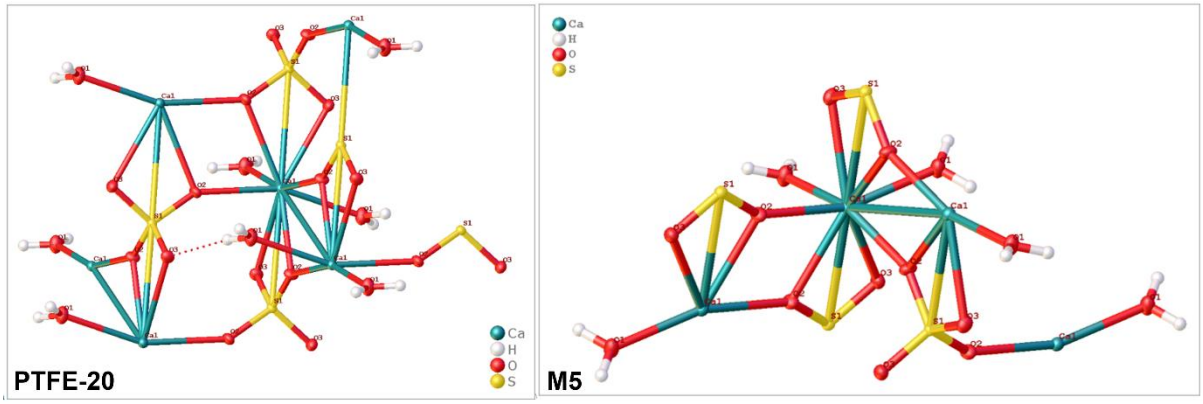

Figure 6.4: Crystal structures of gypsum produced with PTFE-20 and M5, respectively.

6.3.3.3 Powder x-ray diffraction (PXRD)

Powder x-ray diffraction (PXRD) data was used to identify mineral products. This technique was used in conjunction to single crystal XRD because some of the solid product was present in a powder form. This was used to characterise the undissolved solid product of M3. The experimental powder patterns for each membrane may be seen in **Figure 6.5 A-C**. When matching the experimental pattern to those found in databases **(Figure A7)**, it could be seen that PTFE-20 produced gypsum ($CaSO_4.2H_2O$) and M3 produced hydronium jarosite ($(H_3O)Fe^{3+}_3(SO_4)_2(OH)_6$). The data obtained for PTFE-20 corroborated that produced in **Table 6.5.** In addition to producing gypsum single crystals, M5 produced an array of minerals that were identified as 29.66% arcanite (K_2SO_4), 21.77% cobalt sulfate (VI), 1.55% halite (NaCl), 12.71% iron (III) sulfate ($Fe_2(SO_4)_3$, monoclinic), 32.84% mikasite ($Fe_2(SO_4)_3$, rhombohedral), 0.79% nickel sulfate ($NiSO_4$), and 0,65% zinkosite ($ZnSO_4$). This information suggested that the use of M5 could produce a variety of minerals from an MDC set-up. The differences calculated between the experimental pattern and the database patterns could be attributed to noise signals.

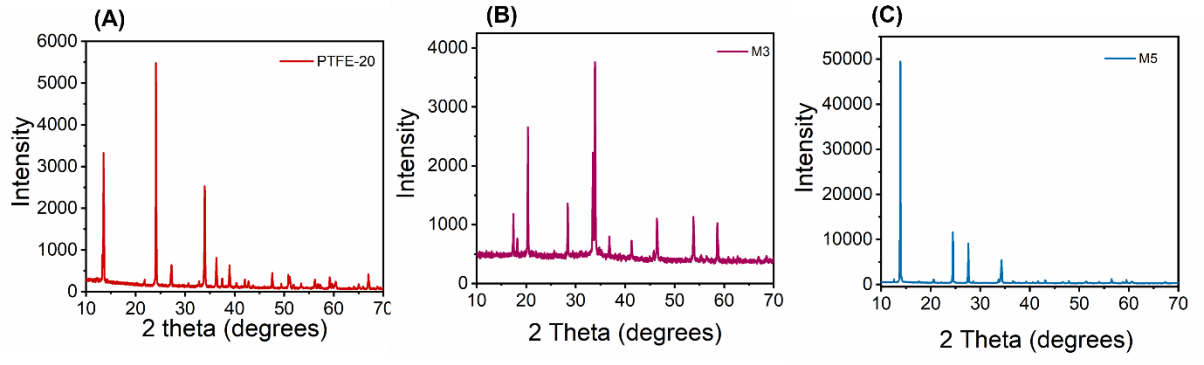

Figure 6.5: Experimental PXRD patterns for using (A) PTFE-20, (B) M3, and (C) M5.

6.3.4 Membrane deposition

Surface deposition in MDC application studies was inevitable and thus understanding its impact on membrane performance at the onset and development is imperative (Chimanlal *et al.*, 2022). Electron microscopy was used to evaluate salt deposition on the surface of the membranes (**Figure 6.6**). Furthermore, EDS graphs presented elemental composition of the deposition layer (**Figure 6.7**). As seen on **Figure 6.6,** the assessed membranes were characterised by a cake layer on the membrane surface. Moreover, these findings were corroborated by EDS analysis which depicts the presence of the feed elements on the membrane surface (**Figure 6.7 A-C**). Notably, the elements that were present at high concentrations such as potassium and iron were present on all EDS spectra. Traces of Au and C from the EDS spectra were due to the membrane coating and membrane additives during SEM preparation. These results provide further substantiation for the deteriorated membrane performance over time as shown in **Figure 6.1 (MDC flux graphs)** above. Notably, calcium is absent from the EDS spectra which indicates that the scaling was not the cause for a decline in the membrane performance. This is because calcium salts are commonly the cause for scaling in membrane processes (Alkhatib, Ayari and Hawari, 2021). Membrane fouling, as a consequence of the feed solution (Yao *et al.*, 2020) may have been a contributing factor toward permeate flux decline. The mechanism for flux decline due to deposition may have been due to pore blockage which may have occurred at the entrance of the pore or within the pores (Choi *et al.*, 2020). In an earlier report, researchers observed a deposition layer on the membrane surface. The cause thereof was ascribed to a decline in the feed velocity to the critical fouling velocity (Zhao *et al.*, 2013). Moreover, previous literature has reported considerable deposition layers were observed which also led to an 18% reduction in the mean pore size (Guillen-Burrieza *et al.*, 2014).

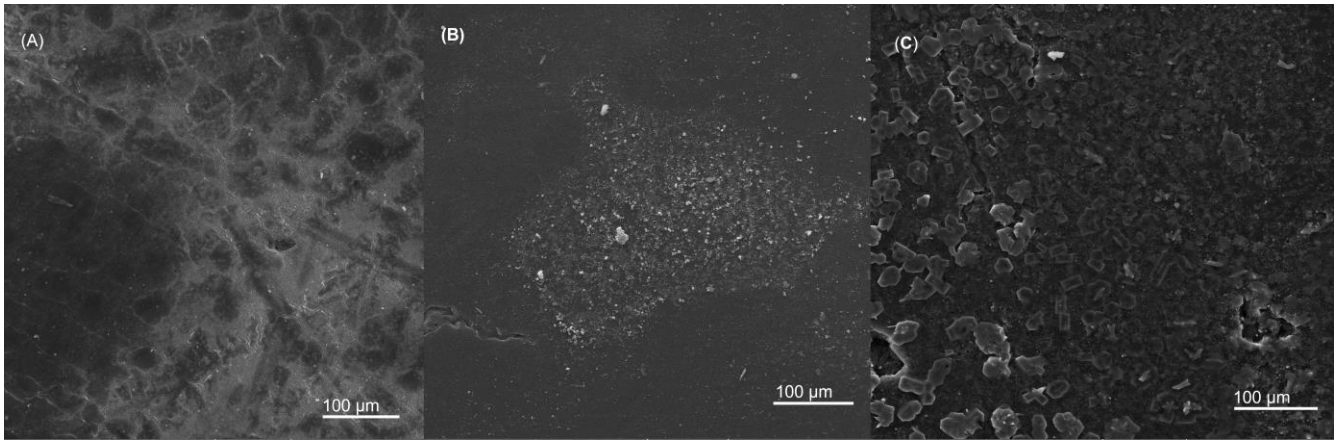

Figure 6.6: SEM micrographs depicting deposition on the membrane surface of **(A)** PTFE-20, **(B)** M3, and, **(C)** M5.

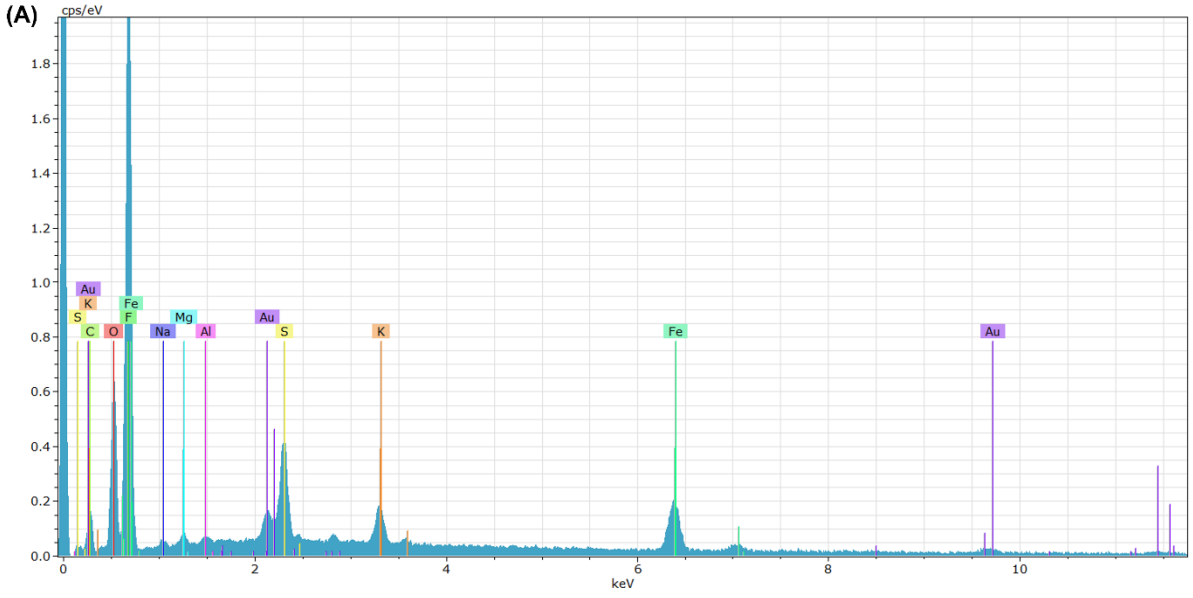

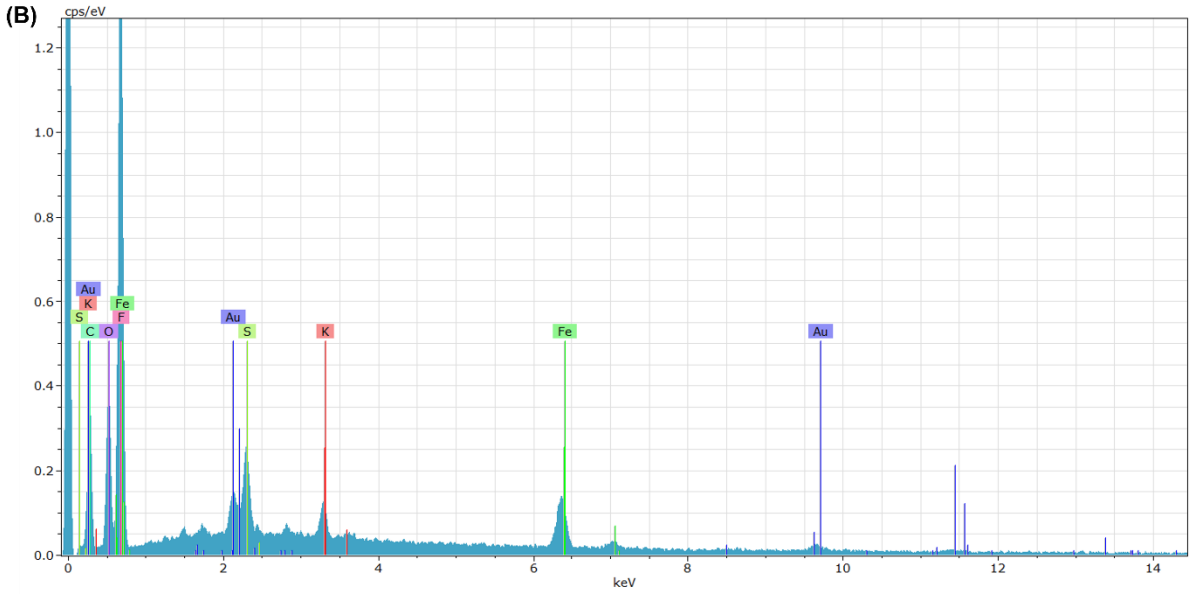

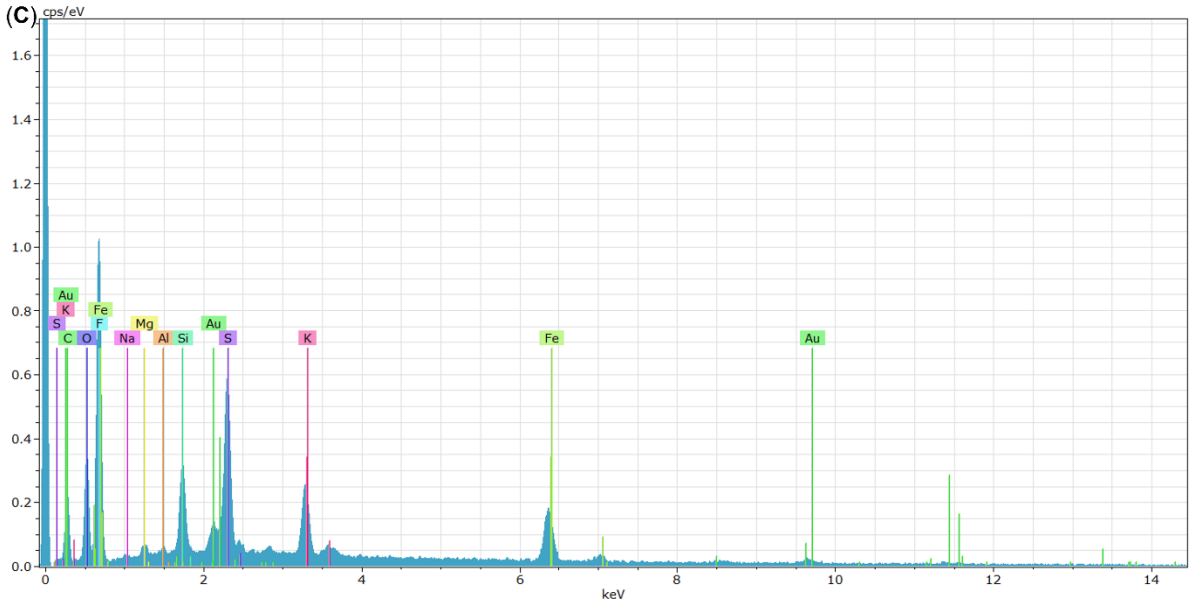

Figure 6.7: EDS spectra showing the elemental composition of membrane fouling deposition on **(A)** PTFE-20, **(B)** M3, and, **(C)** M5.

6.4 Conclusion

The feasibility of synthesised PVDF-modified membranes was evaluated for the recovery of freshwater and minerals from AMD in MDC. M5, containing functionalised nanoparticles (CNTs and SiO_2NPs) had an average permeate flux of 1.459 kg m^{-2} hr^{-1} after 12.5 hrs. Comparatively, a commercial membrane, PTFE-20, achieved an average flux of 2.426 kg m^{-2} hr^{-1}. Additionally, M3 (only containing functionalised CNTs) presented the poorest performance and did not attain supersaturation. Moreover, PXRD analysis revealed that PTFE-20 produced gypsum, while M5 produced an array of mineral salts. These include cobalt sulphate, halite, and iron (III) sulphate, among others. Although M3 was unable to reach supersaturation it could encourage precipitation in the early stages of the experiment as seen from microscopy images. The use of this membrane produced undissolved salts characterised as hydronium jarosite. Its poor performance was a consequence of membrane structural damage and foulant deposition. Nonetheless, SEM micrographs revealed some deposition on the membrane surface which confirmed the susceptibility of all membranes to fouling during MDC application. Nevertheless, the incorporation of nanoparticles into the membrane matrix afforded a satisfactory performance of M5 in MDC. However, further investigation into the longevity of the membrane's performance is required as slight membrane wetting was

responsible for an increased distillate conductivity. This study provided further motivation for the use of nanoparticles to enhance membrane performance. Additionally, this study provided evidence for the use of MDC toward the treatment of AMD which has not been widely researched yet. Furthermore, this provided evidence that MDC and PVDF membranes can treat highly acidic wastewater, which provides groundwork for the application of real samples. Future recommendations include an investigation into properties such as critical fouling velocity and critical feed temperature as it pertains to fouling. Lastly, application with real environmental samples is encouraged as it would afford the deployment of this technology in industrial settings.

References

Akcil, A. and Koldas, S. (2006) 'Acid Mine Drainage (AMD): causes, treatment and case studies', *Journal of Cleaner Production*, 14(12), pp. 1139–1145. doi: https://doi.org/10.1016/j.jclepro.2004.09.006.

Alegbe, M. J. *et al.* (2019) 'Physicochemical characteristics of acid mine drainage , simultaneous remediation and use as feedstock for value added products', *Journal of Environmental Chemical Engineering*, 7(3), p. 103097. doi: 10.1016/j.jece.2019.103097.

Ali, A. *et al.* (2015) 'Application of membrane crystallization for minerals' recovery from produced water', *Membranes*, 5(4), pp. 772–792. doi: 10.3390/membranes5040772.

Alkhatib, A., Ayari, M. A. and Hawari, A. H. (2021) 'Fouling mitigation strategies for different foulants in membrane distillation', *Chemical Engineering and Processing - Process Intensification*, 167(June), p. 108517. doi: 10.1016/j.cep.2021.108517.

Anekwe, S. and Isa, Y. M. (2023) 'Bioremediation of acid mine drainage – Review', *Alexandria Engineering Journal*, 65, pp. 1047–1075. doi: 10.1016/j.aej.2022.09.053.

Bruker (2021) 'APEX4version 2021.4-1 data collection software which includes SAINT version 8.40B, SADABS-2016/2 and XPREP version 2014/2.' Madison, Wisconsin, USA: Bruker AXS Inc.

Chimanlal, I. *et al.* (2022) 'Membrane distillation crystallization for water and mineral recovery : The occurrence of fouling and its control during wastewater treatment', *Frontiers in Chemical Engineering*, (November), pp. 1–14. doi: 10.3389/fceng.2022.1066027.

Chimanlal, I., Lesaoana, M. and Richards, H. (2022) 'Chemical modification of Macadamia - derived activated carbon for remediation of selected heavy metals from wastewater', *Minerals Engineering*, 184(May), p. 107663. doi: 10.1016/j.mineng.2022.107663.

Chimanlal, I. *et al.* (2023) 'Nanoparticle-Enhanced PVDF Flat-Sheet Membranes for Seawater Desalination in Direct Contact Membrane Distillation', *Membranes*. doi: 10.3390/membranes13030317.

Choi, Y. *et al.* (2018) 'Effect of chemical and physical factors on the crystallization of calcium sulfate in seawater reverse osmosis brine', *Desalination*, 426(June 2017), pp. 78–87. doi: 10.1016/j.desal.2017.10.037.

Choi, Y. *et al.* (2020) 'Recovery of sodium sulfate from seawater brine using fractional submerged membrane distillation crystallizer', *Chemosphere*, 238, p. 124641. doi: 10.1016/j.chemosphere.2019.124641.

Cossu, R. *et al.* (2018) 'How can the role of leachate on nitrate concentration and groundwater quality be clarified? An approach for landfills in operation (Southern Italy)', *Waste Management*, 77, pp. 156–165. doi: https://doi.org/10.1016/j.wasman.2018.05.014.

Dhamsaniya, M. *et al.* (2022) 'A review of the techniques for treating the landfill leachate', *Materials Today: Proceedings*. doi: https://doi.org/10.1016/j.matpr.2022.11.496.

Dolomanov, O. V *et al.* (2009) 'OLEX2: a complete structure solution, refinement and analysis program', *Journal of applied crystallography*, 42(2), pp. 339–341.

Edwie, F. and Chung, T.-S. (2013) 'Development of simultaneous membrane distillation–crystallization (SMDC) technology for treatment of saturated brine', *Chemical Engineering Science*, 98, pp. 160–172. doi: 10.1016/j.ces.2013.05.008.

Egashira, R., Tanabe, S. and Habaki, H. (2012) 'Adsorption of heavy metals in mine wastewater by Mongolian natural zeolite', *Procedia Engineering*, 42, pp. 49–57. doi: https://doi.org/10.1016/j.proeng.2012.07.394.

Gaikwad, R. W. and Gupta, D. V. (2008) 'Review on removal of heavy metals from acid mine drainage', *Applied Ecology and Environmental Research*, 6(3), pp. 79–96. doi: 10.15666/aeer/0603_081098.

Gitari, W. M. *et al.* (2008) 'Utilization of fly ash for treatment of coal mines wastewater: Solubility controls on major inorganic contaminants', *Fuel*, 87(12), pp. 2450–2462. doi: 10.1016/j.fuel.2008.03.018.

Greve, P. *et al.* (2018) 'Global assessment of water challenges under uncertainty in water scarcity projections', *Nature Sustainability*, 1(9), pp. 486–494. doi: 10.1038/s41893-018-0134-9.

Gryta, M. (2008) 'Fouling in direct contact membrane distillation process', *Journal of Membrane Science*, 325(1), pp. 383–394. doi: 10.1016/j.memsci.2008.08.001.

Guillen-Burrieza, E. *et al.* (2014) 'Membrane fouling and cleaning in long term plant-scale membrane distillation operations', *Journal of Membrane Science*, 468, pp. 360–372. doi: 10.1016/j.memsci.2014.05.064.

Jiang, X. *et al.* (2016) 'Membrane assisted cooling crystallization: Process model, nucleation, metastable zone, and crystal size distribution', *AIChE Journal*, 62(3), pp. 829–841. doi: https://doi.org/10.1002/aic.15069.

Kijjanapanich, P. *et al.* (2014) 'Chemical sulphate removal for treatment of construction and

demolition debris leachate', *Environmental Technology*, 35(16), pp. 1989–1996. doi: 10.1080/09593330.2014.889219.

Lu, D. *et al.* (2017) 'Simultaneous Recovery and Crystallization Control of Saline Organic Wastewater by Membrane Distillation Crystallization', *AlChE Journal*, 63(6). doi: 10.1002/aic.

Nazzareni, S. *et al.* (2010) 'The crystal structure of gypsum-II determined by single-crystal synchrotron X-ray diffraction data', *American Mineralogist*, 95(4), pp. 655–658. doi: 10.2138/am.2010.3452.

Nthunya, L. N. *et al.* (2019) 'A review of nanoparticle-enhanced membrane distillation membranes : membrane synthesis and applications in water treatment', *Chemical Technology and Biotechnology*, 94(9), pp. 2757–2771. doi: 10.1002/jctb.5977.

Olatunji, S. O. and Camacho, L. M. (2018) 'Heat and Mass Transport in Modeling Membrane Distillation Configurations : A Review', 6(December), pp. 1–18. doi: 10.3389/fenrg.2018.00130.

Ondrasek, G. and Rengel, Z. (2021) 'Environmental salinization processes: Detection, implications & solutions', *Science of the Total Environment*, 754, p. 142432. doi: 10.1016/j.scitotenv.2020.142432.

Pinetown, K. L., Ward, C. R. and van der Westhuizen, W. A. (2007) 'Quantitative evaluation of minerals in coal deposits in the Witbank and Highveld Coalfields, and the potential impact on acid mine drainage', *International Journal of Coal Geology*, 70(1), pp. 166–183. doi: https://doi.org/10.1016/j.coal.2006.02.013.

Sheldrick, G. (2015a) 'Crystal structure refinement with SHELXL', *Acta Crystallographica Section C*, 71(1), pp. 3–8. Available at: https://doi.org/10.1107/S2053229614024218.

Sheldrick, G. (2015b) 'SHELXT - Integrated space-group and crystal-structure determination', *Acta Crystallographica Section A*, 71(1), pp. 3–8. Available at: https://doi.org/10.1107/S2053273314026370.

Skousen, J. G., Ziemkiewicz, P. F. and McDonald, L. M. (2019) 'Acid mine drainage formation, control and treatment: Approaches and strategies', *Extractive Industries and Society*, 6(1), pp. 241–249. doi: 10.1016/j.exis.2018.09.008.

Sparenberg, M. C., Ruiz Salmón, I. and Luis, P. (2020) 'Economic evaluation of salt recovery from wastewater via membrane distillation-crystallization', *Separation and Purification Technology*, 235(April 2019), p. 116075. doi: 10.1016/j.seppur.2019.116075.

Stein, S., Michael, H. A. and Dugan, B. (2021) 'Injection of desalination brine into the saline part of the coastal aquifer; environmental and hydrological implications', *Water Research*, 207(August), p. 117820. doi: 10.1016/j.watres.2021.117820.

Uddin, A. H. *et al.* (2016) 'Comparative study of three digestion methods for elemental analysis in traditional medicine products using atomic absorption spectrometry', *Journal of Analytical Science and Technology*, 7(1). doi: 10.1186/s40543-016-0085-6.

Yadav, A., Labhasetwar, P. K. and Shahi, V. K. (2022) ‘Science of the Total Environment Membrane distillation crystallization technology for zero liquid discharge and resource recovery : Opportunities , challenges and futuristic perspectives’, *Science of the Total Environment*, 806, p. 150692. doi: 10.1016/j.scitotenv.2021.150692.

Yao, M. *et al.* (2020) ‘A review of membrane wettability for the treatment of saline water deploying membrane distillation’, *Desalination*, 479(January), p. 114312. doi: 10.1016/j.desal.2020.114312.

Zhao, Z.-P. *et al.* (2011) ‘Concentration of ginseng extracts aqueous solution by vacuum membrane distillation 2. Theory analysis of critical operating conditions and experimental confirmation’, *Desalination*, 267(2), pp. 147–153. doi: https://doi.org/10.1016/j.desal.2010.09.017.

Zhao, Z. P. *et al.* (2013) ‘Water regeneration from human urine by vacuum membrane distillation and analysis of membrane fouling characteristics’, *Separation and Purification Technology*, 118, pp. 369–376. doi: 10.1016/j.seppur.2013.07.021.

CHAPTER 7 – CONCLUSIONS AND RECOMMENDATIONS

In this study, composite PVDF membranes were successfully fabricated and characterized. Furthermore, additives such as fCNTs and fSiO_2NPs were consecutively incorporated to the polymeric membrane to evaluate their contribution to the anti-wettability of these membranes. Moreover, these membranes were examined in parallel against reference commercial PTFE membranes. The WCA and LEP of M4 were 103.61° and 590 kPa, respectively with a decreased average pore size which was consistent with literature. The high LEP of M4 was attributed to its WCA and reduced pore size, thus improving its mass transfer resistance. Furthermore, the composite membrane demonstrated an increased membrane roughness which was linked to its hydrophobic properties. However, it presented a lower tensile strength when compared to the pristine membrane.

Following membrane characterization, these membranes were evaluated using DCMD for water recovery. The feed solution utilized was a 3.5 wt% NaCl solution which mimicked the salt concentrations typical of seawater. These applications were also evaluated at three different feed temperatures (40, 50, and 60 °C). This was done to investigate its effect on vapor pressure and permeate flux output. The permeate flux increased with an increase in the feed temperature, which was attributed to an improved temperature gradient, thereby enhancing the driving force of this technology. This was corroborated by temperature gradient profiles (dT vs time) whereby a higher feed temperature produced a greater driving force. For example, the average permeate flux produced at 40 and 60 °C for M4 was 19,88 and 39,77 kg m^{-2} hr^{-1}, respectively. In addition, permeate conductivity was also monitored during the experimental time. The conductivity showed slight increases over time which was ascribed to slight membrane wetting. Wetted membranes promoted water passage in a liquid state, therefore, allowing a transfer of dissolved salts. Nonetheless, the slight membrane wetting was negligible and did not negatively impact membrane performance as a 99% salt rejection was still produced.

In comparison to the average permeate flux produced with M1 (14,20 kg m^{-2} hr^{-1}), M4 produced a superior permeate flux which was largely due to the incorporation of membrane additives. Moreover, M3 which only contained fCNTs produced a permeate flux of 22,69 kg m^{-2} hr^{-1} which exceeded that of M1 but was lower than that of M4. The difference was explained by the addition of fSiO_2NPs. The addition of fSiO_2NPs provided a superior membrane performance which was realized by the flux improvement as compared to fCNTs.

In tandem with the DCMD application, membrane distillation crystallization (MDC) was carried out to investigate membrane performance for mineral and freshwater recovery using synthetic AMD. M5 produced an average permeate flux of 1,459 kg m^{-2} hr^{-1} whereas M3 showed poor MDC performance. This was largely due to structural damage and membrane deposition. Moreover, due to its poor performance, it was unable to attain supersaturation and thus could not produce mineral salts. M5 was able to produce both single gypsum crystals and a mixture of powdered crystals. However, SEM/EDX analysis revealed that all membranes suffered membrane deposition which reduced membrane performance.

The addition of fSiO_2NPs considerably improved membrane performance both in DCMD and MDC. Moreover, this study substantiated the necessity for membrane fabrication and modification as it provided an avenue to manipulate membrane properties and investigate the effect of various nanoparticles. In addition, MDC application with synthetic AMD showed the potential of M5 to treat environmental AMD. The successful application of these membranes in DCMD and MDC provided motivation for the use of this technology to treat environmental samples and proved that MDC technologies can treat a variety of feed solutions regardless of their concentrations. Further recommendations include the improvement of the anti-wettability of composite membranes either by incorporating additional hydrophobic particles or by improving the hydrophobicity of SiO_2NPs. This could be achieved by functionalizing the SiO_2NPs with other hydrophobic agents. Furthermore, an improvement in synthetic membrane properties to improve process performance is recommended. Lastly, application with real environmental solutions is recommended as this would provide key information about the suitability of this technology in an industrial setting to alleviate environmental pollution issues.

Appendix

This section includes supplementary information for articles 2 and 3 reported in Chapters Five and Six, respectively.

Appendix for Chapter Five

A1 Fourier transform infrared (FTIR) analysis of the NPs and membranes

A1.1 The FTIR analysis of the nanoparticle additives

The FTIR spectra of SiO_2NPs and fSiO_2NPs are presented in **Figure A1 (A)**. A peak at 1454.23 cm^{-1} was associated with a Si-N stretch contributed by silica and nitrogen reaction from ammonium hydroxide. The appearance of a strong band at 1027.99 cm^{-1} and a medium band at 783.05 cm^{-1} was attributed to a Si-O-Si stretch and bend, respectively. A peak at 1602.74 cm^{-1} was assigned to an -OH bend caused by the physical absorption of water (Cai *et al.*, 2018). In addition to this, a medium band at 933.48 cm^{-1} was associated to the Si-OH bend. The absorption of water evidenced by a weak, broad peak at 3284.55 cm^{-1} was ascribed to an -OH stretch. Notably, the spectra for the SiO_2NPs and fSiO_2NPs did not display significant structural variation. This is because the SiO_2NPs were physically modified with no chemical reaction. Thus, the coating process did not alter the chemical properties of the SiO_2NPs but rather changed particle size as evidenced by the TEM micrographs. **Figure A1 (B)** presents the FTIR spectra of the CNTs. However, the spectra did not show significant differences to fCNTs. Notably, a peak at 1582.04 cm^{-1} and 1487.08 cm^{-1} represented an O-H bend due to chemically absorbed water (Gao *et al.*, 2020), and a CH_2 bend respectively. Gao *et al.* (2020) reported some differences in NP spectra caused by flourination. In their spectra, the appearance of the peaks at 1080 and 1270 cm^{-1} were referred to as Si-O-Si and C-F bands, respectively (Gao *et al.*, 2020). Minor differences were caused by the small addition of silane reagents leading to insignificant fluorination. Though a small addition of silane reagents reduces the production cost of modified CNTs, required properties such as hydrophobicity were compromised. Therefore, optimization processes are required to establish a trade-off between production costs and improved process performance during application.

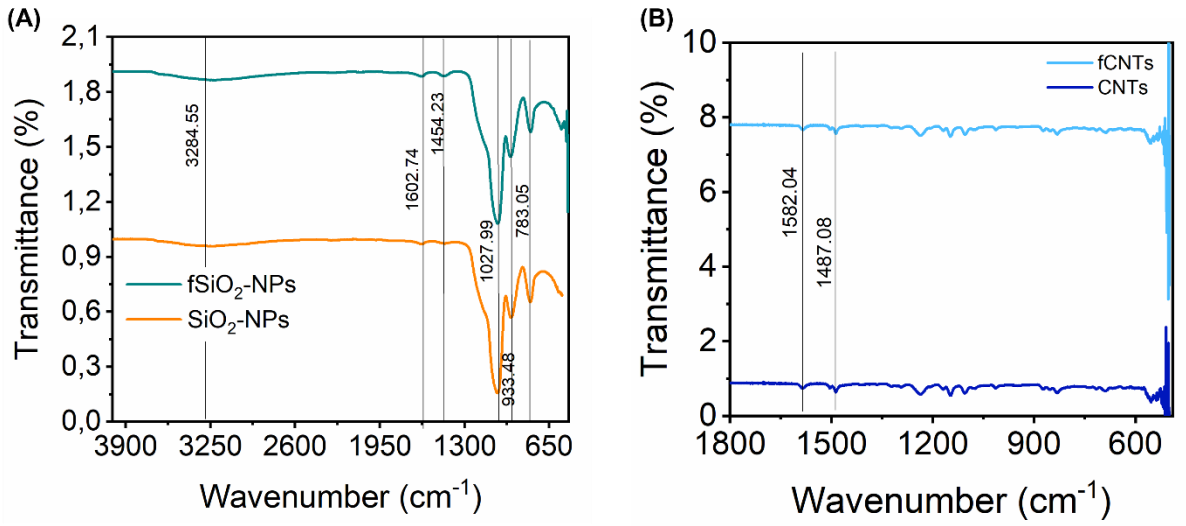

Figure A1: FTIR spectra of unmodified and modified **(A)** SiO_2NPs and **(B)** CNTs.

A1.2 The FTIR analysis of the as-synthesized membranes

FTIR of the as-synthesised and commercial membranes is presented in **Figures A2 (A** and **B)**. The as-synthesised membranes share similar peaks corresponding to bonds characteristic of the PVDF base polymer **(Figure A2 (A))**. The bands at 1398.48 cm^{-1} and 1169.21 cm^{-1} are assigned to C-F stretch, and C-C vibrations. Similar findings were reported by Silva et al. (2015) and Puspitasari et al. (2010). Additionally, bands at 1069.93 – 836.37 cm^{-1} were associated to scissoring vibration of H_2C-CF_2 and CH_2 rocking vibrations, respectively (Puspitasari *et al.*, 2010). Also, the FTIR spectra for M2 – M4 did not vary significantly from that of M1 despite the inclusion of membrane additives due to physical interactions rather than chemical modifications. Upon analyzing PTFE-20, two distinct peaks at 1205.63 and 1149.21 cm^{-1} corresponding to asymmetric and symmetric CF_2 stretching, respectively were observed. In the case of PTFE-45, similar peaks were recorded at 1198.49 and 1146.35 cm^{-1} respectively. Furthermore, peaks appearing range of 640 – 552 cm^{-1} were ascribed to CF_2 wagging and bending vibrations (Wang *et al.*, 2018).

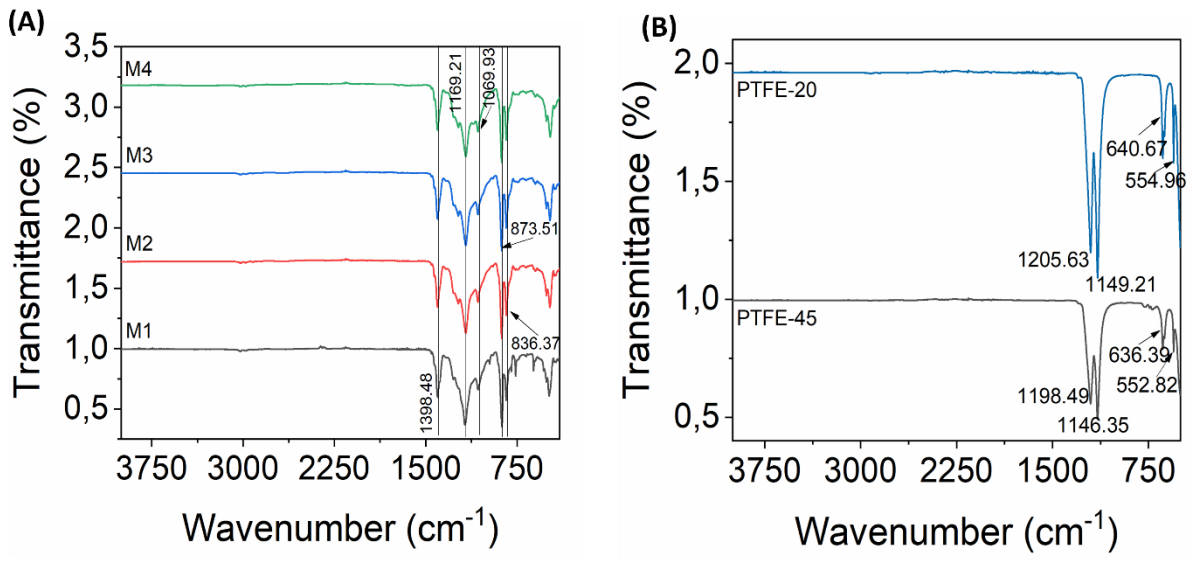

Figure A2: FTIR spectra obtained for **(A)** all synthesised membranes (M1 – M4) and **(B)** commercial membranes (PTFE-20 and PTFE-45).

A1.2 Pure water flux determination in DCMD

Pure water filtration tests were carried out to evaluate MD process performance in the absence of dissolved solutes (**Figure A3).** Evaluations were performed at three different feed temperatures to assess their effect on process performance. The permeate flux (at feed temperature of 40℃) of M1, M2, M3, M4, PTFE-20 and PTFE-45 were 1.89 kg m^{-2} hr^{-1}, 1.26 kg m^{-2} hr^{-1}, 0.63 kg m^{-2} hr^{-1}, 2.21 kg m^{-2} hr^{-1}, 4.42 kg m^{-2} hr^{-1}, and 6.94 kg m^{-2} hr^{-1} respectively. Upon increase the feed temperature to 60℃, the permeate flux increased to 4.10 kg m^{-2} hr^{-1}, 4.73 kg m^{-2} hr^{-1}, 1.89 kg m^{-2} hr^{-1}, 5.05 kg m^{-2} hr^{-1}, 6.62 kg m^{-2} hr^{-1}, and 13.88 kg m^{-2} hr^{-1} respectively. The increase in feed temperature increased vapour pressure gradient resulting high process driving force (Quist-Jensen *et al.*, 2017; Gryta, 2020). Similar findings were reported by Edwie and Chung (2013) at feed temperature range of 40 – 70 ℃. Notably, increased feed temperature does not only improves rate of water recovery, but also the process thermal efficiency (Edwie and Chung, 2013). DeltaT increased significantly upon an increase in feed temperature (**Figure A3 (A2-F2)**), thus translating to the increase in permeate flux (Quist-Jensen *et al.*, 2017). PTFE-45 presented higher flux compared to PTFE-20, thus indicating the role played by the membrane pore size. Also, membrane modifications in order of M1 to M4 presented a progressive increase in permeate flux with some discrepancies for M3. The increased flux at 60 ℃ from M1 (4.10 kg m^{-2} hr^{-1}) to M2 (4.73 kg m^{-2} hr^{-1}) was associated to large pore size caused by incorporation of PVP (a pore former). However, incorporation of fCNTs (M3) caused a decline in water flux (1.89 kg m^{-2} hr^{-1}) due pore

blockage. The M4 presented the highest permeate flux (5.05 kg m^{-2} hr^{-1}) compared to other synthetic membranes. Incorporation of fCNTs and $fSiO_2$NPs improved membrane hydrophobicity significantly, thus minimizing mass transfer resistance by ensuring exclusive vapour transport without competing water molecules in liquid state (Dumée *et al.*, 2013). Moreover, the permeate flux obtained for M4 was relatively comparable PTFE-20, suggesting its promising performances similarly to a commercial membrane.

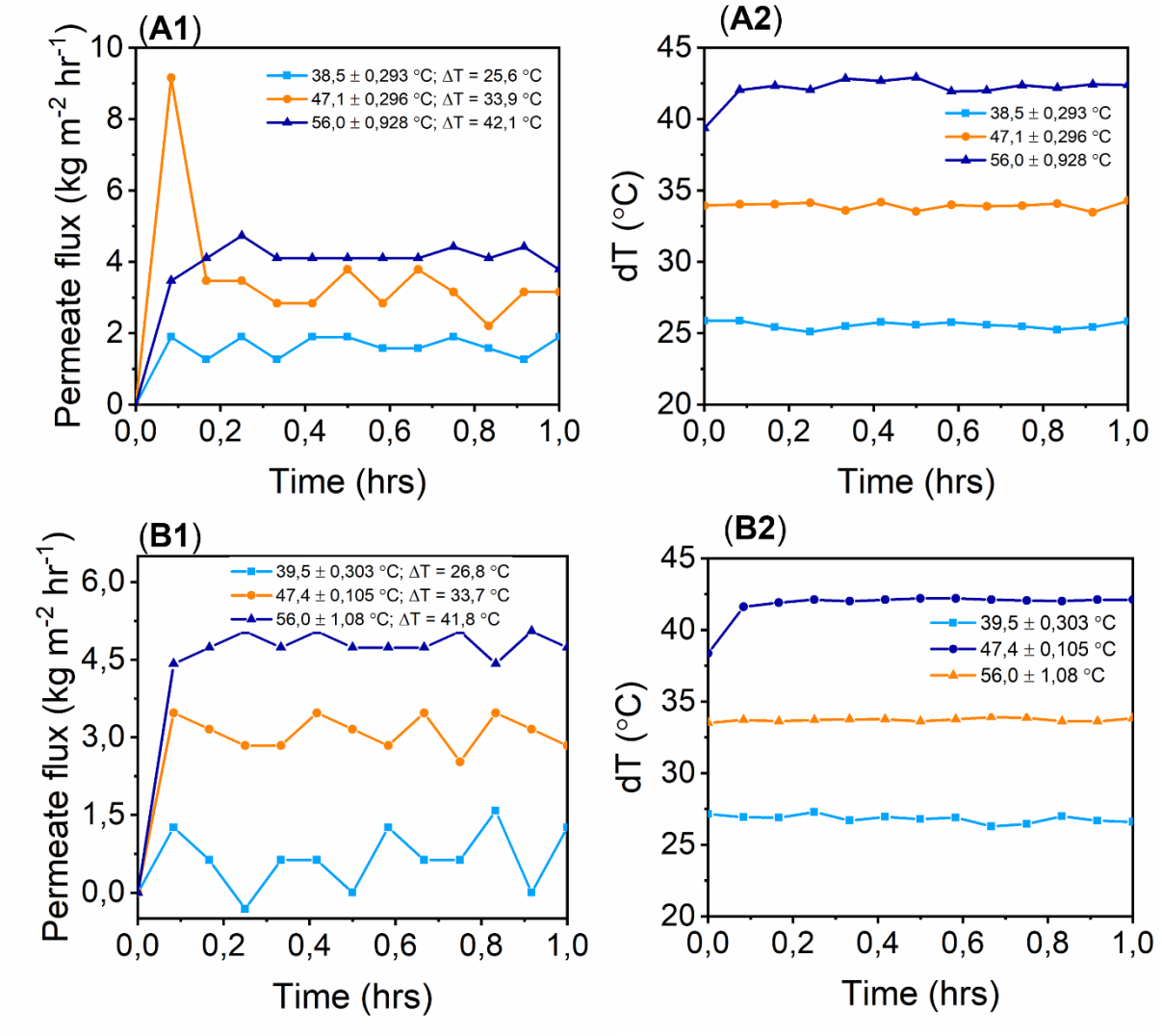

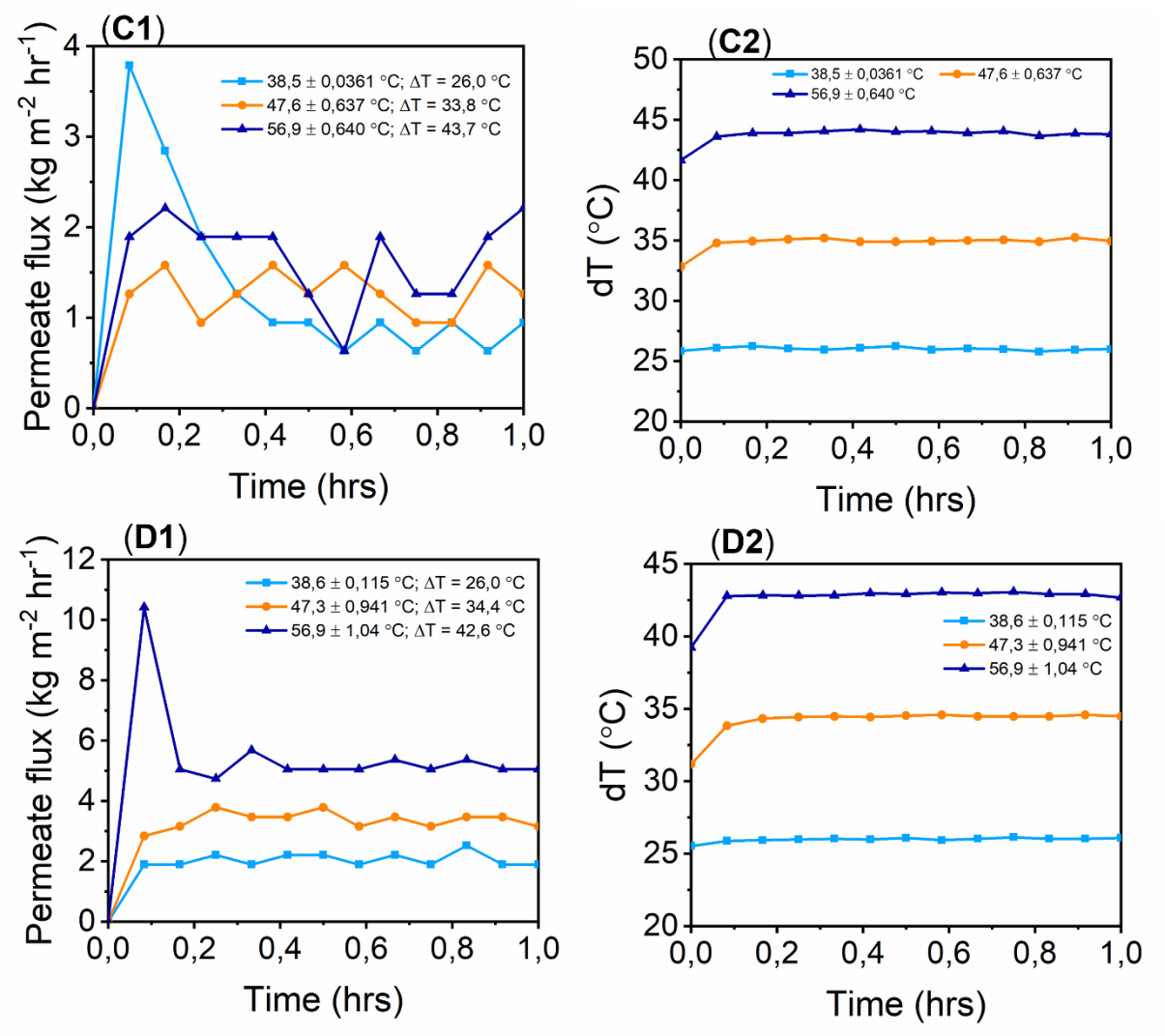
(C1)
Permeate flux (kg m-2 hr-1)
Time (hrs)
38,5 ± 0,0361 °C; ΔT = 26,0 °C
47,6 ± 0,637 °C; ΔT = 33,8 °C
56,9 ± 0,640 °C; ΔT = 43,7 °C
(C2)
dT (°C)
Time (hrs)
38,5 ± 0,0361 °C
47,6 ± 0,637 °C
56,9 ± 0,640 °C
(D1)
Permeate flux (kg m-2 hr-1)
Time (hrs)
38,6 ± 0,115 °C; ΔT = 26,0 °C
47,3 ± 0,941 °C; ΔT = 34,4 °C
56,9 ± 1,04 °C; ΔT = 42,6 °C
(D2)
dT (°C)
Time (hrs)
38,6 ± 0,115 °C
47,3 ± 0,941 °C
56,9 ± 1,04 °C

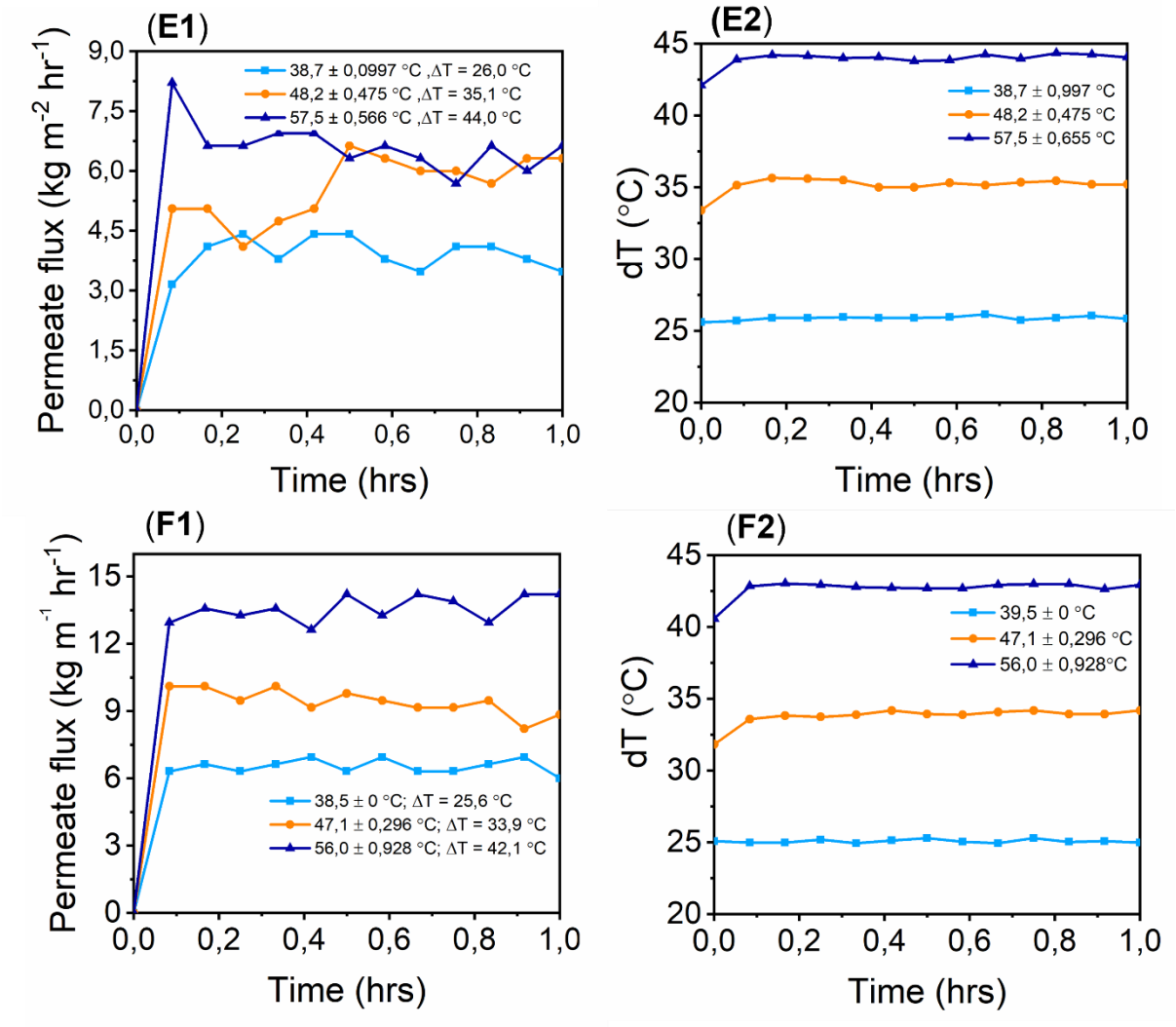

Figure A3: Pure water flux and deltaT vs time at various temperatures for **(A1-A2)** M1, **(B1-B2)** M2, **(C1-C2)** M3, **(D1-D2)** M4, **(E1-E2)** PTFE-20 and **(F1-F2)** PTFE-45.

Appendix for Chapter Six

In this section, the characterization of M5 is provided. This work was compared to that previously reported in **Chapter Five**. Moreover, crystal characterization data is provided which includes single crystal XRD data and PXRD data.

A1.3 Membrane characterization

A1.3.1 Membrane porosity, WCA, and LEP

Physical characteristics were determined for M5, and the results are presented in **Table A1** below. The porosity of this membrane was reported to be 76.58% which was higher than the porosity of M4 with a lower silica content documented previously in **Chapter Five (Table**

5.2). The increased porosity may be attributed to the formation of voids in the membrane structure with an increased concentration of nanoparticle additives (Ding, Liu and Xiao, 2021). However, the WCA and LEP were significantly lower than that reported previously for M4. The lower LEP may be a consequence of irregular pore geometries (Rahimpour and Esmaeilbeig, 2019). Irregular pore geometries mean that the membrane pores may differ in their size, depth, and shape. Therefore, the effect of pore geometry may have surpassed the effect of membrane hydrophobicity. The lower WCA compared to that reported for M4, may have been the consequence of unequal nanoparticle dispersion. Therefore, due to the uncertainty of nanoparticle dispersion, some areas on the membrane may be more hydrophobic than others. However, it was expected that an increased silica content would have significantly improved the membrane hydrophobicity, and its effect would have been realized through these parameters. However, due to time constraints and instrument unavailability, pore size measurements could not be included in this section.

Table A1: Physical characteristics of the membrane, M5 utilized in this study.

Membrane	**Porosity (%)**	**WCA (°)**	**LEP (kPa)**
M5	76.58 ± 1.07	85.84	10 5.24

A1.3.2 Scanning electron microscopy (SEM)

The surface and cross-sectional morphology of M5 utilized in this study is shown in **Figure A4** below. The surface view (**Figure A4 (A)**) of this membrane depicted a relatively smooth surface with irregular surface defects. Furthermore, lighter particles on the surface could be the consequence of the fSiO_2NPs particles added to the membrane. The cross-sectional view of the membrane (**Figure A4 (B)**) illustrates the presence of elongated, finger-like pores along the length of the polymeric structure. These well-defined pores could have derived from the membrane additives as a clear distinction in the internal structure could be seen when compared to a pristine PVDF membrane (**Figure 5.2 A1 and A2).**

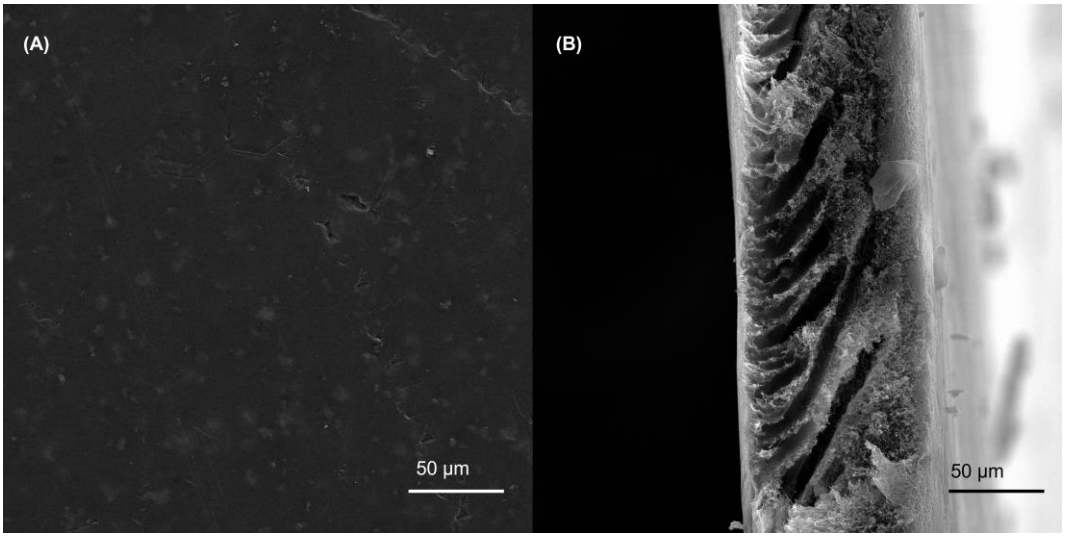

Figure A4: Surface **(A)** and cross-sectional **(B)** of M5 utilized in this study.

A1.3.3 Atomic force microscopy (AFM)

The surface roughness of the synthesized membrane was evaluated with AFM, and the results are shown below in **Figure A5**. This information is indicative of properties such as membrane hydrophobicity, but it may also provide information about membrane fouling, the efficacy of cleaning procedures, and membrane-fouling interactions (Al-Amoudi and Lovitt, 2007). Additionally, this characterization tool may also relay information about nanoparticle dispersion on a polymeric membrane. The root mean square (RMS) roughness of this membrane was found to be 67.86 nm. In previously reported work, M4 displayed an RMS roughness of 129.88 nm which was significantly higher than the pristine PVDF membrane (**Figure 5.3 (A)**). The increased surface roughness was attributed to the contribution of silica nanoparticles. Notably, the surface roughness of M5 was found to be lower than that of M4, despite a higher silica content. However, it was expected that the presence of nanoparticles would increase the surface roughness significantly, therefore the membrane's hydrophobicity. This effect is realized through the formation of macrostructures on the membrane which is caused by the addition of nanoparticles (Rezaei and Samhaber, 2016). The deviation of the experimental results from the effect expected may be due to the dispersion and agglomeration of the nanoparticles on the membrane surface (Hamzah, Leo and Ooi, 2019). Nanoparticle agglomeration and unequal particle dispersion can diminish the effect of the modification such as improving the surface roughness (Berg and Ulbricht, 2020). This may arise due to slight incompatibilities between the polymeric membrane and the nature of the nanoparticles (Kang and Cao, 2014). Moreover, nanoparticle agglomerates increase the particle size which reduces

its surface area and its effective concentration leading to a compromised effect (Berg and Ulbricht, 2020). These factors may have likely contributed to the reduced surface roughness observed despite a higher nanoparticle concentration.

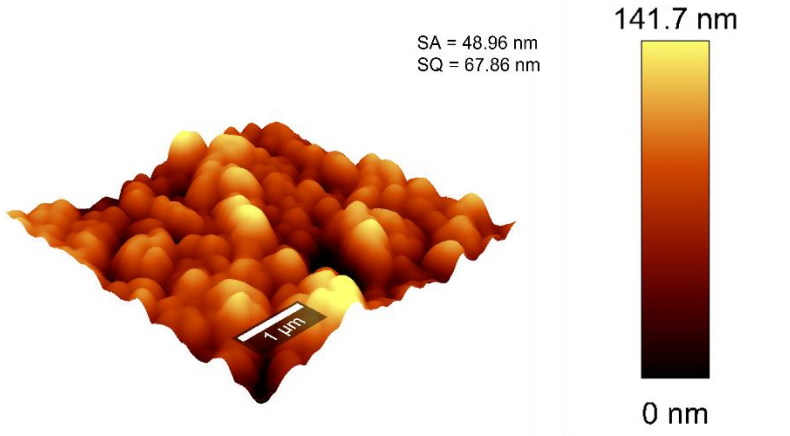

Figure A5: Topographical micrographs evaluating the surface roughness of M5.

A1.3.4 Tensile strength

The mechanical properties were determined for M5 that was employed in this study. The results thereof are represented graphically in **Figure A6** below. The Young's modulus for this membrane was found to be 0.70 ± 0.77 MPa. Compared to the results presented for M4 **(Figure 5.4 (A))**, M5 had a larger Young's modulus compared to M4 which had a Young's modulus of 0.39 ± 0.30 MPa. The increased tensile strength was attributed to the increased silica content as M4 had a lower silica content (3.5 wt%) compared to 7 wt% for M5. These experimental findings were corroborated by that reported previously (Widiyandari *et al.*, 2020). In that study, it was reported that the effect of an increased silica content was realized through an improved mechanical strength (Widiyandari *et al.*, 2020). An improved tensile strength ascribed to the addition of nanoparticles could be associated with the enhanced adeptness of the stress transfer between the nanoparticles and the membrane. Another contributing factor could also be satisfactory interfacial adhesion between the nanoparticles and the membrane (Reddy *et al.*, 2018). Moreover, the tensile strength of M5 was higher than the pristine membrane, M1 (0.45 ± 0.24 MPa), which suggests that the membrane additives contributed to the mechanical strength of the composite membrane. This finding was substantiated by work reported in literature (Rasekh and Raisi, 2021).

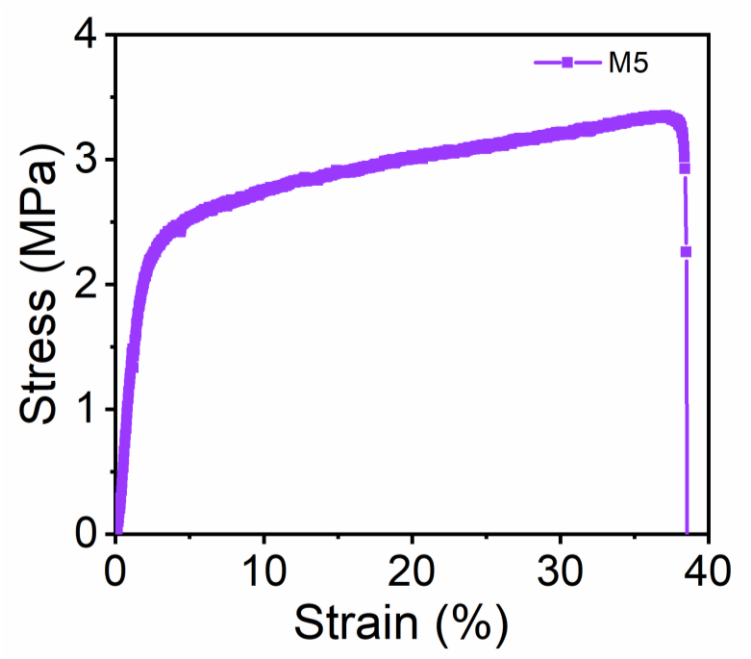

Figure A6: Stress-strain curve for membrane M5.

A1.4 Transition metal analysis

Analyte concentrations for transition metals were obtained using ICP-OES and are reported in **Table A2** below.

Table A2: Concentrations of transition metals from ICP-OES analysis

Sampling area		Transition metals (mg L^{-1})					
		Al^{3+}	Co^{2+}	Fe^{2+}	Mn^{2+}	Ni^{2+}	Zn^{2+}
Leachate A		26.0	BDL	BDL	BDL	BDL	BDL
Leachate B		BDL	BDL	BDL	BDL	BDL	BDL
Co-produced water	Water treatment plant	BDL	BDL	BDL	BDL	BDL	BDL
	Station dirty dam	BDL	BDL	BDL	BDL	BDL	BDL
	Ash dump dam	BDL	BDL	BDL	BDL	BDL	BDL
	Holding dam	BDL	BDL	BDL	101.8 ± 1.6	BDL	1.8 ± 0.1
	FGD blow down	BDL	BDL	BDL	BDL	BDL	BDL
	Clean station dam	BDL	BDL	BDL	BDL	BDL	BDL
	Dirty reclaim dam	BDL	BDL	BDL	BDL	BDL	BDL
	Ash pond	BDL	BDL	BDL	BDL	BDL	BDL
Acid mine drainage	100 m from mine dump	288.2 ± 15.4	32.4 ± 2.4	1210.6 ± 47.5	138.4 ± 3.9	45.7 ± 3.3	69.2 ± 4.7
	200 m from mine dump	30.8 ± 0.3	4.0 ± 0.3	137.0 ± 21.5	126.6 ± 16.3	6.7 ± 0.5	25.9 ± 3.4
	Discharge into Fleurhof dam	20.0 ± 0.6	BDL	11.6 ± 0.5	41.1 ± 1.7	BDL	BDL

A1.5 Crystal characterisation

A1.5.1 Single crystal XRD

Further crystallographic information is provided from single crystal XRD analysis for PTFE-20 and M5 and is shown below in **Table A2**.

Table A2: Additional crystallographic data for gypsum obtained with PTFE-20 and M5.

Crystal data	**PTFE-20**	**M5**
Volume ($Å^3$)	490.25 (4)	490.01 (7)
Z	4	4
ρ_{calc} (g cm^{-3})	2.333	2.334
μ (mm^{-1})	1.648	1.649
F (000)	352.0	352.0
Crystal size (mm^3)	0.379 x 0.084 x 0.077	0.259 x 0.058 x 0.038
Radiation	MoKa (λ = 0.71073)	MoKa (λ = 0.71073)
2Θ range for data collection (°)	5.384 to 56.754	5.384 to 56.554
Index ranges	$-8 \leq h \leq 8$, $-20 \leq k \leq 20$, $-7 \leq l \leq 7$	$-8 \leq h \leq 8$, $-20 \leq k \leq 20$, $-7 \leq l \leq 7$
Reflections collected	4240	8403
Independent reflections	599 [R_{int} = 0.0381, R_{sigma} = 0.0254]	610 [R_{int} = 0.0897, R_{sigma} = 0.0399]
Data/restraints/parameters	599/1/46	610/1/44
Goodness-of-fit on F^2	1.220	1.186
Final R indexes [I>=2σ (I)]	R_1 = 0.0275, wR_2 = 0.0688	R_1 = 0.0330, wR_2 = 0.0854
Final R indexes [all data]	R_1 = 0.0281, wR_2 = 0.0692	R_1 = 0.0353, wR_2 = 0.0889
Largest diff. peak/hole / e $Å^{-3}$	0.41/-0.53	0.33/-0.69

A1.5.2 PXRD analysis

Experimental data obtained using PXRD was compared to those found in databases. The results thereof are displayed in **Figure A7** below.

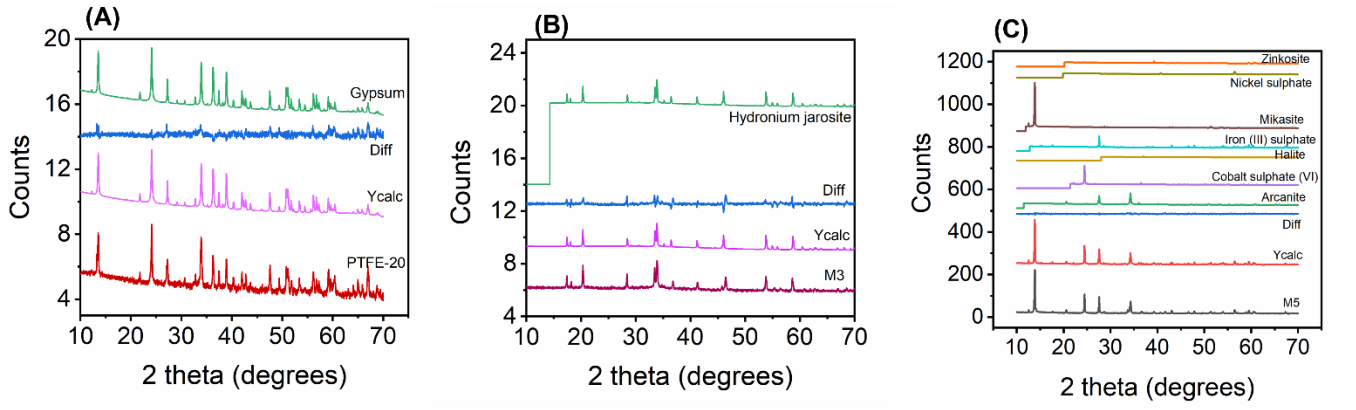

Figure A7: Experimental PXRD patterns with their corresponding databases.

References

Al-Amoudi, A. and Lovitt, R. W. (2007) 'Fouling strategies and the cleaning system of NF membranes and factors affecting cleaning efficiency', *Journal of Membrane Science*, 303(1–2), pp. 4–28. doi: 10.1016/j.memsci.2007.06.002.

Berg, T. van den and Ulbricht, M. (2020) 'Polymer nanocomposite ultrafiltration membranes: The influence of polymeric additive, dispersion quality and particle modification on the integration of zinc oxide nanoparticles into polyvinylidene difluoride membranes', *Membranes*, 10(9), pp. 1–19. doi: 10.3390/membranes10090197.

Cai, Y. *et al.* (2018) 'Applied Surface Science Fabricating superhydrophobic and oleophobic surface with silica nanoparticles modified by silanes and environment-friendly fluorinated chemicals', *Applied Surface Science*, 450, pp. 102–111. doi: 10.1016/j.apsusc.2018.04.186.

Ding, Z., Liu, Z. and Xiao, C. (2021) 'Excellent performance of novel superhydrophobic composite hollow membrane in the vacuum membrane distillation', *Separation and Purification Technology*, 268(October 2020), p. 118603. doi: 10.1016/j.seppur.2021.118603.

Dumée, L. F. *et al.* (2013) 'The role of membrane surface energy on direct contact membrane distillation performance', *Desalination*, 323, pp. 22–30. doi: 10.1016/j.desal.2012.07.012.

Edwie, F. and Chung, T.-S. (2013) 'Development of simultaneous membrane distillation–crystallization (SMDC) technology for treatment of saturated brine', *Chemical Engineering Science*, 98, pp. 160–172. doi: 10.1016/j.ces.2013.05.008.

Gao, C. *et al.* (2020) 'Superhydrophobic Electrospun PVDF Membranes with Silanization and

Fluorosilanization Co-Functionalized CNTs for Improved Direct Contact Membrane Distillation', pp. 35–43. doi: 10.30919/es8d905.

Gryta, M. (2020) 'Separation of saline oily wastewater by membrane distillation', *Chemical Papers*, 74(7), pp. 2277–2286. doi: 10.1007/s11696-020-01071-y.

Hamzah, N., Leo, C. P. and Ooi, B. S. (2019) 'Superhydrophobic PVDF/TiO 2 -SiO 2 Membrane with Hierarchical Roughness in Membrane Distillation for Water Recovery from Phenolic Rich Solution Containing Surfactant', *Chinese Journal of Polymer Science (English Edition)*. doi: 10.1007/s10118-019-2235-y.

Kang, G. dong and Cao, Y. ming (2014) 'Application and modification of poly(vinylidene fluoride) (PVDF) membranes - A review', *Journal of Membrane Science*, 463, pp. 145–165. doi: 10.1016/j.memsci.2014.03.055.

Puspitasari, V. *et al.* (2010) 'Cleaning and ageing effect of sodium hypochlorite on polyvinylidene fluoride (PVDF) membrane', *Separation and Purification Technology*, 72(3), pp. 301–308. doi: 10.1016/j.seppur.2010.03.001.

Quist-Jensen, C. A. *et al.* (2017) 'Reclamation of sodium sulfate from industrial wastewater by using membrane distillation and membrane crystallization', *Desalination*, 401, pp. 112–119. doi: 10.1016/j.desal.2016.05.007.

Rahimpour, M. R. and Esmaeilbeig, M. A. (2019) 'Chapter 6 - Membrane Wetting in Membrane Distillation', in Angelo Basile, Efrem Curcio, I. (ed.) *Current Trends and Future Developments on (Bio-) Membranes*. Elsevier, pp. 143–174. doi: https://doi.org/10.1016/B978-0-12-813551-8.00006-1.

Rasekh, A. and Raisi, A. (2021) 'Electrospun nanofibrous polyether-block-amide membrane containing silica nanoparticles for water desalination by vacuum membrane distillation', *Separation and Purification Technology*, 275(June), p. 119149. doi: 10.1016/j.seppur.2021.119149.

Reddy, J. *et al.* (2018) 'Mechanical, thermal, and water vapor barrier properties of regenerated cellulose/nano-SiO2 composite films', *Cellulose*, 25. doi: 10.1007/s10570-018-2059-x.

Rezaei, M. and Samhaber, W. (2016) 'Wetting behaviour of superhydrophobic membranes coated with nanoparticles in membrane distillation', *Chemical Engineering Transactions*, 47(November), pp. 373–378. doi: 10.3303/CET1647063.

Silva, T. L. S. *et al.* (2015) 'Multi-walled carbon nanotube/PVDF blended membranes with sponge- and finger-like pores for direct contact membrane distillation', *Desalination*, 357, pp. 233–245. doi: 10.1016/j.desal.2014.11.025.

Wang, H. *et al.* (2018) 'Grafting polytetrafluoroethylene micropowder via in situ electron beam irradiation-induced polymerization', *Polymers*, 10(5). doi: 10.3390/polym10050503.

Widiyandari, H. *et al.* (2020) 'Synthesis of PVDF/SiO2nanofiber membrane using electrospinning method as a Li-ion battery separator', *Materials Today: Proceedings*, 44, pp. 3245–3248. doi: 10.1016/j.matpr.2020.11.448.